ASPECTS OF MASS TRANSFER IN GAS-LIQUID OXIDATION REACTIONS

PROEFSCHRIFT

ter verkrijging van
de graad van doctor aan de Universiteit Twente,
op gezag van de rector magnificus,
prof. dr. W.H.M. Zijm,
volgens besluit van het College voor Promoties
in het openbaar te verdedigen
op vrijdag 9 december 2005 om 13.15 uur

door

Johannes Adriaan Aris Hoorn
Geboren op 1 december 1968
te Zaandam

Dit proefschrift is goedgekeurd door de promotor

prof. dr. ir. G.F. Versteeg

Hoorn, J.A.A.

Aspects of mass transfer in gas-liquid oxidation reactions

Thesis, University of Twente, The Netherlands

ISBN-10: 9090201300

ISBN-13: 9789090201306

Key words: absorption, diffusion, enhancement, radicals, homogeneous catalysis, design

Contents

Chapter 3. (continued.)

1

Introduction

Abstract

The context and the outline of this thesis are described in this Chapter. Also a number of frequently applied technical terms and definitions are explained.

1. Context

A chemical reactor is a vessel designed for carrying out a reaction. Reactors are frequently called 'the heart of a chemical plant' but when comparing the chemical plant to a human body more differences than similarities are found. In the human body the heart is, although ingeniously engineered, nothing more than a fluid pump. Among the organs the liver has probably the highest resemblance with industrial reactors: waste processing, catalyst production, sugar processing and the conversion of ammonia to urea. Just as a human body contains a variety of specialized cells also chemical reactors occur in various shapes and sizes.

The classification of reactors is often based on the phases present and the operating mode of the reactor (Levenspiel, 1972; Trambouze et al., 1988). Single phase reactors operate with a gas or liquid. With multiple phases a variety of combinations is encountered: gas-liquid, liquid-liquid, gas-solid, gas-liquid-solid, liquid-solid and even reactors comprising 4 phases (gas-liquid-liquid-solid) have been studied (Rode et al., 2001). The operation mode of a reactor is batch or continuous, mixed forms also occur. The naming of a type of reactor is also determined by other factors such as for example energy input (stirred tank reactor, bubble column), flow patterns (fluidised bed, fixed bed) and construction details (tubular reactor).

Within the chemical processes operated by DSM today gas-liquid reaction systems occur frequently. Among the large scale applications is the oxidation of cyclohexane to cyclohexanone as one of the two routes for the first step in the production of ε-caprolactam (van de Moesdijk, 1979). In the production of cyclohexanone air is contacted with liquid cyclohexane at elevated temperature and pressure. A similar type of process applied within DSM is the oxidation of toluene for the production of benzoic acid. This reaction is catalysed by a homogeneous metal salt (Keading et al, 1965). Another large scale process involving a gas-liquid reactor is the production of urea from ammonia and carbon dioxide. The development of the reactor is an interesting example of incremental optimisation (see urea documentation at http://www.stamicarbon.com; access date 25 August 2005). In the alternative process for the production of caprolactam developed by DSM and DuPont two of the four main reaction steps comprise gas-liquid reactors: step 1 is a carbonylation reaction (Drent et al., 2003) and step 2 is a hydroformylation reaction (Gelling et al., 2000). Both type of reactions are catalysed by homogeneous metal catalyst.

The reactors in the former processes are clearly visible as gas-liquid operations, but gas-liquid reactions also occur other types of equipment: the absorption and reaction of nitrous gases in water in the production of nitric acid and the scrubbing of components from various gas effluents (nitrous and sulphuric oxides, bromine and hydrogen cyanide). When the study of gas-liquid phenomena is not restricted to purely gas-liquid, the number of reactions is even greater. The number of processes operated at DSM involving gas, liquid and a third phase is even larger than the pure gas-liquid processes. Among these processes are the synthesis of hydroxyl amine from nitric acid (also part of the manufacturing of caprolactam), the hydrogenation of succinonitrile to diaminobutane and various hydrogenations in fine chemicals or food production. The reaction engineering on fermenters is generally considered a specialist topic; the metabolism of the micro-organisms is often so complex that 'ordinary' chemical kinetics is not adequate.

In view of the large number of reactors involving gases and liquids operated within DSM, the need for expertise in this area of chemical reaction engineering is evident. This expertise is among others concerned with the design and optimisation of chemical reactors. Through clever design and maximum optimisation the profit of the plant is increased, as well as the safety of the reactor including operation and finally the environmental impact of the production is reduced. In the design and optimisation a large number of physical, chemical and technological aspects is involved. Knowledge of these aspects has to be gathered through theory and experiments. Only in special cases large scale experiments can be performed directly in the plant. Most often plant experiments are not feasible (operational, economic, technical or safety) and experiments on a much smaller scale are the only option. As an indication: a typical plant scale for a bulk chemical process is 200 kt/yr, that is 25000 kg/hr. Experiments at smaller scales include a pilot plant (10 kg/hr), lab scale (100 g/hr) or micro scale (1 g/hr). The translation of the results obtained with experiments to the situation in the plant is the art of scaling-up. The basic assumption of any scale-up procedure is by knowing the essential steps of the chemical process the behaviour on a different scale can be predicted by taking into account the (different) scale-rules accompanying the essential steps. Scale rules can be quite simple (the intrinsic kinetics of the reaction rates do not change with the size of the reactor) or subject of expert fields (for example the hydrodynamics of fluidised bed reactors). The knowledge of all the relevant steps involved in the processes occurring in a chemical reactor is not evident in all situations. In that case an extended program of various experiments is required to unravel and quantify the essential steps. The collection of ideas on those relevant steps including the quantifications is called a model. The term model does not necessarily refers to a computer model, although most often computer support is essential.

In a gas-liquid reactor, components are transferred between the gas and liquid phase. This transport of molecules between different phases is called mass transfer. There are several mechanisms by which mass transport between phases occurs, but the most commonly encountered driving force is molecular diffusion. A detailed treatise of the theory on gas-liquid mass transfer with reaction can be found in Westerterp et al. (1984), here only the basic concepts are discussed.

The most simple gas-liquid mass transfer with reaction system consists of a gaseous component that is transferred to the liquid phase and in the liquid is converted to a product component:

$$A(g) \longrightarrow A(l) \quad (1)$$

$$A(l) \longrightarrow P(l) \quad (2)$$

The driving force for the transfer of A from gas to liquid is the concentration gradient that is maintained by the disappearance of A in the liquid. In non-reactive systems, the concentration gradient is reduced as time progresses to a situation where thermodynamic equilibrium is reached. In the film theory it is assumed that the interface between gas and liquid can be represented by two stagnant films where the transport of components occurs through diffusion: a layer in the gas side and a layer in the liquid. Between the liquid and the gas phase equilibrium exists. In combination with the reaction of A in the liquid a concentration profile is established as shown in Figure 1.

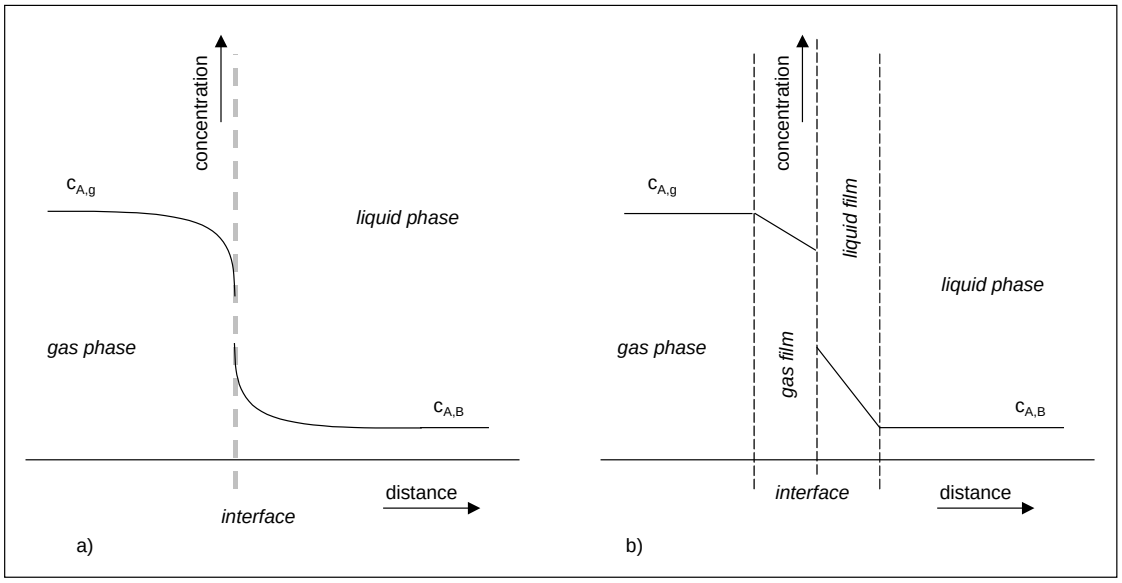

Figure 1. a) Physical representation of absorption and reaction, b) schematic representation of the two-film model.

For only a minor number of absorption-reaction systems the gas and liquid film are equally important. With high liquid solubility's or very small gas phase diffusivity the gas phase resistance is significant. In most practical cases, the gas phase resistance can be ignored.

The two-film model is widely applied in chemical engineering as well as related scientific disciplines as a result of its simplicity and the user-friendliness of the mathematical equations. For more accurate physical descriptions alternative theories have been developed that provide better predictions over a wide range of applications. The penetration model proposed by Higbie (1935) is derived from the idea that the gas-liquid interface is not a static surface but a dynamic area where fluid elements (small packages) are exchanged with the bulk of the liquid. During the period that a fluid element is located on the surface gaseous component A is absorbed from the gas phase and after some contact time the element returns to the bulk of the liquid where it is mixed with the rest. The other well-known theory proposed by Danckwerts (1968) is a modification of Higbie's theory. Instead of a contact time it is assumed that each liquid element at the surface has a similar chance of disappearing in the liquid bulk. Although the theories by Higbie and Danckwerts provide a better physical representation and often a more accurate description of experimental observations, the equations are more complicated and only for the very simple systems analytical solutions are available. In other cases numerical techniques have to be applied to solve the equations.

Reaction and diffusion are coupled processes. In the absence of a chemical reaction differences in concentrations are settled as time progresses unless some other factor than reaction is involved (like for example mass transfer to a solid or secondary liquid). In a gas-liquid reaction system, the reaction increases the mass transfer rate in comparison to the pure physical absorption, the extend depends on the relative rate of the reaction. For slow reactions the major part of the components is converted in the bulk of the liquid. A lot of chemical engineers and chemists call this the kinetic regime. In this regime the kinetics of the reactions are the limiting factor but this does not exclude the occurrence of gradients in the liquid and/or gas film.

For fast reactions, the concentration of absorbent A near the interface is significantly decreased in comparison to pure physical absorption. The concentration gradient increases the diffusion rate and mass transfer is enhanced. The ratio between mass transfer rate and kinetics is expressed through the Hatta number.

For simple reactions, the Hatta number is well defined and can be calculated from a limited number of process parameters. The Hatta number for a first order irreversible reaction rate is defined by:

$$\varphi = \frac{\sqrt{k_1 \cdot D_A}}{k_L} \tag{3}$$

In most expressions the enhancement of mass transfer is incorporated by means of an enhancement factor E. The rate of physical absorption is calculated with:

$$J = k_L \cdot \left(c_{A,i} - c_{A,b}\right) \tag{4}$$

The absorption rate of absorption with reaction can be expressed as:

$$J = k_L \cdot E \cdot \left(c_{A,i} - c_{A,b}\right) \tag{5}$$

For the single first order reaction all models predict in case of slow reactions E = 1 whereas for fast reactions $c_{A,b}$ is zero and E = φ. In other situations, the various theories have different results for enhancement factors. In addition, the evaluation of enhancement factors is dependent upon the type of reaction(s) where the absorbing component is involved. Overviews can be found in for example van Swaaij and Versteeg (1992) and Doraiswamy and Sharma (1994).

A very large amount of literature regarding experimental procedures for gas-liquid reactions is available. Experiments can be designed to determine whether a reaction is slow, fast or instantaneous. Once this classification has been made suitable kinetic rate expressions can be determined from dedicated experiments. In practice, the experimental recipes are not so simple as the text books claim. For example many reactions proceed by means of a catalyst where the condition of the catalyst is influenced by a large number of process variables (concentrations, temperature, pressure, contaminants, etc.). Often it is not possible to control the condition of the catalyst in lab equipment in the same way as in the plant. For reaction systems where catalyst deactivation occurs specialized equipment and experiments are often required to determine reaction rates and other scale-up parameters. In systems where the absorption of a component occurs in a strong evaporating liquid the description of diffusion by Fick's law and the derived mass transfer theories are no longer valid. In that case, application of the Stefan-Maxwell equations with multi component mass transfer is the recipe for better descriptions as has been shown for a number of separation processes (Taylor and Krishna, 1993). Finally, in systems with high reaction rates and strong exothermic heats of reaction temperature gradients are likely to occur in the liquid film, affecting physical properties, reaction rates and altering transport rates.

2. Outline of this thesis

Despite of the difficulties and pitfalls in experimentation and interpretation, once a model is completed and verified to agree with all experimental observations it can be used for a range of purposes:

- scale-up and design,
- optimisation,
- process control,
- flow sheet improvement,
- study of stability and dynamic behaviour.

The study of the stability and dynamic behaviour was the initial objective at the start of the PhD project resulting in this thesis. For the gas-liquid reactors in operation at DSM this type of study had not been performed earlier and it was shown by Van Elk (2001) that this field of expertise promised opportunities for further research. The study of dynamic behaviour and the development of stability criteria is very much dependent on the availability of well defined and verified models for the specific reactors. Instead of suitable models the internal reports and data on gas-liquid reactors at DSM very much reflected the open literature: a vast amount of data and reports but with different results, experiments, conditions and opposing hypotheses. Therefore setting-up a model sufficiently simple and well validated became the initial task. Toluene oxidation was chosen as the model process for a number of practical reasons.

Construction of a model and the identification of the ratio between mass transfer and reaction under conditions closely resembling the plant reactor situation was the objective of the initial task. The results of this study are reflected in *Chapter 2*. The conclusion with respect to the enhancement of mass transfer was that for most conditions the system is in a kinetically controlled regime.

Once it was clear that enhancement of mass transfer does not occur to a significant extend, the optimisation of the descriptions of the reaction rates had to be performed through alterations in the kinetic equations. In *Chapter 3* the improvement of the kinetic expressions to increase the model predictions is described. The detailed reaction network of the toluene oxidation comprising both radical and non-radical reactions and intermediates is well established from literature. Including all these reactions in a model is not feasible since for a large part the reaction rates are unknown.

By modifying the basic rate equations, it was possible to increase the description of the formation and reaction of benzyl alcohol. The rate equations were derived from an assumption of a new path in the reaction network.

From the work leading to the results described in Chapters 2 and 3, the interesting question emerged how reactive intermediates behave in the vicinity of the gas-liquid interface. The efforts to address this topic in a more theoretical framework is described in *Chapter 4*. The specific aspects from the toluene oxidation were transformed to a general form of a gaseous absorbent that reacts with a liquid component B to form product P by means of elementary radical reactions. The tools for numerically solving the diffusion-reaction equations was already well established by Cornelisse et al. (1980) and lately applied by van Elk (1999). The study of the diffusion and mass transfer and radicals was concluded with a paragraph on design aspects and for that purpose it was required that the results of models with different numbers of parameters could be compared. For the example systems applied a methodology is presented that is easy to use while the potential of tuning models to desired accuracy and degree of simplicity is high.

Finally, in *Chapter 5* the analysis for the radical reactions is extended to another class of reactions where complex reaction networks frequently occur: homogeneous catalysis. The principle question again was what is the behaviour of catalytic complexes that exist as intermediates near the gas-liquid interface. What kind of effect do those catalytic complexes have on the enhancement of mass transfer?

Nomenclature

Notation

$c_{A,i}$	concentration of A at the gas-liquid interface	kmol/m^3
$c_{A,b}$	concentration of A in the bulk of the liquid	kmol/m^3
D_A	diffusion coefficient of A	m^2/s
E	enhancement factor	-
J	flow across gas-liquid interface	kmol/m^2/s
k_1	reaction rate constant (first order)	s^{-1}
k_L	liquid side mass transfer coefficient	m/s

Greek

φ	Hatta number	-

References

Cornelisse, R., Beenackers, A.A.C.M., van Beckum, F.P.H., van Swaaij, W.P.M., (1980), Numerical calculation of simultaneous mass transfer of two gases accompanied by complex reversible reactions, *Chem. Eng. Sci.* **35**, 1245-1260.

Danckwerts, P.V., (1968), Gas absorption with instantaneous reaction, *Chem. Eng. Sci.* **23**, 1045-1051.

Doraiswamy, L.K., Sharma, M.M, (1984), Heterogeneous reactions: Analysis, Examples, and Reactor Design. Volume 2: Fluid-Fluid-Solid Reactions, John Wiley & Sons, New York.

Drent, E., van Broekhoven, J.A.M., Breed, A.J.M., (2003), Patent PCT/NL02/00461 (Jan. 23).

Gelling, O.J., Borman, P.C., van Leeuwen, P.W.N.M., (2000), U.S. Patent 6,153,800 (Nov. 28).

Higbie, R., (1935), The rate of absorption of a pure gas into a still liquid during short periods of exposure, *Trans. Am. Inst. Chem. Eng.* **31** 365-389.

Keading, W.W., Lindblom, R.O., Temple, R.G., Mahon, H.I., (1965), Oxidation of toluene and other alkylated aromatic hydrocarbons to benzoic acids and phenols, *Ind. Eng. Chem. Process Des. Dev.* **4**, 97-101.

Levenspiel, O., (1972). Chemical Reaction Engineering, John Wiley & Sons, New York, pp 1-7.

Rode, C.V., Vaidya, M.J., Jaganathan, R., Chaudhari, R.V., (2001), Hydrogenation of nitrobenzene to p-aminophenol in a four-phase reactor: reaction kinetics and mass transfer effects, *Chem. Eng. Sci.* **56**, 1299-1304.

Taylor, R., Krishna, R., (1993), Multicomponent mass transfer, John Wiley & Sons, New York.

Trambouze, P., Van Landeghem, H., Wauquier, J.P., (1988), Chemical Reactors - design/engineering/operation, Éditions Technip, Paris, pp. 53-61.

van de Moesdijk, C.G.M., (1979), The catalytic reduction of nitrate and nitric oxide to hydroxylamine: kinetics and mechanism, Thesis, Technische Hogeschool Eindhoven.

van Elk, E.P., Borman, P.C., Kuipers, J.A.M., Versteeg, G.F., (1999), Modelling of gas-liquid reactors - stability and dynamic behaviour of gas-liquid mass transfer accompanied by irreversible reaction, *Chem. Eng. Sci.* **54**, 4869-4879.

van Elk, E.P., (2001), Gas-liquid reactions - Influence of liquid bulk and mass transfer on process performance, Thesis, Twente University.

van Swaaij, W.P.M., Versteeg, G.F., (1992), Mass transfer accompanied with complex reversible chemical reactions in gas-liquid systems: an overview, *Chem. Eng. Sci.* **47**, 3181-3195.

Westerterp, K.R., van Swaaij, W.P.M., Beenackers, A.A.C.M., (1984), Chemical Reactor Design and Operation, John Wiley & Sons, New York.

2

Modelling toluene oxidation, incorporation of mass transfer phenomena

Abstract

The kinetics of the oxidation of toluene have been studied in close interaction with the gas-liquid mass transfer occurring in the reactor. Kinetic parameters for a simple model have been estimated on basis of experimental observations performed under industrial conditions. The conclusions for the mass transfer and reaction regime on basis of experimental observations and model calculations are in good agreement: toluene oxidation under industrial conditions can be characterized as a slow reaction with respect to mass transfer.

1. Introduction

The site of DSM Special Products Rotterdam has the largest toluene oxidation plant in the world, producing benzoic acid that for the major part is converted to phenol. In addition, benzoic acid and its derivative sodium benzoate also find their applications in the food and fine chemicals industry. The DSM site at Rotterdam also has the largest production unit for benzaldehyde, a specialty chemical. Since the development of the process (Keading et al., 1965) a large number of studies on the chemistry of toluene oxidation and related hydrocarbons have been published. Most of the earlier publications have in common that the main focus is on the kinetics and that other process items are not considered (Borgaonkar et al., 1984; Lozar et al., 2001; Mulkay and Rouchaud, 1967; Quiroga et al., 1980; Scott and Chester, 1972). This approach is not sufficient when considering scale-up and modelling of the plant reactors. For safety reasons, oxygen levels in the reactor offgas have to be kept below the explosion limits. This means that at least in part of the reactor the oxygen partial pressure is so low that the liquid concentration is significantly decreased. In the range of low oxygen concentrations, the radical chain mechanism produces different by-products (Bateman, 1951). In addition, it is expected that the mass transfer of oxygen influences the productivity of the reactor. It is essential to quantify kinetics in close interaction with the mass transfer phenomena occurring in the reactor in order to increase the control of the productivity and selectivity.

2. Kinetics and mass transfer

The oxidation of toluene with air at elevated temperatures and pressures proceeds via a mechanism consisting of a chain of radical reactions and is initialised by cobalt ions. The use of elementary reactions in this radical mechanism is at this moment too complicated (lack of basic data and the need for extensive numerical solving techniques) to be of much practical use in the analyses on mass transfer and reaction. Instead a more simplified kinetic description is applied in the present study. The kinetic scheme in Figure 1 is directly derived from the stoichiometric equations (assuming elementary reactions) and has been proposed earlier for toluene oxidation (Quiroga et al., 1980) as well as xylene oxidation (Cao et al., 1994). For oxidation reactions proceeding through radical intermediates, a zero-order reaction rate is commonly encountered (Helfferich, 2001).

Morimoto and Ogata (1967) concluded from their batch experiments that for oxygen levels below 42 vol% (the oxygen concentration in the reactor was kept constant by maintaining a constant pressure through suppletion of pure oxygen to the oxygen/nitrogen mixture). Bhattacharya et al. (1973) give a reaction order for oxygen of ½, but the experimental conditions are not fully given.

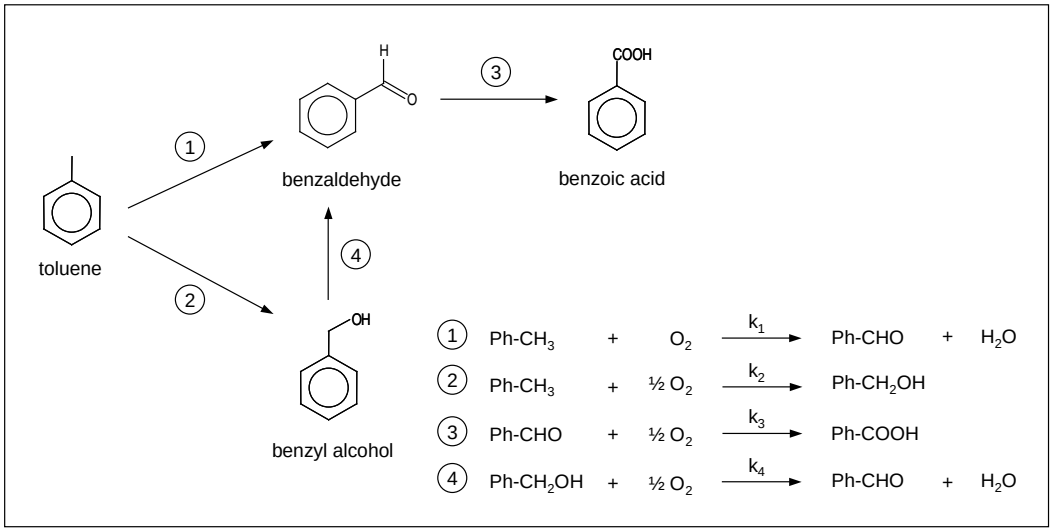

Figure 1. Basic scheme for the kinetics.

The rates for the reactions in Figure 1 are assumed to be first-order in the reactants, also for oxygen. As it mathematically can be shown, it is not possible to determine the individual rate constants for reactions 1, 2 and 4 independently without experiments comprising benzyl alcohol added to the feed. These experiments have not been performed while the availability of the experimental set-up for kinetic experiments was very limited. In addition, benzyl alcohol is known to inhibit the oxidation (Morimoto and Ogata, 1967) making the operation of a continuous tank reactor more difficult than it is already. A correlation between R_1 and R_2 was made on basis of the observation that in the oxidation mechanism the primary termination reaction takes place between two alkoxy radicals (Russell, 1957; Kondratiev, 1969) whereby alcohol and aldehyde are formed in a 1:1 ratio. For this reason, the parameters k_1 and k_2 were replaced by a single parameter k_{12} giving the following expressions for the reaction rates:

$$R_1 = k_{12} \cdot c_{TOL} \cdot c_{O2} \tag{1}$$

$$R_2 = k_{12} \cdot c_{TOL} \cdot c_{O2} \tag{2}$$

$$R_3 = k_3 \cdot c_{BALD} \cdot c_{O2} \tag{3}$$

$$R_4 = k_4 \cdot c_{BALC} \cdot c_{O2} \tag{4}$$

The influence of the catalyst was not included in the rate equations because all experimental data have been performed at a constant cobalt concentration. The expression for the Hatta number (φ) depends on the reaction rate equation. For a first-order irreversible reaction with respect to the absorbing component φ is defined by:

$$\varphi = \frac{\sqrt{k \cdot D}}{k_L} \tag{5}$$

For systems consisting of multiple reactions involving the gaseous component the most commonly applied simplification is to evaluate the Hatta number on the assumption that an overall pseudo zero-order or first-order rate equation is applicable. The model of the xylene oxidation by Cao et al. (1994) comprises a zero order reaction for oxygen where Hatta is calculated according to the correlation of Hikita and Asai (1964). This approach is also applied by Suresh et al. (1988) in the modelling of the cyclohexane oxidation. Pohorecki et al. (2001) apply a first order dependence for oxygen in the cyclohexane oxidation with a kinetic scheme that has a close resemblance to the toluene oxidation scheme given in Figure 1. The mass transfer flux for a first-order irreversible reaction according to the Danckwerts modification of the penetration theory is defined by (Westerterp et al., 1984):

$$J = k_L \cdot \left[c_{A,i} - \frac{c_{A,b}}{1+\varphi^2} \right] \cdot \sqrt{1+\varphi^2} \tag{6}$$

The extremes for small and large Hatta numbers are convenient for simple evaluations on basis of analytical solutions.

$$\varphi > 2 \qquad J = k_L \cdot c_{A,i} \cdot \varphi \tag{7}$$

$$\varphi < 0.3 \qquad J = k_L \cdot \left(c_{A,i} - c_{A,b} \right) \tag{8}$$

The enhancement factor is the ratio of the flux in presence of reaction (Eq. (6)) and pure physical mass transfer under identical conditions (expression is equivalent to Eq. (8)).

$$E = \sqrt{1+\varphi^2} \cdot \frac{\left(c_{A,i} - \frac{c_{A,b}}{1+\varphi^2} \right)}{c_{A,i} - c_{A,b}} \tag{9}$$

The extremes for small and large Hatta numbers are:

$$\varphi > 2 \qquad E = \varphi \tag{10}$$

$$\varphi < 0.3 \qquad E = 1 \tag{11}$$

The Hatta number and the enhancement factor are calculated from experimental observations, respectively included in the modelling.

3. Experiments and observations

The reactor and auxiliary equipment for the toluene oxidation experiments are operated in a continuous mode, a schematic drawing of the set-up is given in Figure 2. All equipment is accommodated in an explosion proof facility.

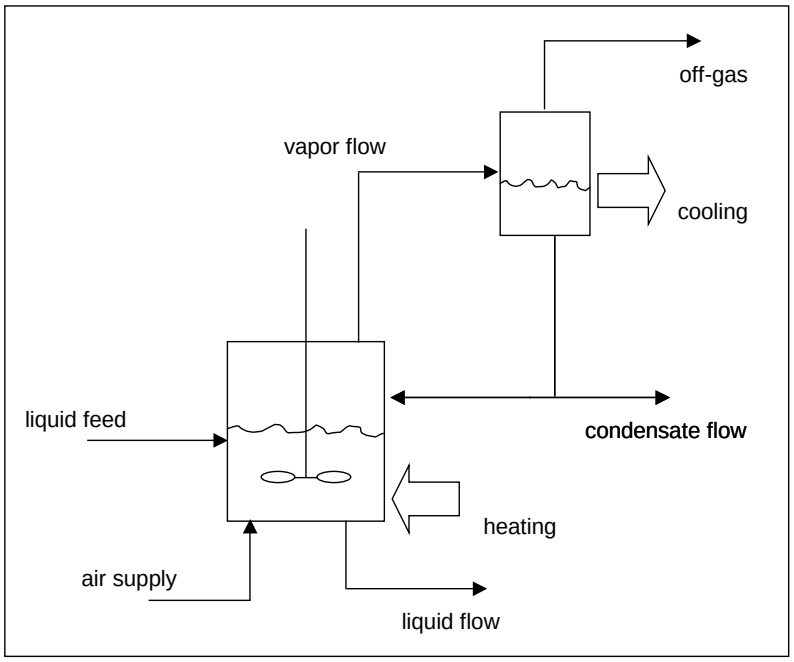

Figure 2. Experimental set-up.

From the continuous monitoring of the reactor temperature and the oxygen concentration in the off-gas during experiments it appeared that small fluctuations are present in the reaction set-up. The standard deviations of the results of five reference experiments having identical process conditions are shown in Table 1 as an indication of the extend of experimental inaccuracy's. The range of process variables of all experiments is included for comparison. A number of experiments have been performed with insufficient tracing in part of the piping from the reactor vessel to the condenser causing a partial condensation of the vapour and subsequent reflux of components to the reactor. The rate of oxygen transferred to the liquid phase (F_{GL}) was calculated from the difference between the gas feed and off-gas flow.

Table 1. Data from a series of standard experiments.

			Range of operation	Standard deviation in reference experiments
Reactor temperature		°C	140-160	0.8%
Reactor pressure		bar	4-7	0.2%
Off-gas inert flow		Nl/hr	100-300	1.1%
Feed flow toluene		kg/hr	1-2	1.0%
Feed flow air		Nl/hr	100-300	0.3%
Flow liquid discharge		kg/hr	0.5-1.5	2.1%
Flow condensate		kg/hr	0.5-1.5	2.3%
Off-gas oxygen level		vol%	0-6	32.5%
condensate	Balc	mol/hr	0.0003-0.005	12.5%
	Bald	mol/hr	0.003-0.02	7.3%
	BzA	mol/hr	0-0.02	20.8%
	H_2O	mol/hr	0.6-1.6	11.0%
	Tol	mol/hr	2.1-5.6	4.8%
liquid discharge	Balc	mol/hr	0.003-0.05	3.9%
	Bald	mol/hr	0.03-0.2	1.8%
	BzA	mol/hr	0.4-1.1	3.3%
	Tol	mol/hr	1.5-10.9	1.5%

Both the liquid and the gas phase were assumed to be ideally mixed; the residence times for the liquid were in the order of 1 hr. To address the gas phase mixing qualitatively a visual check was performed in an glass vessel comprising identical baffle and stirrer configuration. With cyclohexane as liquid at room temperature and nitrogen as gas feed, it was observed that at 1600 rpm stirrer speed a significant amount of gas backmixing occured into the liquid by means of vortex formation around the stirrer and turbulences behind the baffles. In addition, it was assumed that no oxygen is present in the liquid feed and the system operates at steady state. The oxygen concentration in the liquid at saturation was calculated according to Henry's law. The Henry coefficients were calculated from gas-liquid equilibirum data retrieved from the Dortmund Data Bank (program version DDBSP 2003; http://www.ddbst.com, president and CEO of DDBST is Prof. Dr. J. Gmehling, access date 26 November 2004). Typical values are in the range of 1500-2000 bar. The partial pressure of oxygen was determined from the off-gas and condensate composition. In Figure 3 the conversion rates for oxygen are shown as function of the oxygen concentration in the liquid.

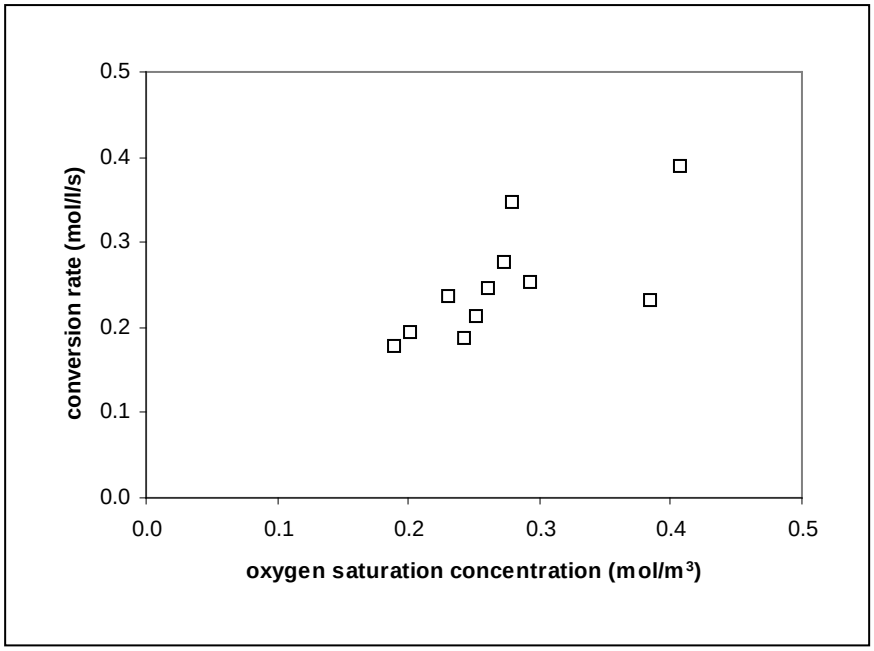

Figure 3. Observed conversion rates for oxygen as function of the oxygen concentration in the liquid at saturation.

The conversion rate for oxygen is defined as the transfer rate of oxygen divided by the liquid volume; in this way the outflow of dissolved oxygen is neglected. The experimentally observed oxygen transfer rate F_{GL} is related with the flux through the interfacial area:

$$F_{GL} = J \cdot V_R \cdot a \tag{12}$$

In case $\varphi > 2$ substitution of the expression for the observed transfer rate gives (taking into account the definition for the Hatta number):

$$k = \frac{1}{D} \cdot \left(\frac{F_{GL}}{V_R \cdot a \cdot c_{A,i}} \right)^2 \tag{13}$$

For $\varphi < 0.3$ the bulk concentration can be calculated from a balance for oxygen in the liquid phase:

$$0 = -\phi_V \cdot c_{A,b} - (1-\varepsilon) \cdot V_R \cdot k \cdot c_{A,b} + J \cdot V_R \cdot a \tag{14}$$

The outflow of dissolved oxygen is considered to be much smaller than the reaction term and the transfer rate through the gas-liquid interface; therefore Eq. (14) can be simplified to:

$$0 = -(1-\varepsilon) \cdot V_R \cdot k \cdot c_{A,b} + J \cdot V_R \cdot a \tag{15}$$

With the substitution for J (Eq. (8)):

$$\frac{c_{A,b}}{c_{A,i}} = \frac{1}{1+Al\cdot\varphi^2} \tag{16}$$

Where Al is the Hinterland ratio:

$$Al = \frac{(1-\varepsilon)\cdot k_L}{a\cdot D} \tag{17}$$

Combining the expression for the bulk concentration with the flux and the observed conversion rate gives an equation that can be solved with respect to the kinetic rate constant:

$$F_{GL} = V_R\cdot a\cdot k_L\cdot\left(c_{A,i} - \frac{c_{A,i}}{1+Al\cdot\varphi^2}\right) \tag{18}$$

Solving for k gives:

$$k = \frac{k_L^2}{Al\cdot D}\cdot\frac{F_{GL}}{V_R\cdot k_L\cdot a\cdot c_{A,i} - F_{GL}} \tag{19}$$

Values for specific surface areas were estimated with the correlation of Shridhar and Potter (1980), diffusion coefficients were estimated with the correlation of Wilke and Chang (1955). Mass transfer coefficients were estimated for water with the equation of van 't Riet (1979). To translate the mass transfer coefficients from water to toluene at reactor conditions, a result from Higbie's penetration theory was applied:

$$\frac{k_L(\text{toluene}, 150\ ^\circ C)}{k_L(\text{water}, 25\ ^\circ C)} = \sqrt{\frac{D(\text{toluene}, 150\ ^\circ C)}{D(\text{water}, 25\ ^\circ C)}} \tag{20}$$

The experimental conditions in the experiments were such that the volumetric mass transfer coefficient could be taken as constant at a value of 0.75 s^{-1}. The interfacial area was taken as a constant at 300 m^2/m^3. Under the hypothesis that the reaction is fast, i.e. $\varphi > 2$, the calculated rate constant (Eq. (13)) is 100 s^{-1} ($\pm$ 56 s^{-1}, standard deviation for the experimental observations). The corresponding Hatta number on basis of this rate constant can then be estimated to be 0.60 $\pm$ 0.16. This is not in line with the assumption of a fast reaction with $\varphi > 2$. For the hypothesis of a slow reaction, i.e. $\varphi < 0.3$, the calculated rate constant is 2.2 $\pm$ 3.2 s^{-1} giving a Hatta number of 0.079 $\pm$ 0.048 which is in line with the assumption made for the Hatta number. Therefore it is concluded that on basis of the experimental observations the reaction rate is slow in comparison to the mass transfer rate of oxygen.

4. Modelling of the experimental reactor

A model was constructed to determine the kinetic parameters under conditions of mass transfer limitations while taking into account partial condensation of the vapour phase. To include a description of the partial condensation between the reactor and the condenser the model comprised two flash calculations for the reactor part of the set-up. A scheme of the model is given in Figure 4.

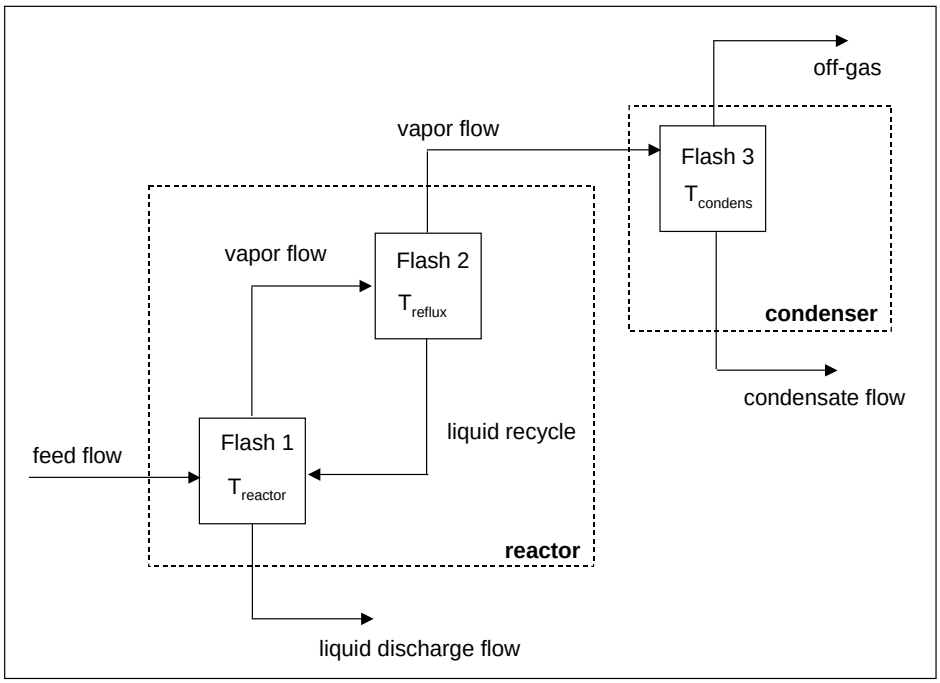

Figure 4. Schematic drawing of model. The symbols in this scheme are utilized in the overview of model equations.

For an overview on the model equations see Appendix. The model calculations were performed in Aspen Custom Modeler. Thermodynamic properties for the liquid phase were calculated with Aspen Plus Properties. The pure component properties were taken from the DIPPR Handbook (http://dippr.byu.edu, American Institute of Chemical Engineers, access date 25 May 2004) or DDBST (http://www.ddbst.com). The interaction between components was described by the NRTL-model. The thermodynamic property files generated in Aspen Plus were included in the ACM file.

The liquid from the second flash is totally refluxed to the first flash (“liquid recycle”). The temperature of the second flash was varied for each experiment in such a way that the differences between experimental and model values for the gas and liquid mole flows of all components were minimized.

The calculations to determine the temperatures of the second flash were performed with a simulated combined feed of the liquid discharge and vapour flows. For experiments performed with the correct tracing, the temperature of the second flash was fixed at the temperature of the first flash. The temperatures of the second flash were 5 to 15 °C lower than the reactor temperature depending on the composition of the condensate flow. The liquid recycle amounts to 10 to 20% (mole flow basis) compared to the vapour flow feeding the second flash. The statistical results of the calculations are given in Table 2.

Table 2. Statistics for vapour-liquid calculations.

		SSO (mol^2/hr^2)	SSR (mol^2/hr^2)	Standard deviation	SSR without reflux (mol^2/hr^2)	Standard deviation without reflux
condensate	Balc	$3.24 \cdot 10^{-5}$	$5.61 \cdot 10^{-6}$	35.5%	$8.74 \cdot 10^{-5}$	127.5%
	Bald	$9.29 \cdot 10^{-4}$	$1.69 \cdot 10^{-4}$	21.7%	$1.38 \cdot 10^{-3}$	61.3%
	BzA	$4.45 \cdot 10^{-4}$	$1.87 \cdot 10^{-4}$	34.2%	$1.34 \cdot 10^{-4}$	37.3%
	H_2O	$1.26 \cdot 10^{1}$	$2.23 \cdot 10^{-1}$	11.0%	$2.57 \cdot 10^{-1}$	12.6%
	Tol	$1.61 \cdot 10^{2}$	$2.72 \cdot 10^{0}$	11.0%	$3.34 \cdot 10^{1}$	36.1%
liquid discharge	Balc	$6.92 \cdot 10^{-3}$	$5.61 \cdot 10^{-6}$	2.4%	$8.74 \cdot 10^{-5}$	9.4%
	Bald	$1.53 \cdot 10^{-1}$	$1.69 \cdot 10^{-4}$	3.0%	$1.38 \cdot 10^{-3}$	8.7%
	BzA	$5.09 \cdot 10^{0}$	$1.87 \cdot 10^{-4}$	0.5%	$1.34 \cdot 10^{-4}$	0.4%
	Tol	$4.84 \cdot 10^{2}$	$2.72 \cdot 10^{0}$	11.0%	$3.34 \cdot 10^{1}$	38.5%

The kinetic parameters in Figure 1 were estimated by a least squares minimization procedure. In the estimation procedure (and in the subsequent model calculations) the temperatures in the second flash were fixed at the values calculated earlier. The most suitable variables as experimental data points and the optimal weighting were identified after some trial and error. Best results were obtained with the toluene conversion, selectivity's for benzyl alcohol, benzaldehyde and benzoic acid and the oxygen off-gas concentration. The weights of the experimental values for a particular variable were set as reciprocals of the average values, except for oxygen which was given a lower value (10% of the reciprocal average). The results are given in Table 3. In Table 4 the sums of the squared residuals of model prediction and experimental values (SSR) are shown.

Table 3. Estimated parameter values and correlation matrix.

Parameter values			Reactions		Correlation matrix			
k_{12}	0.015 ± 0.004	m^3/mol/s	Tol ⟶ Balc			k_{12}	k_3	k_4
			Tol ⟶ Bald		k_{12}	1		
k_3	1.35 ± 0.36	m^3/mol/s	Bald ⟶ BzA		k_3	0.98	1	
k_4	3.9 ± 1.0	m^3/mol/s	Balc ⟶ Bald		k_4	0.99	0.98	1

Table 4. Sum of Squares for experiments and model.

	Experiment SSO	Model SSR
O_2 off-gas	$7.2 \cdot 10^{1}$	$4.3 \cdot 10^{1}$
Tol conversion	$7.2 \cdot 10^{-2}$	$1.8 \cdot 10^{-3}$
Balc selectivity	$9.6 \cdot 10^{-3}$	$1.4 \cdot 10^{-4}$
Bald selectivity	$2.4 \cdot 10^{-1}$	$1.7 \cdot 10^{-3}$
BzA selectivity	$7.5 \cdot 10^{0}$	$1.6 \cdot 10^{-3}$

The model results for the data applied in the estimation procedure are shown in the parity plots in Figures 5 to 8. Comparison between experimental values and model calculations for the oxygen concentration in the off-gas are shown in Figure 9.

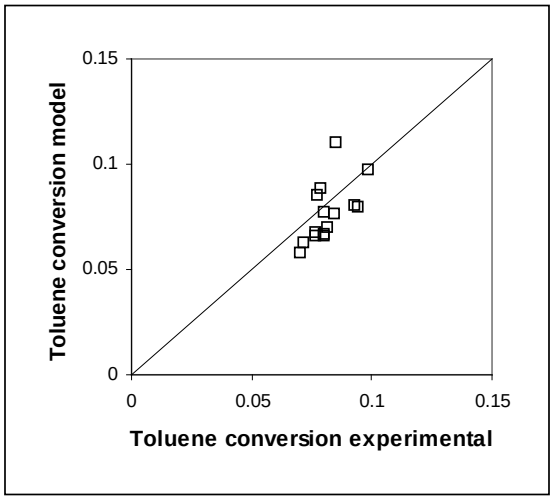

Figure 5. Comparison between experimental values and model calculations for the conversion of toluene.

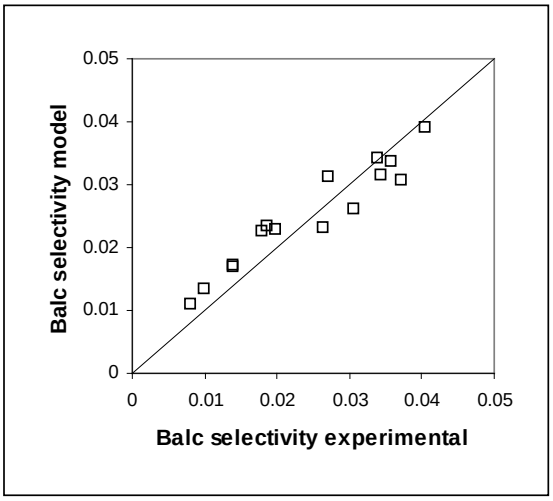

Figure 6. Comparison between experimental values and model calculations for the selectivity of benzyl alcohol.

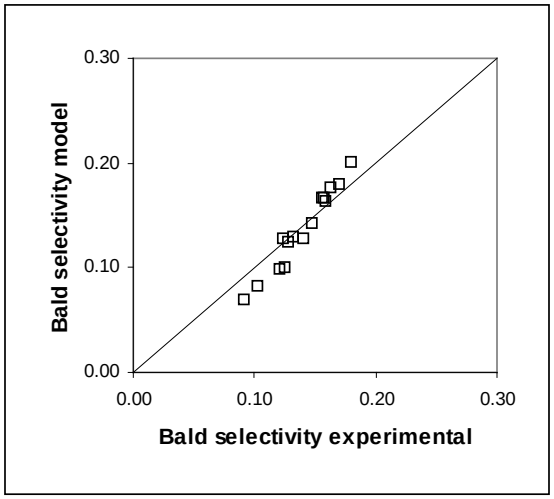

Figure 7. Comparison between experimental values and model calculations for the selectivity of benzaldehyde.

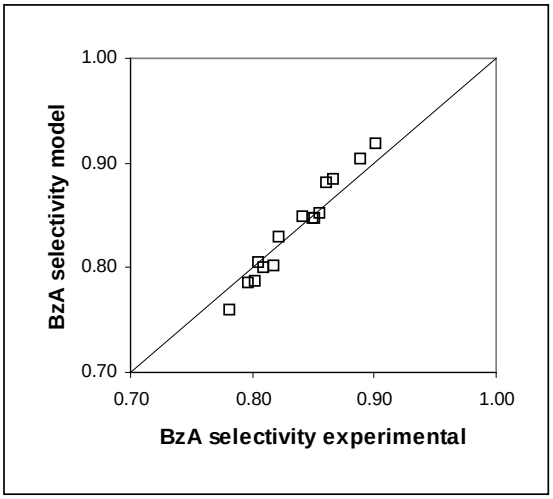

Figure 8. Comparison between experimental values and model calculations for the selectivity of benzoic acid.

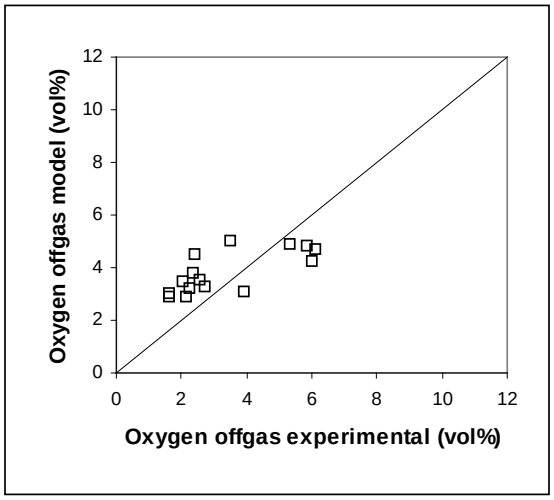

Figure 9. Comparison between experimental values and model calculations for the oxygen concentration in the off-gas.

The residuals for benzyl alcohol, benzaldehyde and benzoic acid selectivity are shown in Figures 10 and 11. Residual values are given as the difference in selectivity between experiment and model relative to the observed experimental value. The calculated pseudo first-order rate constant is $k_{fo} = 295 \pm 14\ s^{-1}$, the Hatta number is $\varphi = 0.92 \pm 0.05$ and the enhancement factor is $E = 1.36 \pm 0.03$.

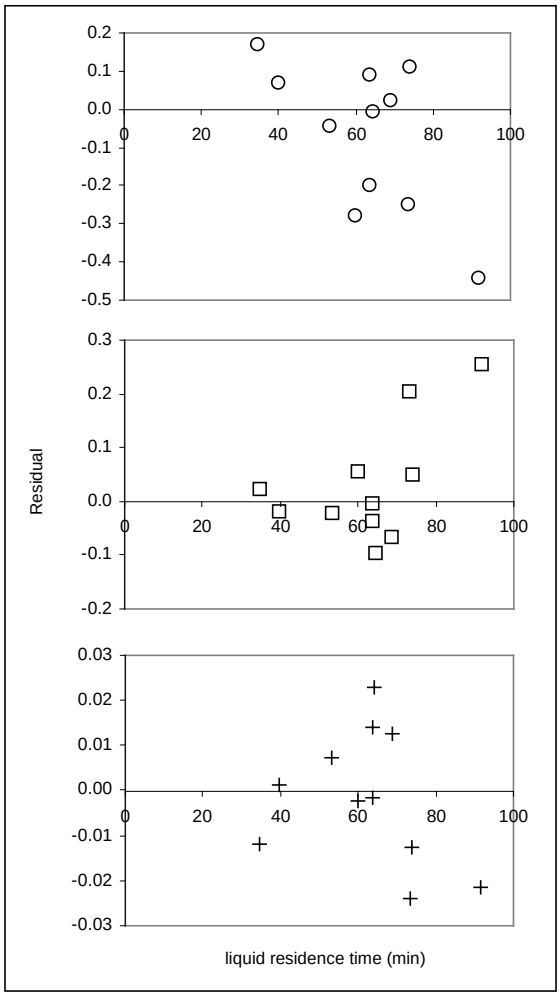

Figure 10. Residuals between experimental and model values as function of the residence time based on the liquid feed flow rate; (○) = benzyl alcohol; (□) = benzaldehyde; (+) = benzoic acid.

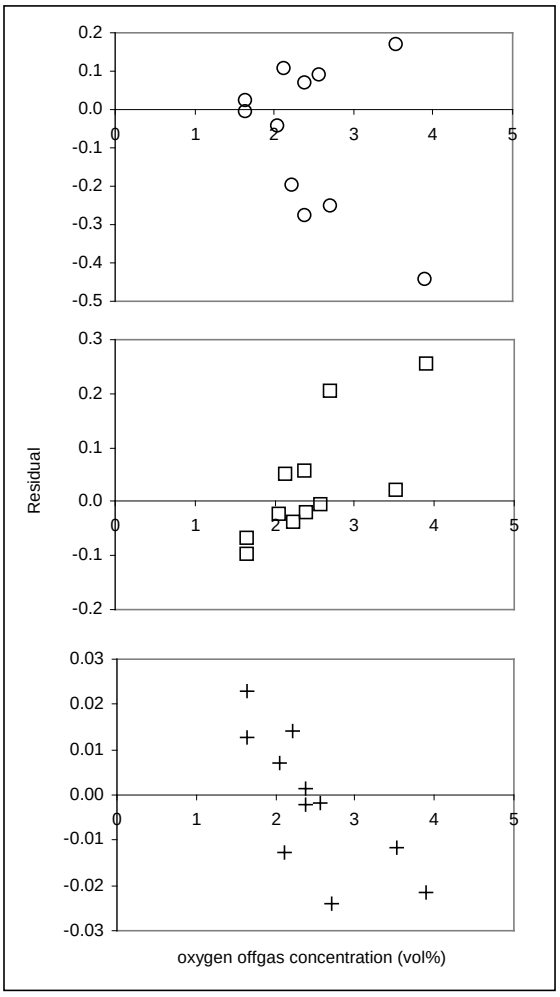

Figure 11. Residuals between experimental and model values as function of the experimental observed oxygen concentration in the offgas; (○) = benzyl alcohol; (□) = benzaldehyde; (+) = benzoic acid.

5. Discussion

From Table 1 it appears that the input process parameters are controlled with acceptable accuracy of approximately 1%. The response variables differ in accuracy in the range of 1.5% for toluene in the liquid discharge flow to 20% for benzoic acid in the condensate flow. Benzoic acid concentrations in the condensate flow are difficult to analyse because at room temperature the condensate separates into a water and an organic phase. The low accuracy for the oxygen measurement is a combination of the analytical measurement and the length of the sample pipe from the off-gas vessel to the instrument. The simulation of the partial condensation in the piping to the condenser vessel is successfully performed by modelling the reactor part with an additional flash calculation (Figure 4) and this is illustrated when the results in Table 2 are compared. The differences between model predictions and experimental observations are clearly reduced with respect to the situation where there is no liquid recycle. When compared to the indication of experimental errors in Table 1, the model describing the partial condensation has a scatter in the model predictions that is much closer to the experimental error than the model version without the reflux mechanism. Tables 3 and 4 summarize results of the estimated kinetic parameters. The values of the standard deviations as well as the correlation parameters are in acceptable limits for further scale-up purposes, but improvement is still desired. The residual sums are acceptable in comparison to the experimental values. This picture is confirmed by the graphs of the residual plots of the toluene conversion and the selectivity's of benzyl alcohol, benzaldehyde and benzoic acid (Figures 5 to 8). The parity plot for oxygen exhibits a fair off-set (Figure 9). This is caused by the low weighting value for oxygen which was based on the inaccuracy of the experimental value.

The residuals are larger when the liquid residence time increases or when the oxygen concentration is higher. (There is no direct relation between liquid residence time and oxygen concentration because the gas flow rate is set independent of the liquid feed flow rate). For the determination of the reaction rate order in oxygen the results in Figure 3 do not exclude other than simple first order kinetics. The choice for a first-order oxygen dependence is quite arbitrary and has been done for practical reasons, a zero-order model is more difficult to handle because of the discontinuity's with the reaction rates. When some reaction rate equation other than a power law is required to improve the model accuracy, mass transfer rates have to be solved by numerical procedures. The combination of these numerical solutions with parameter estimation procedures has not been performed so far. The value of the Hatta number that was directly derived from the experimental observations indicates that the oxidation of toluene can be considered to be slow.

The Hatta number of 0.09 derived from the experimental observations is in good agreement with the value calculated with the model. The enhancement factor calculated by the model is also close to unity. The results obtained with the model show a more narrow distribution of errors. The standard deviations in the average Hatta number is smaller (5% relative) than with the experimentally determined Hatta number (50%). The low values of Hatta and the enhancement factor imply the presence of an oxygen concentration in the liquid bulk, suggesting that reaction of oxygen with some kind of radical intermediate can not be the rate-determining step in the overall mechanism. This is in general agreement with the picture for autoxidation reactions (Helfferich, 2001).

6. Conclusions

Experiments performed in a reactor that was operated under industrial conditions have been successfully applied in the estimation of kinetic parameters in a model with inclusion of the description of mass transfer phenomena. Analyses of the mass transfer characteristics reveal that toluene oxidation under industrial conditions is a slow reaction with respect to mass transfer.

Nomenclature

Notation

a	interfacial area per unit volume of dispersion	m^2/m^3
Al	Hinterland ratio	-
c	concentration	$kmol/m^3$
$c_{A,b}$	concentration of A in the liquid bulk	$kmol/m^3$
$c_{A,i}$	concentration of A at the gas-liquid interface	$kmol/m^3$
$c_{O2,sat}$	saturation concentration of oxygen	$kmol/m^3$
$c_{O2,out}$	oxygen concentration in the gas outflow	$kmol/m^3$
D	diffusion coefficient	m^2/s
E	enhancement factor	-
F	flow	kmol/s
F_{GL}	flow across gas-liquid interface	kmol/s
J	flow across gas-liquid interface	$kmol/m^2/s$
k	reaction rate constant (second order)	$m^3/kmol/s$

k	reaction rate constant (first order)	s^{-1}
k_{fo}	reaction rate constant (pseudo first order)	s^{-1}
k_L	liquid side mass transfer coefficient	m/s
k_La	volumetric liquid side mass transfer coefficient	1/s
n	reaction order	-
p	partial pressure	bar
P_{tot}	total pressure (absolute)	bar
R	reaction rate	$kmol/m^3/s$
V_R	dispersion volume (liquid + gas)	m^3
w	mole fraction in liquid	mol/mol
x	mole fraction in liquid	mol/mol
$x_{O2,sat}$	oxygen mole fraction in liquid at saturation	mol/mol
y	mole fraction in vapour	mol/mol
z	mole fraction in vapour	mol/mol

Greek

ε	gas volume per unit volume dispersion	m^3/m^3
χ	conversion	mol/mol
ϕ	fugacity coefficient	-
ϕ_V	volumetric flow	m^3/s
φ	Hatta number	-
$\rho_{mol,L}$	liquid molar density	$kmol/m^3$
σ	selectivity	mol/mol
τ_L	residence time	s

Sub- and superscripts

i	any component
BALC	benzyl alcohol
BALD	benzaldehyde
BzA	benzoic acid
F	feed flow
G	vapour flow
H2O	water
L	liquid flow

N2	nitrogen
R	liquid flow
O2	oxygen
TOL	toluene
V	vapour flow

Abbreviations

ACM	Aspen Custom Modeler
SSO	Sum of Squared Observations
SSR	Sum of Squared Residuals

References

Bateman, L., (1951), Olefin oxidation, *Quart. Revs. (London)* **31**, 147-167.

Bhattacharya, D., Guha, D.K., Roy, A.N., (1973), Liquid phase air oxidation of toluene to benzoic acid. II. Kinetics and mechanism, *Chem. Age India* **24**, 87-90.

Borgaonkar, H.V., Raverkar, S.R., Chandalia, S.B., (1984), Liquid phase oxidation of toluene to benzaldehyde by air, *Ind. Eng. Chem. Prod. Res. Dev.* **23**, 455-458.

Cao, G., Servida, A., Pisu, M., Morbidelli, M., (1994), Kinetics of p-xylene liquid-phase catalytic oxidation, *AIChE J.* **40**, 1156-1166.

Helfferich, F.G., (2001), Kinetics of homogeneous multistep reactions, in: Compton, R.G., Hancock, G., (Eds.), *Comprehensive Chemical Kinetics, vol. 38*, Elsevier, Amsterdam, pp. 283-286.

Hikita, H., Asai, S., (1964), Gas absorption with (m,n)-th order irreversible chemical reaction, *Int. Chem. Eng.* **4**, 332-340.

Keading, W.W., Lindblom, R.O., Temple, R.G., Mahon, H.I., (1965), Oxidation of toluene and other alkylated aromatic hydrocarbons to benzoic acids and phenols, *Ind. Eng. Chem. Process Des. Dev.* **4**, 97-101.

Kondratiev, V.N, (1969), The theory of kinetics, in: Bamford, C.H., Tipper, C.F.H., (Eds.), *Comprehensive Chemical Kinetics, vol. 2*, Elsevier, Amsterdam, pp. 165-173.

Lozar, J., Falgayrac, G., Savall, A., (2001), Kinetics of the electrochemically assisted autoxidation of toluene in acetic acid, *Ind. Eng. Chem. Res.* **40**, 6055-6062.

Morimoto, T., Ogata, Y., (1967), Kinetics of the autoxidation of toluene catalyzed by cobaltic acetate, *J. Chem. Soc. (B)*, 62-66.

Mulkay, P., Rouchaud, J., (1967), Solvatation des catalyseurs d'oxydation en phase liquide homogène, *Bull. Soc. Chim. Fr.* **12**, 4653-4657.

Pohorecki, R., Baldyga, J., Moniuk, W., Podgórska, W., Zdrójkowski, A., Wierzchowski, P.T., (2001), Kinetic model of cyclohexane oxidation, *Chem. Eng. Sci.* **56**, 1285-1291.

Quiroga, O.D., Gottifredi, J.C., Capretto de Castillo, M.E., (1980), Liquid phase catalytic toluene oxidation, formulation of a kinetic model, *Lat. Am. J. Chem. Eng. Appl. Chem.* **10**, 77-88.

van 't Riet, K., (1979), Review of measuring methods and results in nonviscous gas-liquid mass transfer in stirred vessels, *Ind. Eng. Chem. Process. Des. Dev.* **18**, 357-364.

Russell, G.A., (1957), Deuterium-isotope effects in the autoxidation of aralkyl hydrocarbons. Mechanism of the interaction of peroxy radicals, *J. Am. Chem. Soc.* **79**, 3871-3877.

Scott, E.J.Y., Chester, A.W., (1972), Kinetics of the cobalt-catalyzed autoxidation of toluene in acetic acid, *J. Phys. Chem.* **76**, 1520-1524.

Shridhar, T., Potter, O.E., (1980), Interfacial areas in gas-liquid stirred vessels, *Chem. Eng. Sci.* **35**, 683-695.

Suresh, A.K., Sridhar, T., Potter, O.E., (1988), Autocatalytic oxidation of cyclohexane - mass transfer and chemical reaction, *AIChE J.* **34**, 81-93.

Westerterp, K.R. , van Swaaij, W.P.M., Beenackers, A.A.C.M., (1984), Chemical Reactor Design and Operation, John Wiley & Sons, New York, pp. 371-377.

Wilke, C.R., Chang, P., (1955), Correlation of diffusion coefficients in dilute solutions, *AIChE J.* **1**, 264-270.

Appendix

Overall pseudo first-order rate constant for oxygen

$$k_{fo} = \frac{3}{2} \cdot k_{12} \cdot c_{TOL} + \frac{1}{2} \cdot \left(k_3 \cdot c_{BALD} + k_4 \cdot c_{BALC} \right)$$

Definition of Hatta number and mass transfer equations

$$\varphi = \frac{\sqrt{k_{fo} \cdot D}}{k_L}$$

$$F_{GL} = J \cdot V_R \cdot a$$

$$E = \sqrt{1+\varphi^2} \cdot \frac{\left(c_{O2,sat} - \frac{c_{O2}}{1+\varphi^2} \right)}{c_{O2,sat} - c_{O2}}$$

$$J = k_L \cdot \left(c_{O2,sat} - c_{O2} \right) \cdot E$$

Reaction rate expressions (according to Figure 1)

$$R_1 = k_{12} \cdot c_{TOL} \cdot c_{O2}$$

$$R_2 = k_{12} \cdot c_{TOL} \cdot c_{O2}$$

$$R_3 = k_3 \cdot c_{BALD} \cdot c_{O2}$$

$$R_4 = k_4 \cdot c_{BALC} \cdot c_{O2}$$

$$R_{BALC} = R_2 - R_4$$

$$R_{BALD} = R_1 - R_3 + R_4$$

$$R_{BzA} = R_3$$

$$R_{H2O} = R_1 + R_4$$

$$R_{O2} = -R_1 - \frac{1}{2} \cdot \left(R_2 + R_3 + R_4 \right)$$

$$R_{TOL} = -R_1 - R_2$$

Definition for toluene conversion

$$\chi = \frac{F_{F,TOL} - \left(F_{L,TOL} + F_{G,TOL} \right)}{F_{F,TOL}}$$

Definition for benzoic acid, benzaldehyde and benzyl alcohol selectivity

$$\sigma_i = \frac{F_{L,i} + F_{G,i}}{\sum_j F_{L,j} + \sum_j F_{G,j}}$$

Definition for off-gas oxygen concentration

$$c_{O2,out} = \frac{F_{G,O2}}{F_{G,N2} + F_{G,O2}}$$

Mole fractions and concentrations for all components

$$c_i = \rho_{mol,L} \cdot x_i$$

$$x_i = \frac{F_{L,i}}{\sum_i F_{L,i}}$$

$$y_i = \frac{F_{G,i}}{\sum_i F_{G,i}}$$

$$z_i = \frac{F_{VAP,i}}{\sum_i F_{VAP,i}}$$

$$w_i = \frac{F_{REC,i}}{\sum_i F_{REC,i}}$$

Mass balances for all components except oxygen for Flash 1 and Flash 2 (see Figure 4)

$$\phi_{L,i} \cdot x_i = \phi_{V,i} \cdot z_i$$

$$\phi_{G,i} \cdot y_i = \phi_{R,i} \cdot w_i$$

$$F_{F,i} + F_{R,i} + V \cdot R_i = F_{L,i} + F_{V,i}$$

$$F_{V,i} = F_{G,i} + F_{R,i}$$

Mass balances for oxygen

$$\phi_{L,O2} \cdot x_{O2,sat} = \phi_{V,O2} \cdot z_{O2}$$

$$\phi_{G,O2} \cdot y_{O2} = \phi_{R,O2} \cdot w_{O2}$$

$$F_{F,O2} = F_{GL,O2} + F_{V,O2}$$

$$F_{GL,O2} + F_{R,O2} + V_R \cdot R_{O2} = F_{L,O2}$$

$$F_{V,O2} = F_{G,O2} + F_{R,O2}$$

3

A kinetic model for toluene oxidation comprising benzylperoxy benzoate ester as reactive intermediate in the formation of benzaldehyde

Abstract

During the oxidation of toluene under semibatch conditions, the formation of benzyl alcohol is initially equal to the rate of formation of benzaldehyde. As the overall conversion increases the benzyl alcohol concentration at first decreases much faster than benzaldehyde, but this decrease slows down causing the benzyl alcohol concentration to reduce to zero only very slowly. To account for this phenomenon a new reaction pathway has been proposed where the formation of benzaldehyde out of benzylhydroperoxide is catalysed by benzoic acid. Incorporation of this new reaction in a model improves the description of benzyl alcohol concentration prophiles while maintaining good predictions for benzaldehyde and benzoic acid.

1. Introduction

Toluene oxidation is a reaction system in which chemistry, kinetics, thermodynamics, transport processes and hydrodynamics interact in a complex fashion. Although the initial development of the process took place already more than 50 years ago (Palmer and Bibb, 1942; Hearne et al., 1951) and a lot of details have been published (Keading et al., 1965; Mulkay and Rouchoud, 1967; van Goolen and van den Berg, 1967), there is still room for improvement especially in the area of integration of the aforementioned disciplines. As an integrating tool, modelling is very suitable to perform that task. Early model developments have in common that the main focus is on the kinetics and that other process items are not considered. The interaction of the mass transfer of oxygen with the toluene oxidation reactions has been addressed by Hoorn et al. in a recent paper (Hoorn et al., 2005). In order to develop a model suitable for combination with more detailed mass transfer phenomena the kinetic mechanism is simplified to interactions between the basic components. The simplest model possible is derived from the overall reaction stoichiometry (Figure 1).

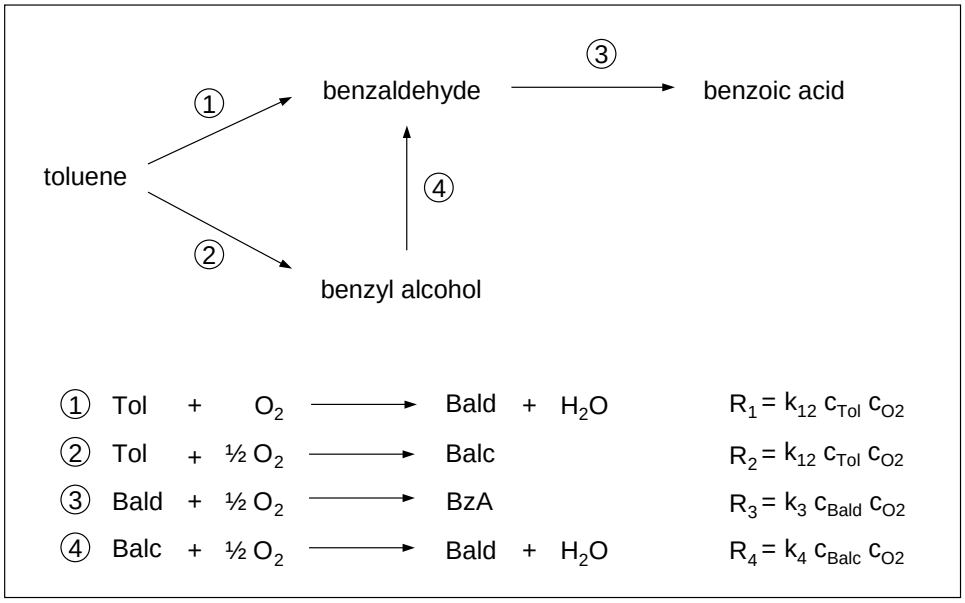

Figure 1. Basic model kinetic scheme.

It has to be noted that the expressions for the reaction rates of the above model were generated on basis of a best-fit procedure during parameter estimations. In particular the oxygen dependence in the expressions, i.e. first order is in contrast with the general view on autoxidation reaction rates: zero-th order with respect to oxygen concentration (Helferrich, 2001).

However, with the implementation of the mass transfer rate of oxygen substantially improved results were obtained when the oxygen concentration was incorporated in the equations. Other model parameters than those for the kinetic rate constants have been estimated using literature correlations. The values for the specific surface area were estimated with the correlation of Shridhar and Potter (1980), diffusion coefficients were estimated with the correlation of Wilke-Chang (1955). Mass transfer coefficients were calculated for water with the equation of van 't Riet (1979). To translate the mass transfer coefficients from water at ambient conditions to toluene at reactor conditions, it was assumed on basis of the penetration theory from Higbie (1935) that the mass transfer coefficient varies with the square root of the diffusion coefficient as shown in Eq. (1).

$$\frac{k_L(\text{toluene}, 150\ ^\circ\text{C})}{k_L(\text{water}, 25\ ^\circ\text{C})} = \sqrt{\frac{D(\text{toluene}, 150\ ^\circ\text{C})}{D(\text{water}, 25\ ^\circ\text{C})}} \tag{1}$$

The reactor models have been programmed in Aspen Custom Modeler. The equations are given in Appendix A. Within Aspen Custom Modeler a least squares method is applied to minimize the differences between experimental values and model calculations. The parameters for this basic kinetic model have been determined in an experimental set-up comprising a reactor/condenser system operated in a continuous mode (Hoorn et al., 2005). This is suitable for testing under industrial conditions, but not optimal for kinetic parameter estimations. To validate the model under different conditions a number of experiments have been performed in a semibatch laboratory autoclave. In these experiments oxygen was the only reactant that was supplied continuously.

2. Experimental

A Parr autoclave is used for toluene oxidation experiments. The reactor set-up comprises a batch liquid and a continuous gas phase. The Parr autoclave has a volume 250 ml, is equipped with a mechanical stirrer and has a sample device. The autoclave is equipped with a reflux condenser of sufficient capacity with respect to the heating power of the reactor jacket. The reflux rates are fairly high in a typical experiment. Application of a cold trap after the condenser shows that the amount of condensable components passing through the reflux condenser is very little compared to the total liquid content. A scheme is shown in Figure 2.

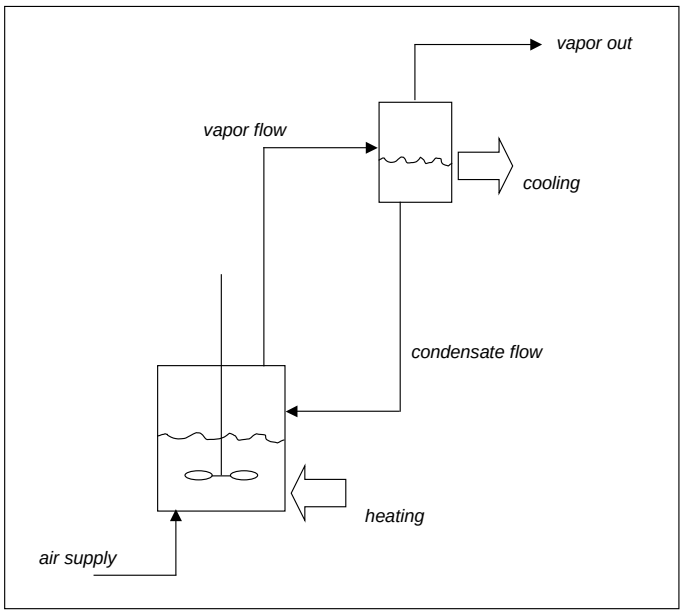

Figure 2. Principles of toluene oxidation in Parr autoclave.

The temperature for the experiments was in the range of 155 – 165 °C and the total pressure in the autoclave was kept constant at 7 bar. Air was applied as gas feed. The oxygen concentration in the off-gas flow was kept below 8 vol% for safety reasons. Five experiments were performed at a gas flow of 50 Nl/hr. Oxygen concentrations were typically in the range of 2 vol%. The differences in induction period were taken into account by taking the initial increase in temperature in the liquid as the starting time of the reaction.

The estimations of kinetic parameters were performed by a least squares minimization procedure. The objective function was the sum of the weighted differences between model and experimental observed mass fractions in the liquid for the components benzyl alcohol, benzaldehyde and benzoic acid. Toluene was not included in the objective function because the toluene concentrations were not analysed but derived from the mass balance. The weights of the experimental values for the mass fractions were determined by a combination of methods. The weight for benzyl alcohol was fixed at a value of 1, the benzaldehyde weight was adjusted to 0.8 on basis of the (average) slightly higher mass fractions. The weight for benzoic acid was determined by trial and error; the results of several estimated parameter sets with varying benzoic acid weights showed that best results were obtained with a value of 0.2.

The statistical output of the results is given as sums of the squared residuals of model prediction and experimental values (SSR). Also the sum of squared observations (SSO) are given as reference for the SSR. These definitions and as well as the standard deviation of data are given in Appendix A.

The standard deviations for parameters are the variances as calculated by the standard procedure provided by Aspen Custom modeler (covariance matrix calculation from Jacobian and Hessian matrices of the objective function and the parameters).

3. Results

The results from 5 runs with identical settings are listed in Table 1. The toluene concentration is not analysed but calculated from the balance.

Table 1. Experimental data.

Experiment#	Time (min)	BzA (wt%)	Balc (wt%)	Bald (wt%)
1	7	0.10	0.54	0.51
	15	0.91	1.41	1.28
	27	3.51	1.70	2.07
	41	7.28	1.26	2.59
	60	13.04	0.78	2.49
	79	21.36	0.78	2.20
	95	25.72	0.83	2.10
	104	27.87	0.82	2.04
2	9	0.13	0.58	0.60
	20	1.63	1.33	1.70
	34	5.08	1.04	2.41
	49	9.05	0.85	2.40
	64	13.49	0.69	2.41
	79	18.33	0.59	2.33
	98	23.51	0.57	2.17
	106	25.93	0.58	2.13
3	1.25	0.04	0.19	0.14
	6.5	0.22	0.84	0.70
	9.8	0.64	1.29	1.25
	18	2.12	1.46	1.86
	44	9.05	0.74	2.60
	60.5	14.01	0.51	2.49
	89	18.64	0.41	2.34
	119	29.77	0.34	2.03

Table 1. (continued.)

Experiment#	Time (min)	BzA (wt%)	Balc (wt%)	Bald (wt%)
4	0.5	0.00	0.02	0.03
	5.8	0.04	0.46	0.53
	10	0.33	0.96	1.07
	20	1.95	1.34	1.98
	30.25	4.43	0.98	2.48
	45	8.57	1.19	2.29
	59.8	12.09	0.61	2.46
5	6.35	0.14	0.64	0.49
	12.2	0.66	1.27	1.19
	26	3.76	1.39	2.36
	45.8	9.21	0.59	2.68
	63	14.57	0.47	2.41

With the basic model the simulation results for benzaldehyde and benzoic acid are in good agreement with experiments. The description for benzyl alcohol was not satisfying, it proved not to be possible to qualitatively describe the "camel hump" in the concentration of benzyl alcohol as is shown in Figure 3.

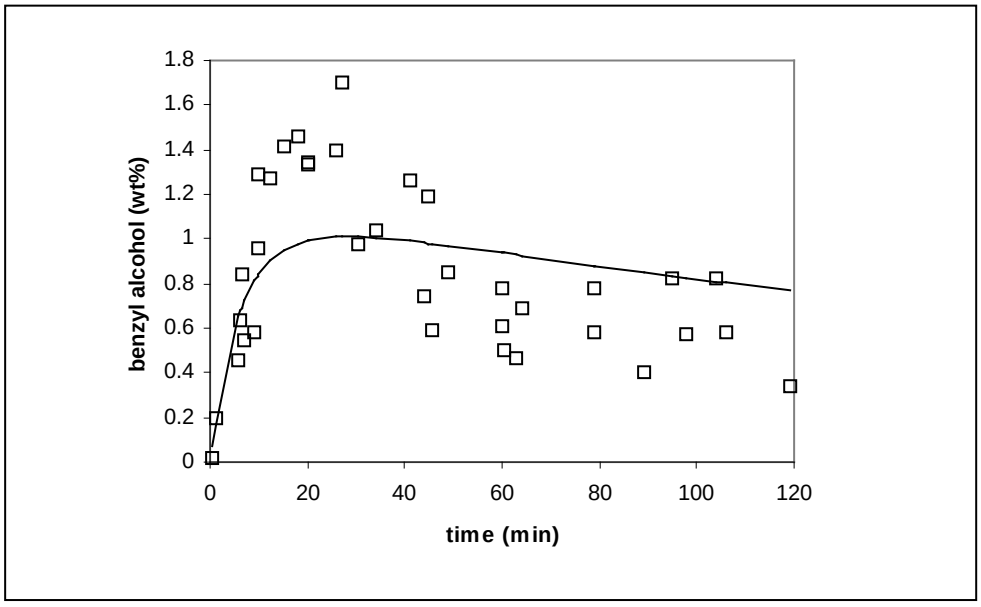

Figure 3. Model prediction versus experimental values for benzyl alcohol, basic model.

The results presented in Figure 3 clearly suggested that some adaptation on the basic model was required to improve the model prediction for benzylalcohol.

One of the possible routes was to change the reaction order coefficients and modifiy the reaction rate expressions, for example to a more flexible power law. This option was not preferred because the relation of power law expressions to chemical or mass transfer effects is difficult to make. In other words, power law models are not convenient when kinetic expressions are to be derived from chemical principles. Instead, it was preferred to extend the basic model with an effect that occurs preferentially at higher conversions. To identify possible reaction pathways where such effects can occur (part of) the toluene oxidation reaction network is explained in the next section.

4. Toluene oxidation reaction network

Bukharkina and Digurov (2004) published a comprehensive review on the field of the kinetics and chemistry on liquid-phase oxidations. This field can be subdivided into three main systems: metal catalysed oxidation in non-polar solvents, oxidation in acetic acid as solvent and oxidation in presence of bromide catalysts. Each of the reaction systems has a number of particular properties, but all systems have in common that the reactions proceed through radical intermediates. These radical reactions are part of a network comprising initiation, propagation and termination steps. In addition, non-radical reaction steps also can occur.

4.1. Initiation

Chain-initiating benzyl radicals are generated from toluene by cobalt(III) through one-electron oxidation (Morimoto and Ogata, 1967) as shown in Eq. (2).

$$PhCH_3 + Co^{3+} \longrightarrow PhCH_2\bullet + Co^{2+} + H^+ \quad (2)$$

Peroxides in general are considered as radical initiation sources. The decomposition of peroxides is catalysed by cobalt(II)/cobalt(III) in a Haber-Weiss redox cycle (Helfferich, 2001), Eq. (3) and (4).

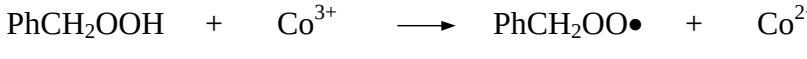

$$PhCH_2OOH + Co^{3+} \longrightarrow PhCH_2OO\bullet + Co^{2+} + H^+ \quad (3)$$

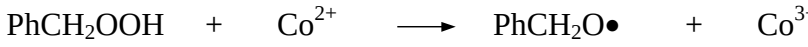

$$PhCH_2OOH + Co^{2+} \longrightarrow PhCH_2O\bullet + Co^{3+} + OH^- \quad (4)$$

The role of cobalt in the autoxidation of toluene and related components is not limited to these reactions (Scott and Chester, 1972; Kagami, 1968). More examples of cobalt interactions are given in the next paragraphs.

4.2. Propagation

Independent of the specific reaction system, all mechanisms presented in literature comprise a diffusion controlled oxygen-coupling reaction with benzyl radical to form a peroxy radical (Bhattacharya et al., 1973; Quiroga et al., 1980; Gadelle and Clément, 1968; Korthals Altes and van den Berg, 1966; Ivanov et al., 1983) as shown in Eq. (5).

$$PhCH_2\bullet + O_2 \longrightarrow PhCH_2OO\bullet \quad (5)$$

This peroxy radical can substract hydrogen from any suitable substrate but most often it will be from toluene or benzaldehyde (Eq. (6) and (7)). Similar reactions also occur with the benzoyl radical instead of the benzyl radical as shown in Eqs. (8) to (10).

$$PhCH_2OO\bullet + PhCH_3 \longrightarrow PhCH_2OOH + PhCH_2\bullet \quad (6)$$

$$PhCH_2OO\bullet + PhCH(O) \longrightarrow PhCH_2OOH + PhC\bullet(O) \quad (7)$$

$$PhC\bullet(O) + O_2 \longrightarrow PhC(O)OO\bullet \quad (8)$$

$$PhC(O)OO\bullet + PhCH_3 \longrightarrow PhC(O)OOH + PhCH_2\bullet \quad (9)$$

$$PhC(O)OO\bullet + PhCH(O) \longrightarrow PhC(O)OOH + PhC\bullet(O) \quad (10)$$

The formed perbenzoic acid takes part in the oxidation of benzaldehyde to benzoic acid (Baeyer-Villiger reaction, see next paragraph). Perbenzoic acid can also be decomposed to benzoic acid by Co(II) through an overall reaction described by Hendriks et al. (1978a), see Eq. (11).

$$PhC(O)OOH + 2\,Co^{2+} + 2\,H^{+} \longrightarrow 2\,Co^{3+} + H_2O + PhC(O)OH \quad (11)$$

Some other radicals are also involved in transfer reactions producing a stable product, for example the reaction of benzyloxy radical (formed in the initiation reactions) substracts hydrogen from toluene or benzaldehyde to form benzyl alcohol, Eq. (12) and (13).

$$PhCH_2O\bullet + PhCH_3 \longrightarrow PhCH_2OH + PhCH_2\bullet \quad (12)$$

$$PhCH_2O\bullet + PhCH(O) \longrightarrow PhCH_2OH + PhC\bullet(O) \quad (13)$$

4.3. Termination and Sequential Reactions

Experiments on toluene oxidation are mostly carried out with high oxygen concentrations in the gas phase. The reaction rate of C-centered radicals with oxygen is in general very fast. Traces of oxygen in the liquid decrease the concentration of C-centered radicals drastically. For these reasons termination products from C-centered radicals such as benzyl radicals only occur at very low oxygen pressures.

The primary termination reaction proceeds according to a Russell mechanism (1957) between two benzylperoxy radicals forming oxygen, benzyl alcohol and benzaldehyde (Eq. (14) and Figure 4).

$$2\ PhCH_2OO\bullet \longrightarrow PhCH(O) + PhCH_2OH + O_2 \qquad (14)$$

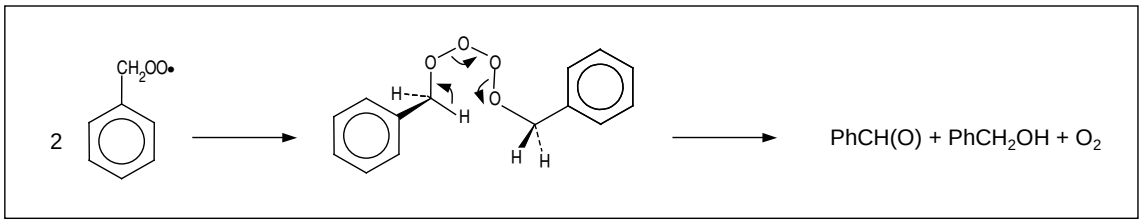

Figure 4. Russell mechanism for benzylperoxy radical termination reaction.

The oxidation of benzaldehyde to benzoic acid is a Baeyer-Villiger type reaction. In Figure 5 it is shown that perbenzoic acid oxidizes benzaldehyde forming two benzoic acid equivalents (Hendriks et al., 1978b).

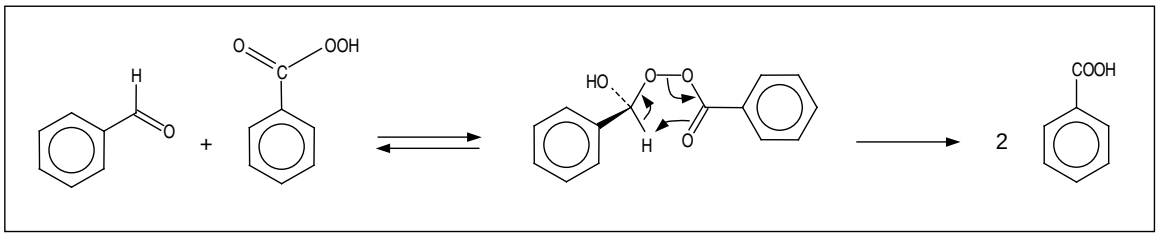

Figure 5. Baeyer-Villiger reaction.

Formation of benzaldehyde from benzylhydroperoxide proceeds through a Co(II)/Co(III) cycle as shown in Eqs. (15) and (16).

$$PhCH_2OOH + Co^{3+} \longrightarrow PhCH_2OO\bullet + Co^{2+} + H^{+} \qquad (15)$$

$$PhCH_2OO\bullet + Co^{2+} \longrightarrow PhCH(O) + Co^{3+} + OH^{-} \qquad (16)$$

A pathway involving a hydrogen abstraction from the benzylic position of benzyl alcohol under the influence of Co(III) also accounts for benzaldehyde formation. The radical intermediate ("center-OH radical") reacts with oxygen to form an peroxy hydrate which decomposes in turn to hydrogen peroxide and benzaldehyde (Figure 6).

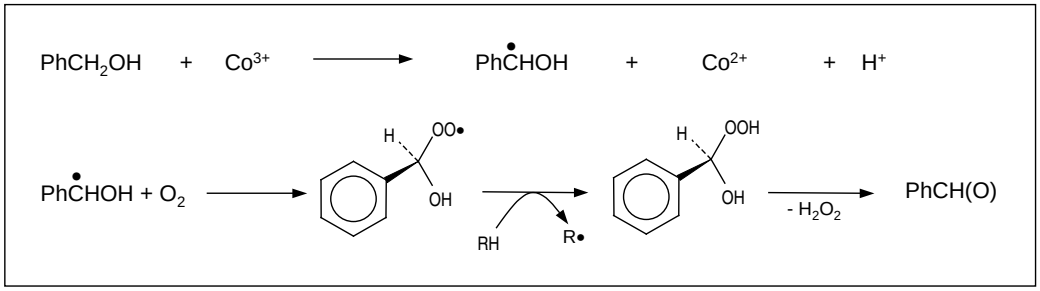

Figure 6. Oxidation of benzyl alcohol to benzaldehyde.

To summarize the (main) reactions pathways, a simplified scheme is presented in Figure 7. All secundairy transformations that occur in multiple reactions such as the cobalt oxidations or reductions and the hydrogen abstraction reactions have not been taken into account in the scheme for clarity purposes.

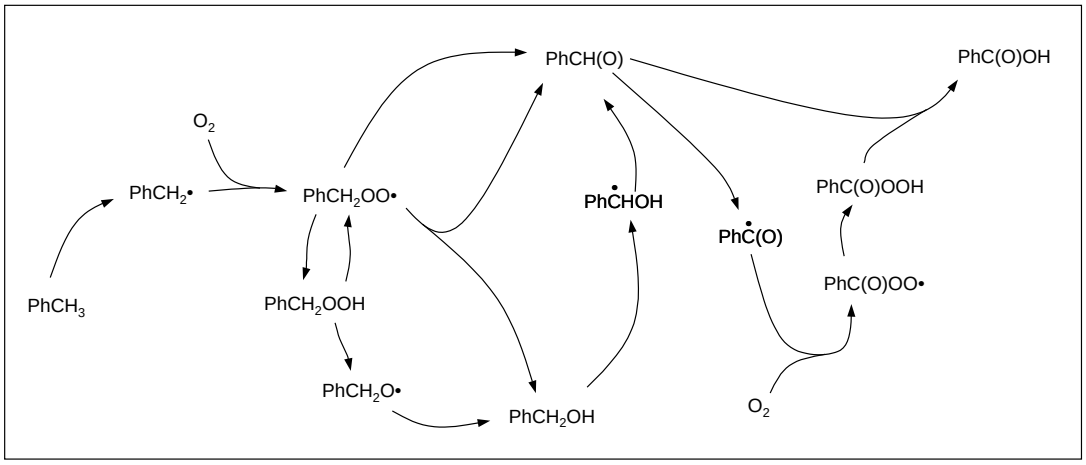

Figure 7. Reaction network for toluene oxidation showing main reactions.

Only a fraction of the reaction rates of the reactions mentioned in Figure 7 are known. In a series of papers by Howard and Ingold reaction rates for a variety of alkyl aromatic compounds have been determined (1967). The developments on the estimation of reaction rate constants through molecular modelling are very promising but still not that accurate for predicting the pre-exponential factors (van Speybroeck and Meier, 2003). The number of reactions studied in detail is also quite limited still. The reactions shown in Figure 7 have no indication for a decreased formation or increased reaction of benzyl alcohol at higher conversions. The primary component formed at high conversion is benzoic acid. It is postulated here that benzoic acid reacts with benzylhydroperoxide to form an intermediate peroxyester (Figure 8).

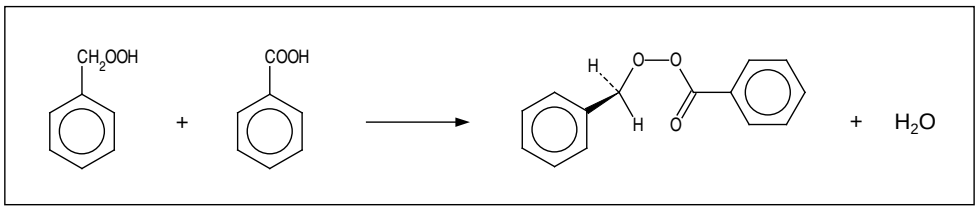

Figure 8. Formation of benzylperoxy benzoate ester.

The peresterification is followed by a decomposition to form benzaldehyde and benzoic acid. The postulated six-membered transition state of the perester decomposition strongly resembles the commonly accepted transition state for the Baeyer-Villiger type of rearrangement shown in Figure 9.

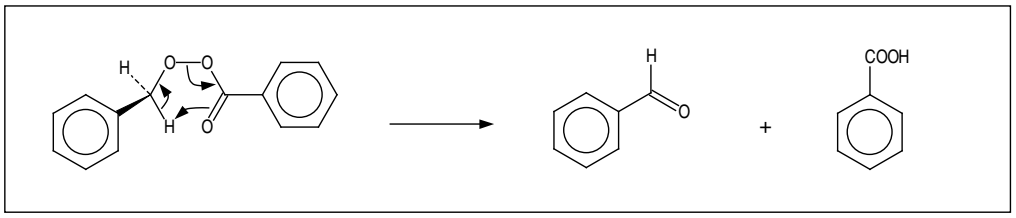

Figure 9. Formation of benzaldehyde by benzylperoxy benzoate ester decomposition.

In this way the formation of benzaldehyde will have a dependency on the benzoic acid concentration, i.e. as the reaction progresses the rate of benzaldehyde formation will be increased relative to that of benzyl alcohol. Note that benzoic acid effectively acts as a catalyst for benzylhydroperoxide dehydration to benzaldehyde, since it is regenerated in the peroxyester decomposition step.

5. Extended model

To incorporate the concept of a peroxyester intermediate benzylhydroperoxide (peroxide) and its radical equivalent are added to the basic kinetic scheme (Figure 10).

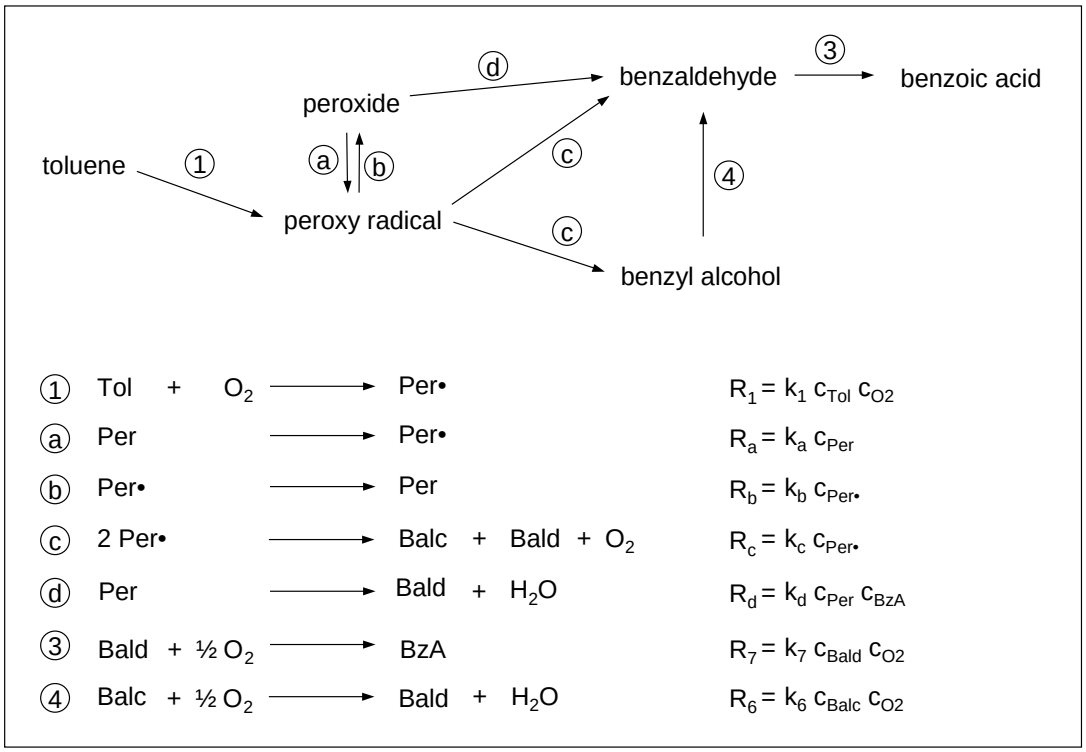

Figure 10. Extended model kinetic scheme.

The naming of the rate constants in comparison to the basic scheme in Figure 1 has been kept identical as much as possible. The rate constants that are involved in equations comprising reactive intermediates have been designated letters instead of numbers because these constants will be simplified later.

To eliminate the reactive intermediates from the rate expressions, no distinction is made between initiation and termination rates on one hand and propagation rates on the other hand (which is commonly applied in reducing radical networks (Helfferich, 2001) because several components are involved in both radical and non-radical reactions. Instead, the peroxy radical and peroxide concentrations are eliminated with an overall steady-state assumption, see Eq. (17) and (18).

peroxy radical: $$R_1 + R_a = R_b + 2 \cdot R_c \quad (17)$$

peroxide: $$R_b = R_a + R_d \quad (18)$$

In order to reduce the number of parameters, it is also assumed that the radical reactions (a) and (b) are much faster than the other reactions. The peroxy radical and the hydroperoxide maintain in equilibrium throughout the reaction progress. On basis of Eqs. (17) and (18), it is not difficult to derive equations for R_c and R_d in which the intermediates have been eliminated (see Appendix B). The explicit expressions for R_c and R_d allow all component reaction rates to be expressed as functions of observable concentrations:

$$R_c = \frac{k_1 \cdot c_{Tol} \cdot c_{O_2}}{2 + k_2 \cdot c_{BzA}} \tag{19}$$

$$R_d = \frac{k_1 \cdot k_2 \cdot c_{BzA} \cdot c_{Tol} \cdot c_{O_2}}{2 + k_2 \cdot c_{BzA}} \tag{20}$$

6. Comparison of the models

The modified reaction rate expressions after optimising the kinetic parameters improves the benzyl alcohol description indeed substantially as is shown in Figure 11 (Right side). The comparison of the results generated by the two models is shown in graphical form in Figures 11-14. The values for the kinetic parameters of the two models are given in Table 2 and 3. The interval values in Table 3 are the standard deviations. The correlation matrices show how much the parameters dependent on each other. The statistics on the data points and the goodness-of-fit are given in Table 4.

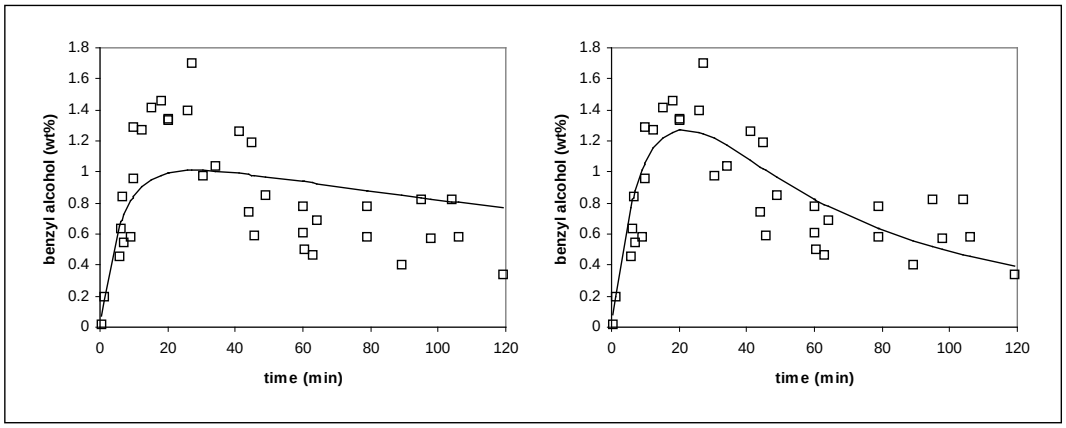

Figure 11. Model prediction (line) versus experimental values (symbol) for benzyl alcohol concentration as function of reaction time. Left: basic model. Right: extended model.

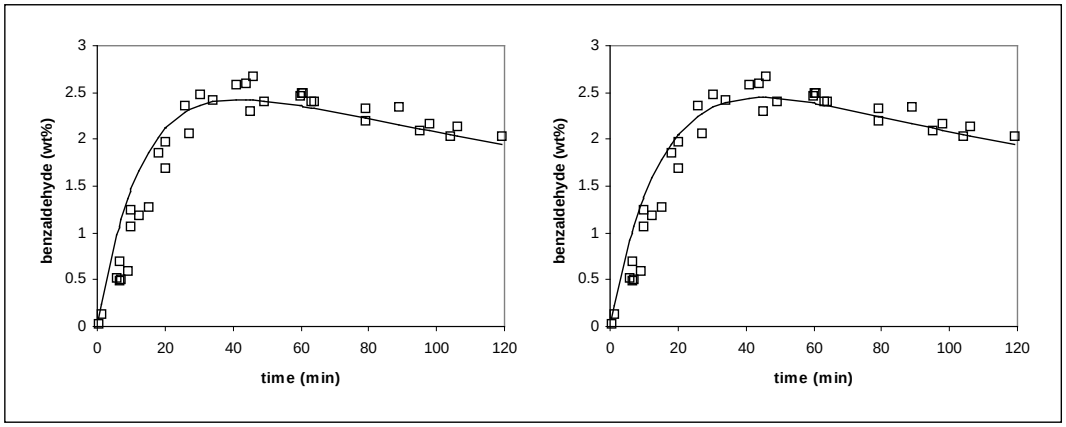

Figure 12. Model prediction (line) versus experimental values (symbol) for benzaldehyde concentration as function of reaction time. Left: basic model. Right: extended model.

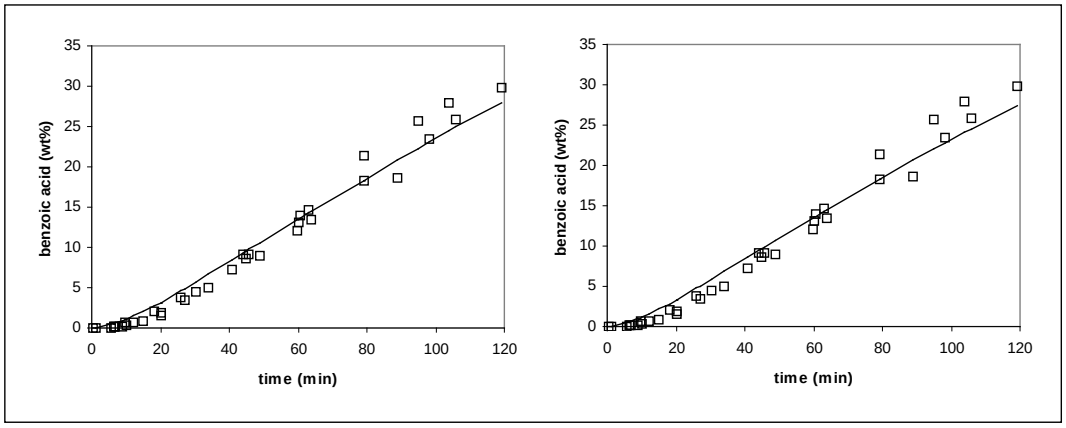

Figure 13. Model prediction (line) versus experimental values (symbol) for benzoic acid concentration as function of reaction time. Left: basic model. Right: extended model.

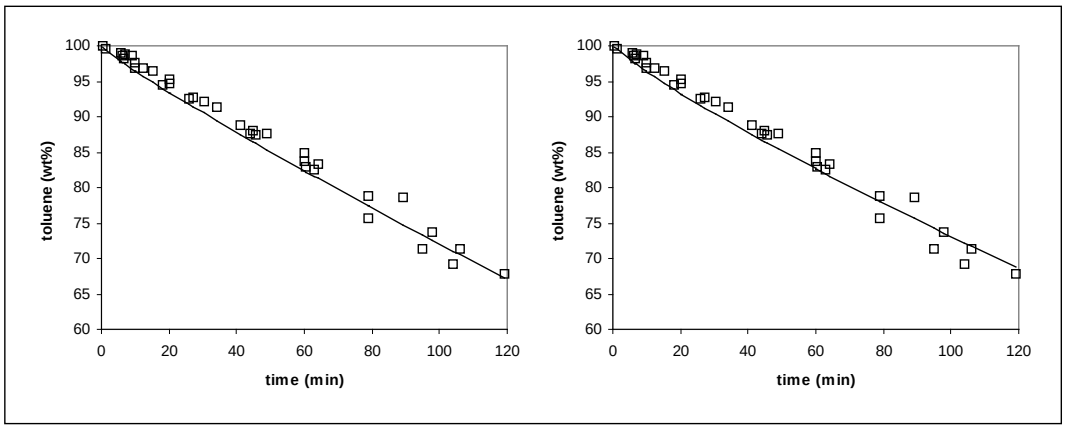

Figure 14. Model prediction (line) versus experimental values (symbol) for toluene concentration as function of reaction time. Left: basic model. Right: extended model.

Table 2. Kinetic parameters basic model.

Parameter values			Correlation matrix			
				k_{12}	k_3	k_4
k_{12}	0.018 ± 0.002	l/mol/s	k_{12}	1		
k_3	1.52 ± 0.15	l/mol/s	k_3	0.99	1	
k_4	1.93 ± 0.20	l/mol/s	k_4	0.96	0.95	1

Table 3. Kinetic parameters extended model.

Parameter values			Correlation matrix				
				k_1	k_2	k_3	k_4
k_1	0.020 ± 0.002	l/mol/s	k_1	1			
k_2	0.051 ± 0.022	l/mol	k_2	-0.12	1		
k_3	0.87 ± 0.06	l/mol/s	k_3	0.97	-0.07	1	
k_4	0.65 ± 0.08	l/mol/s	k_4	0.46	-0.92	0.40	1

Table 4. Statistical output for both models.

Component	Weight	Statistic*	Experimental data	Basic model	Extended model
Benzyl alcohol	1	SSO	30.6		
		SSR		3.33	1.79
		SDD		0.31	0.23
Benzaldehyde	0.8	SSO	139		
		SSR		3.01	2.28
		SDD		0.24	0.21
Benzoic acid	0.2	SSO	6056		
		SSR		66	79
		SDD		0.28	0.31
Toluene	0	SSO	270213		
		SSR		536	661
		SDD		-	-

* SSO = Sum of Squared Observations, SSR = Sum of Squared Residuals, SDD = Standard Deviation of Data.

7. Discussion

The estimation of kinetic parameters on the batch autoclave experiments has been successful for both model versions, but the extended model with benzoic acid concentrations in the reaction rate expressions gives a better qualitative and quantitative description of the benzyl alcohol concentrations. Also with regard to the description of benzaldehyde the extended model has a slightly better performance than the basic model as can be seen from the statistical values in Table 4.

The differences are not very substantial however; comparing the ratio of the sum of squared residuals and the sum of squared observations the improvement for benzaldehyde is a decrease from 1.3% to 0.9% in favour of the extended model. The benzoic acid concentration is better described by the basic model. The changes are not very substantial as can be verified by the visual comparison of Figure 13 and Figure 14. For both models it is observed that the concentrations for benzaldehyde appear to be somewhat lower than the experimental values. By changing the weights for the different datasets in the parameter estimation procedure it is possible to improve the description for benzaldehyde by a few percent but at the same time the good fit for benzyl alcohol is lost. Extension of the number of experiments and increasing the variation in the reaction conditions should be the strategy to improve the model in this respect.

The extended model includes a peresterification of benzylhydroperoxide and benzoic acid as an important step in order to describe the kinetic behaviour of benzyl alcohol properly. This assumption is reasonable, since peroxyesters can be prepared through condensation of a hydroperoxide with carboxylic acid (Sanchez and Meyers). Other models, such as those described by Bukharkina and Digurov (2004), appear to be able to describe the kinetics of benzyl alcohol properly. Unfortunately, the lack of details with respect to their model and experimental conditions precludes a more accurate comparison with our extended model.

Five experiments with identical conditions provide a useful estimation of the accuracy of the results. As can be seen from Figure 12 and Figure 13 the spread in the benzyl alcohol values is larger than the benzaldehyde percentages. This is caused by a combination of factors. The concentrations for benzyl alcohol are a factor 2 lower than benzaldehyde after the initial reaction period. Benzyl alcohol is also more difficult to analyse accurately than benzaldehyde. A third reason is the involvement of benzyl alcohol in side reactions such as esterfication with benzoic acid to benzyl benzoate.

Although the limited number of and variation in experiments make it impossible to estimate a larger number of kinetic parameters, it is questionable whether all kinetic parameters of a reaction network presented in Figure 7 can be determined on the basis of experiments alone. The most promising route to manipulate complex reaction networks appears to be a synthesis of experiments and molecular modelling. One of the major challenges is to maintain the balance between the number of parameters and the predictive quality of the model. At the same time it is very much desired to increase the number of significantly determined parameters at the lowest experimental effort.

On the basis of the theoretical correlations it was found that the high rotational speed of the autoclave stirrer and the small liquid volume gave high values for the mass transfer coefficient, making the exact value for mass transfer coefficient not very critical.

In a previous investigation (Hoorn et al., 2005) it was found that the oxidation of toluene is a slow reaction with respect to mass transfer. In combination with a sufficiently high oxygen concentration in the gas phase it can therefore be concluded that the mass transfer for oxygen is not important in these experimental settings. However, the models are set-up in such a way that also non-ideal conditions can be described.

8. Conclusions

In a batch operated autoclave the benzyl alcohol concentrations are initially increasing equally fast as benzaldehyde. As the oxidation of toluene progresses, the benzyl alcohol concentration diminishes faster in comparison with benzaldehyde, but the benzyl alcohol concentration approaches zero only very slowly at longer reaction times. In order to describe this behaviour by means of a model a dependency on the benzoic acid concentration is suggested. Through the hypothesis that the decomposition of benzylhydroperoxide to benzaldehyde is catalysed by benzoic acid the formation rate of benzaldehyde is increased relative to benzyl alcohol at higher benzoic acid concentrations. Through estimation of the kinetic parameters the modifications in the model indeed improve the description of the benzyl alcohol concentration profiles observed during the oxidation of toluene.

Nomenclature

Notation

c	concentration in liquid phase	kmol/m^3
F	flow	kmol/s
k	kinetic rate constant	s^{-1} or m^3/kmol/s
k^P_{flow}	constant for controlling flows	kmol/bar/s
k^V_{flow}	constant for controlling flows	kmol/m^3/s
k_La	volumetric liquid side mass transfer coefficient	s^{-1}
m	mass in liquid phase	kg
M_r	molar mass	kg/kmol
n	number of moles	kmol

n_{obs}	number of observations	-
n_{par}	number of parameters	-
P	pressure	bar
R	reaction rate	kmol/m^3/s
V	volume	m^3
w	weight factor for estimation	-
x	mole fraction in liquid phase	kmol/kmol
y	mole fraction in gas phase	kmol/kmol
Y_{calc}	calcultated variable	-
Y_{exp}	observed variable	-

Greek

ρ	molar density	kmol/m^3
ϕ	fugacity coefficient	-

Sub- and superscripts

i	component
gas	vapor phase
vap	vapor phase
liq	liquid phase
tot	total
nv	non-volatiles
set	set point
in	feed stream
out	exit stream
sat	saturated

Abbreviations

Balc	benzyl alcohol
Bald	benzaldehyde
BzA	benzoic acid
Per	benzylhydroperoxide
Per•	benzylperoxy radical
Tol	toluene

References

Bhattacharya, D., Guha, D.K., Roy, A.N., (1973), Liquid phase air oxidation of toluene to benzoic acid. II. Kinetics and mechanism, *Chem. Age India* **24**, 87-90.

Bukharkina, T.V., Digurov, N.G., (2004), Kinetics of aerobic liquid-phase oxidation of organic compounds, *Org. Proc. Res. Dev.* **8**, 320-329.

Gadelle, C., Clément, G., (1968), Étude cinétique de l'oxydation radicalaire par l'oxygène des alcoylaromatiques en phase liquide, *Bull. Soc. Chim. De France* **1**, 44-54.

Hearne, G.W., Evans, T.W., Buls, V.W., (1951), U.S. Patent 2,578,654 (Dec. 18).

Helfferich, F.G., (2001), Kinetics of homogeneous multistep reactions, in: Compton, R.G., Hancock, G., (Eds.), *Comprehensive Chemical Kinetics, vol. 38*, Elsevier, Amsterdam, pp. 283-286.

Hendriks, C.F., van Beek, H.C.A., Heertjes, P.M., (1978a), The oxidation of substituted toluenes by cobalt(III) acetate in acetic acid solution, *Ind. Chem. Prod. Res. Dev.* **17**, 256-260.

Hendriks, C.F., van Beek, H.C.A., Heertjes, P.M., (1978b), The kinetics of the autoxidation of aldehydes in the presence of cobalt(II) and cobalt(III) acetate in acetic acid solution, *Ind. Chem. Prod. Res. Dev.* **17**, 260-264.

Higbie, R., (1935), The rate of absorption of a pure gas into a still liquid during short periods of exposure, *Trans. Am. Inst. Chem. Eng.* **35**, 36-60.

Hoorn, J.A.A., van Soolingen, J., Versteeg, G.F., (2005), Modelling toluene oxidation, incorporation of mass transfer phenomena, *Chem. Eng. Res. Des.* **83**, 187-195.

Howard, J.A., Ingold, K.U., (1967), Absolute rate constants for hydrocarbon autoxidation, *Can. J. Chem.* **45**, 793-802.

Ivanov, S.K., Kalitchin, Z.H.D., Hinkova, M.K., (1983), Direct oxidation of toluene to benzaldehyde in the presence of N-bromosuccinimide, *Oxidation Communications* **3**, 89-102.

Kagami, K., (1968), Anomalous effect of the concentration of metal-salt catalysts in the liquid-phase oxdation of p-xylene and toluene, *Bull. Chem. Soc. Jap.* **41**, 1552-1557.

Keading, W.W., Lindblom, R.O., Temple, R.G., Mahon, H.I., (1965), Oxidation of toluene and other alkylated aromatic hydrocarbons to benzoic acids and phenols, *Ind. Eng. Chem. Process Des. Dev.* **4**, 97-101.

Korthals Altes, F.W., van den Berg, P.J., (1966), Kinetics of the autoxidation of ethylbenzene, *Receuil* **85**, 538-544.

Morimoto, T., Ogata, Y., (1967), Kinetics of the autoxidation of toluene catalyzed by cobaltic acetate, *J. Chem. Soc. (B)*, 62-66.

Mulkay, P., Rouchaud, J., (1967), Solvatation des catalyseurs d'oxydation en phase liquide homogène, *Bull. Soc. Chim. Fr.* **12**, 4653-4657.

Palmer, R.C., Bibb, C.H., (1942), U.S. Patent 2,302,462 (Nov. 17).

Quiroga, O.D., Gottifredi, J.C., Capretto de Castillo, M.E., (1980), Liquid phase catalytic toluene oxidation, formulation of a kinetic model, *Rev. Latinoam. Ing. Quim. Quim. Apl.* **10**, 77-88.

Russell, G.A., (1957), Deuterium-isotope effects in the autoxidation of aralkyl hydrocarbons. Mechanism of the interaction of peroxy radicals, *J. Am. Chem. Soc.* **79**, 3871-3877.

Sanchez, J., Meyers, T.N., (2004), Peroxides and peroxide compounds, organic peroxides in: Kirk-Othmer, Encyclopedia of chemical technology, John Wiley & Sons, online edition.

Scott, E.J.Y., Chester, A.W., (1972), Kinetics of the cobalt-catalyzed autoxidation of toluene in acetic acid, *J. Phys. Chem.* **76**, 1520-1524.

Shridhar, T., Potter, O.E., (1980), Interfacial areas in gas-liquid stirred vessels, *Chem. Eng. Sci.* **35**, 683-695.

van Goolen, J.T.J., van den Berg, P.J., (1967), The catalytic oxidation of toluene in the liquid phase, *Industrie Chimique Belge* **32**, 658-661.

van Speybroeck, V., Meier, R.J., (2003), A recent development in computational chemistry: chemical reactions from first principles molecular dynamics simulations, *Chem. Soc. Rev.* **32**, 151-157.

van 't Riet, K., (1979), Review of measuring methods and results in nonviscous gas-liquid mass transfer in stirred vessels, *Ind. Eng. Chem. Process Des. Dev.* **18**, 357-364.

Wilke, C.R., Chang, P., (1955), Correlation of diffusion coefficients in dilute solutions, *AIChE J.* **1**, 264-270.

Appendix A. Model equations and statistical definitions

Kinetics – basic

$$R_1 = k_{12} \cdot c_{TOL} \cdot c_{O2}$$

$$R_2 = k_{12} \cdot c_{TOL} \cdot c_{O2}$$

$$R_3 = k_3 \cdot c_{BALD} \cdot c_{O2}$$

$$R_4 = k_4 \cdot c_{BALC} \cdot c_{O2}$$

$$R_{BALC} = R_2 - R_4$$

$$R_{BALD} = R_1 - R_3 + R_4$$

$$R_{BzA} = R_3$$

$$R_{H2O} = R_1 + R_4$$

$$R_{O2} = -R_1 - \frac{1}{2} \cdot (R_2 + R_3 + R_4)$$

$$R_{TOL} = -R_1 - R_2$$

Kinetics – extended

$$R_1 = k_1 \cdot c_{Tol} \cdot c_{O2}$$

$$R_c = \frac{k_1 \cdot c_{Tol} \cdot c_{O2}}{2 + k_2 \cdot c_{BzA}}$$

$$R_d = \frac{k_1 \cdot k_2 \cdot c_{BzA} \cdot c_{Tol} \cdot c_{O2}}{2 + k_2 \cdot c_{BzA}}$$

$$R_3 = k_3 \cdot c_{BALD} \cdot c_{O2}$$

$$R_4 = k_4 \cdot c_{Balc} \cdot c_{O2}$$

$$R_{Balc} = R_c - R_4$$

$$R_{Bald} = R_c + R_d + R_4 - R_3$$

$$R_{BzA} = R_3$$

$$R_{H2O} = R_d + R_4$$

$$R_{O2} = -R_1 + R_c - \frac{1}{2}(R_3 + R_4)$$

$$R_{Tol} = -R_1$$

Definitions

$$m_i = n_{liq,i} \cdot M_{r,i}$$

$$(wt\%)_i = 100 \cdot \frac{m_i}{m_{nv}}$$

$$m_{nv} = \sum_i m_i - m_{O2} - m_{N2}$$

Reactor

For all components i :

$$\phi_{gas,i} \cdot y_i = \phi_{liq,i} \cdot x_i^{sat}$$

$$n_{gas,tot} \cdot y_i = n_{gas,i}$$

$$n_{liq,tot} \cdot x_i = n_{liq,i}$$

$$c_i = \rho_{liq} \cdot x_i$$

$$c_i^{sat} = \rho_i^{sat} \cdot x_i^{sat}$$

$$F_{gas,i}^{out} = y_i \cdot F_{gas,tot}^{out}$$

$$\frac{dn_{liq,i}}{dt} = F_{liq,i}^{in} + k_L a \cdot V_{tot} \cdot \left(c_i^{sat} - c_i\right) + V_{liq} \cdot R_i$$

$$\frac{dn_{gas,i}}{dt} = F_{gas,i}^{in} - F_{gas,i}^{out} - k_L a \cdot V_{tot} \cdot \left(c_i^{sat} - c_i\right)$$

Other equations :

$$F_{gas,tot}^{out} = \sum_i F_{gas,i}^{in} + k_{flow} \cdot \left(P_{tot} - P_{set}\right) \text{ if } P_{tot} \geq P_{set} \quad \text{else} \quad F_{gas,tot}^{out} = 0$$

$$V_{gas} \cdot \rho_{gas} = n_{gas,tot}$$

$$V_{liq} \cdot \rho_{liq} = n_{liq,tot}$$

$$V_{liq} + V_{gas} = V_{tot}$$

$$n_{gas,tot} = \sum_i n_{gas,i}$$

$$n_{liq,tot} = \sum_i n_{liq,i}$$

Cooler

For all components i :

$$\phi_{gas,i} \cdot y_i = \phi_{liq,i} \cdot x_i^{sat}$$

$$n_{gas,tot} \cdot y_i = n_{gas,i}$$

$$n_{liq,tot} \cdot x_i = n_{liq,i}$$

$$c_i = \rho_{liq} \cdot x_i$$

$$c_i^{sat} = \rho_i^{sat} \cdot x_i^{sat}$$

$$F_{gas,i}^{out} = y_i \cdot F_{gas,tot}^{out}$$

$$F_{liq,i}^{out} = x_i \cdot F_{liq,tot}^{out}$$

$$\frac{dn_{liq,i}}{dt} = k_L a \cdot V_{tot} \cdot \left(c_i^{sat} - c_i\right) + V_{liq} \cdot R_i - F_{liq,i}^{out}$$

$$\frac{dn_{gas,i}}{dt} = F_{gas,i}^{in} - F_{gas,i}^{out} - k_L a \cdot V_{tot} \cdot \left(c_i^{sat} - c_i\right)$$

Other equations :

$$F_{gas,tot}^{out} = k_{flow}^{P} \cdot \left(P_{tot} - P_{set}\right) \text{ if } P_{tot} \geq P_{set} \quad \text{else} \quad F_{gas,tot}^{out} = 0$$

$$F_{liq,tot}^{out} = k_{flow}^{V} \cdot \left(V_{liq} - V_{set}\right) \text{ if } V_{liq} \geq V_{set} \quad \text{else} \quad F_{liq,tot}^{out} = 0$$

$$V_{gas} \cdot \rho_{gas} = n_{gas,tot}$$

$$V_{liq} \cdot \rho_{liq} = n_{liq,tot}$$

$$V_{liq} + V_{gas} = V_{tot}$$

$$n_{gas,tot} = \sum_{i} n_{gas,i}$$

$$n_{liq,tot} = \sum_{i} n_{liq,i}$$

Statistical definitions:

Sum of Squared Observations, $$SSO = \sum_{i=1}^{n_{obs}} Y_{exp,i}^{\ 2}$$

Sum of Squared Residuals, $$SSR = \sum_{i=1}^{n_{obs}} \left(Y_{exp,i} - Y_{calc,i} \right)^2$$

Standard Deviation of Data, $$SDD = \sqrt{\frac{\sum_{i=1}^{n_{obs}} \left(w_i \cdot \left(Y_{exp,i} - Y_{calc,i} \right) \right)^2}{n_{obs} - n_{par}}}$$

Appendix B. Simplification of reaction network

Reaction rate equations:

$$R_1 = k_1 \cdot c_{Tol} \cdot c_{O_2}$$

$$R_a = k_a \cdot c_{Per}$$

$$R_b = k_b \cdot c_{Per\bullet}$$

$$R_c = k_c \cdot c_{Per\bullet}$$

$$R_d = k_d \cdot c_{Per} \cdot c_{BzA}$$

Steady state assumption on peroxy radical and peroxide:

$$R_1 + R_a = R_b + 2 \cdot R_c \qquad \text{and} \qquad R_b = R_a + R_d$$

Substitution of the expressions for the reaction rates and some rearrangements gives:

$$c_{Per\bullet} = \frac{k_1 \cdot (k_a + k_d \cdot c_{BzA}) \cdot c_{Tol} \cdot c_{O_2}}{2 \cdot k_a \cdot k_c + (k_b + 2 \cdot k_c) \cdot k_d \cdot c_{BzA}}$$

$$c_{Per} = \frac{k_1 \cdot k_b \cdot c_{Tol} \cdot c_{O_2}}{2 \cdot k_a \cdot k_c + (k_b + 2 \cdot k_c) \cdot k_d \cdot c_{BzA}}$$

These expressions are substituted in the reaction rates R_c and R_d:

$$R_c = \frac{k_1 \cdot k_c \cdot (k_a + k_d \cdot c_{BzA}) \cdot c_{Tol} \cdot c_{O_2}}{2 \cdot k_a \cdot k_c + (k_b + 2 \cdot k_c) \cdot k_d \cdot c_{BzA}}$$

$$R_d = \frac{k_1 \cdot k_b \cdot k_d \cdot c_{BzA} \cdot c_{Tol} \cdot c_{O_2}}{2 \cdot k_a \cdot k_c + (k_b + 2 \cdot k_c) \cdot k_d \cdot c_{BzA}}$$

When k_a and k_b are much larger than the other constants the equations for R_c and R_d become:

$$R_c = \frac{k_1 \cdot c_{Tol} \cdot c_{O_2}}{2 + \frac{k_b \cdot k_d}{k_a \cdot k_c} \cdot c_{BzA}} \qquad \text{and} \qquad R_d = \frac{k_1 \cdot \frac{k_b \cdot k_d}{k_a \cdot k_c} \cdot c_{BzA} \cdot c_{Tol} \cdot c_{O_2}}{2 + \frac{k_b \cdot k_d}{k_a \cdot k_c} \cdot c_{BzA}}$$

The parameters k_a through k_d in these two expressions can be replaced by one independent constant (k_2 for naming convenience) giving the following final expressions for the rate equations:

$$R_c = \frac{k_1 \cdot c_{Tol} \cdot c_{O_2}}{2 + k_2 \cdot c_{BzA}} \qquad \text{and} \qquad R_d = \frac{k_1 \cdot k_2 \cdot c_{BzA} \cdot c_{Tol} \cdot c_{O_2}}{2 + k_2 \cdot c_{BzA}}$$

4

Modelling of mass transfer in combination with radical reactions

Abstract

The diffusion-reaction equations for different model versions have been solved using a finite-differencing technique. In all models a reactant A is transferred from the gas to the liquid phase and reacts in the liquid with B to form P. The calculations comprised a simple stoichiometric model, a system with radical intermediates involved in the propagation steps and a version where also the termination reactions were included. The results show that the diffusion coefficients of radical intermediates can have significant influence on the profiles of concentrations and reaction rates near the G/L interface. Furthermore, it is shown that for very fast reactions differences in diffusion coefficients of the intermediates influence the by-product formation. For systems of two radical intermediates, the so-called mixed termination product is only formed in low quantities whereas the other two termination products dominate. The calculation of enhancement factors required in the design of a G/L reaction system can be performed with simplified models where the reactive intermediates do not occur in the expressions for the reaction rates. The optimum model for a specific design purpose can be found by tuning the functions that correlate the parameters of the complex model to the parameters of the simplified model. In principle it is possible to very easily evaluate a large number of alternatives.

1. Introduction

The calculation of the rate of mass transfer in the absorption of gases followed by complex chemical reaction is a challenging task. The textbook example of a single first-order irreversible reaction is often a drastic simplification of real reaction systems. However, the concepts of Hatta number and enhancement factor are simple and well established. A great number of researchers have investigated a wide variety of chemical reaction systems in which one ore more reactants or product species absorbs or desorbs. The spectrum of reactive systems includes single and multiple reactions (parallel and in-series), irreversible as well as reversible reactions and auto catalytic reactions. A comprehensive overview on the literature on mass transfer accompanied by complex chemical reactions can be found in Van Swaaij and Versteeg (1992). In industry, reactions involving radical intermediates are frequently encountered. Examples are oxidation and chlorination reactions. In the fine chemicals industry, gas/liquid processes such as bromination or ozonolysis proceed through radical intermediates. Already the simplest reaction mechanisms involving radical intermediates comprises multiple reaction schemes. Only in the case of a specific definition, a single irreversible reaction, analytic solutions to the diffusion-reaction equations can be found. One example of such a special case is given by Sim and Mann (1975). They studied the autocatalytic reaction:

$$A + R\bullet \longrightarrow R\bullet + R\bullet \qquad (1)$$

The authors applied the film theory to calculate the rate of absorption and the enhancement factors. The equations were solved through a numerical procedures involving integration of a system of first order differential equations by a modified Rung-Kutta method (Juvekar (1976) suggested an improved solution technique). In addition, Flores-Fernandez and Mann (1978) published a paper with a comparison between film and penetration models for the aforementioned reaction. Another example, not directly in the field of chemical reactors, was presented by Burns et al. (1970). The radiolysis of cyclohexane was described with the following set of reactions:

$$\begin{aligned} C_6H_{12} &\longrightarrow C_6H_{12}^{**} \longrightarrow H_2 + C_6H_{10} \\ C_6H_{12} &\longrightarrow C_6H_{12}^{*} \longrightarrow H\bullet + C_6H_{11}\bullet \end{aligned} \qquad (2)$$

A point source of radicals was created by the radiation energy in the liquid. In the models the point sources were approximated by Gaussian spherical or cylindrical distributions. Burns et al. (1970) included a number of propagation and termination reactions in their models.

Reactions involving radical intermediates are in general fast to very fast reactions. For radicals, the reaction rate constants are typically in the range of 10^5 to 10^9 m^3/kmol/s for second order reactions (Carey and Sundberg, 1990; Sitarski, 1981). For very fast or instantaneous reactions the equations of Higbie's penetration theory can be solved analytically.

For a single irreversible instantaneous reaction of the type A + B $\rightarrow$ P the enhancement factor and the location of the reaction plane can be found from an implicit equation that has to be solved for a parameter β (definitions according to Froment and Bischof, 1990):

$$\exp\left(\frac{\beta^2}{D_B}\right)\cdot \mathrm{erfc}\left(\frac{\beta}{\sqrt{D_B}}\right)=\frac{a}{b}\cdot\frac{c_{B,0}}{c_{A,i}}\cdot\sqrt{\frac{D_B}{D_A}}\cdot\exp\left(\frac{\beta^2}{D_A}\right)\cdot\mathrm{erf}\left(\frac{\beta}{\sqrt{D_A}}\right) \tag{3}$$

The constants a and b are the stoichiometric coefficients for the reactants A and B respectively. For any time t the position of the reaction front (δ_r) is given by:

$$\delta_r = 2\cdot\beta\cdot\sqrt{t} \tag{4}$$

The enhancement factor is given by:

$$E_{A,\infty} = \frac{1}{\mathrm{erf}\left(\frac{\beta}{\sqrt{D_A}}\right)} \tag{5}$$

2. Model systems studied

Three model systems have been considered, all concerned with A as a gaseous component from the gas phase transferring to the liquid and reacting with B to form product P. The reaction pathways make the difference. The models have been given short names to reflect their essential feature.

2.1. Model ABP

This is the model for the stoichiometric reaction:

$$A + B \longrightarrow P \tag{6}$$

2.2. Model 3T

This model is based on a small network of reactions involving radical intermediates. The system comprises six reactions as shown in Figure 1.

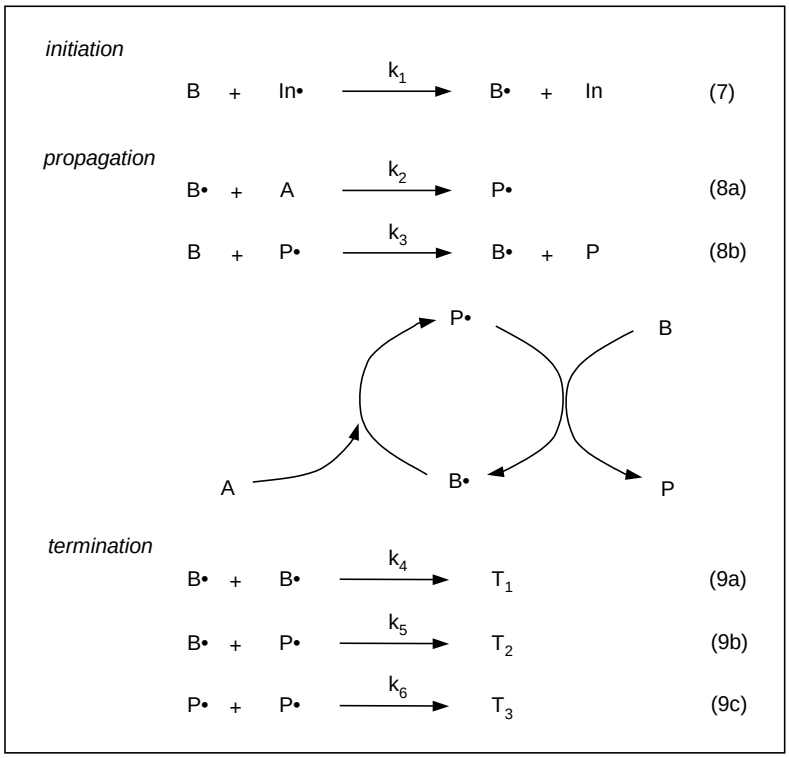

Figure 1. Components and reactions in the model 3T.

The source of radicals originates from a suitable initiator (In•) that reacts with B to generate the radical equivalent of B. The propagation steps are formed by two reactions: B• reacts with A to form P•, reaction of this radical with B gives P and B•. Three by-products from termination reactions can be formed. The number of parameters in model 3T is already quite large. Besides reaction rate constants also diffusion coefficients, volatility for each component and mass transfer parameters can be varied.

2.3. Model BPdot

This third model is a simplified version of model 3T comprising only the two propagation reactions, Eqs. (8a) and (8b) respectively. The initiation reaction, Eq. (7), has been left out because it is assumed that the reaction is so fast that all radicals are in the form of B• at the start. Model BPdot has been incorporated in the analysis because part of the effects can be studied more effectively in a system with fewer parameters.

2.4. Absorption model

For all model systems assumptions have been made:

- diffusion is described by Fick's laws; there are no convective contributions in the liquid phase to mass transport,
- the solvent is inert,
- the temperature is constant, heat effects of reactions and absorption are not included,
- the density of the liquid is constant,
- mass transfer resistance in the gas phase is negligible.

For the description of mass transfer the penetration theory according to Higbie has been applied. The disadvantage of more complicated numerical calculations in the penetration theory in comparison to the film theory is compensated by more physically realistic descriptions (Versteeg et al., 1987). In the penetration theory the equation for a single diffusing and reacting component (i) is given by:

$$\frac{\partial C_i}{\partial t} = D_i \cdot \frac{\partial^2 C_i}{\partial x^2} + R_i \tag{10}$$

Initial condition: $t = 0$ and $x \geq 0$ $\quad C_i = C_{i,bulk}$ (11)

Boundary conditions: $t > 0$ and $x = \infty$ $\quad C_i = C_{i,bulk}$ (12)

$t > 0$ and $x = 0$ $\quad J_{i,gas} = J_{i,liquid}$ (13)

In the application of the first boundary condition, Eq. (12), the bulk concentration of the absorbing species A is set to zero. This is allowed in the present study because only irreversible reactions are considered. The second boundary condition states that the flux of component i in the gas phase is equal to the flux in the liquid phase. The expressions for the reaction rates differ for each model but all reaction rates are derived from the stoichiometry of the molecular reactions. For the BPdot- and 3T- model the rates for the reactions are defined by Eq. (14). The overall component reaction rate expressions are given in Table 1.

$$R_1 = k_1 \cdot c_{In\bullet} \cdot c_B$$

$$R_2 = k_2 \cdot c_A \cdot c_{B\bullet}$$

$$R_3 = k_3 \cdot c_B \cdot c_{P\bullet}$$

$$R_4 = k_4 \cdot c_{B\bullet}^2$$

$$R_5 = k_5 \cdot c_{B\bullet} \cdot c_{P\bullet}$$

$$R_6 = k_6 \cdot c_{P\bullet}^2 \tag{14}$$

Table 1. Component reaction rates.

Component	Model ABP	Model BPdot	Model 3T
A	$R_A = -k_1 \cdot c_A \cdot c_B$	$R_A = -R_2$	$R_A = -R_2$
B	$R_B = -k_1 \cdot c_A \cdot c_B$	$R_B = -R_3$	$R_B = -R_1 - R_3$
P	$R_P = k_1 \cdot c_A \cdot c_B$	$R_P = R_3$	$R_P = R_3$
In•	-	-	$R_{In\bullet} = -R_1$
In	-	-	$R_{In} = R_1$
T_1	-	-	$R_{T1} = R_4$
T_2	-	-	$R_{T2} = R_5$
T_3	-	-	$R_{T3} = R_6$
B•	-	$R_{B\bullet} = -R_2 + R_3$	$R_{B\bullet} = R_1 - R_2 + R_3 - 2 \cdot R_4 - R_5$
P•	-	$R_{P\bullet} = R_2 - R_3$	$R_{P\bullet} = R_2 - R_3 - R_5 - 2 \cdot R_6$

The concentration profiles and derived properties are evaluated at the end of the contact time, τ_p. The contact time for absorption according to the penetration model is directly related to the liquid mass transfer coefficient and the diffusion coefficient of component A by means of:

$$\tau_p = 4 \cdot \frac{D_A}{\pi \cdot k_L^2} \tag{15}$$

To display the concentration profiles in a more convenient way a scaling factor is derived from the solution of the penetration model for a non-reacting diffusion system (Westerterp et al., 1990):

$$c_A(x,t) = c_{A,i} \cdot \left[1 - \mathrm{erf}\left(\frac{x}{2\sqrt{D_A \cdot t}} \right) \right] \tag{16}$$

At any time t, the value of x for which the error function is close enough to unity to reduce the concentration of A to zero is not precisely determined. The error function of the square root of π is close to 0.99 and this value is combined with τ_p to define the penetration depth, δ_p:

$$\frac{\delta_p}{2\sqrt{D_A \cdot \tau_p}} = \sqrt{\pi} \tag{17}$$

Substitution of Eq. (15) for τ_p gives:

$$\delta_p = 4 \cdot \frac{D_A}{k_L} \tag{18}$$

The choice for the square root of π is arbitrary, but as any other value for x would be equally disputable the esthetical result of Eq. (18) is preferred.

3. Numerical treatment

The system of coupled non-linear parabolic partial differential equations has been solved by application of a method presented by Cornelisse et al. (1980). This approach is based on a three-point backward scheme for finite differencing by Baker and Oliphant (1960). For an efficient use of grid point allocation, transformation of both the time and spatial variables has been applied (Versteeg et al., 1989). The transformation of the time variable is given by:

$$t = \tau_p \cdot s^4 \tag{19}$$

Where τ_p is the specific contact time defined by Eq. (8). The spatial grid is allocated through a transform function comprising a parameter p (varied between 0 and 1) through which the curvature can be controlled.

$$x = p \cdot z + (1-p) \cdot z^4 \tag{20}$$

For small values of p the number of grid points per distance increases in the direction of the gas/liquid interface. The method for finite differencing requires all equations to be linear in the domain of interest. Besides the differential terms the reaction rates are non-linear and therefore need to be transformed. The linearization of the reaction rate terms is performed through a first-order Taylor expansion around the reference component concentrations that have been calculated in the previous time step. The reaction rate equation can be written in general terms as:

$$R_j = k_j \cdot \prod_{p=1}^{comp} C_p^{\beta_{p,j}} \tag{21}$$

The exponent $\beta_{p,j}$ is the reaction order of component p in the j^{th} reaction. The component rate equation is:

$$R_i = \sum_{j=1}^{reac} \nu_{i,j} \cdot R_j \tag{22}$$

The stoichiometric coefficient $\nu_{i,j}$ indicates the coefficient of component i in reaction j. The combination of Eq. (21) and (22) in the linearization based on a Taylor expansion around C_i° gives:

$$R_i = \sum_{j=1}^{reac} \nu_{i,j} \cdot k_j \cdot \left[1 - \sum_{p=1}^{comp} \beta_{p,j} \right] \cdot \prod_{p=1}^{comp} \left(C_p^\circ \right)^{\beta_{p,j}} + \sum_{p=1}^{comp} \left\{ \sum_{j=1}^{reac} \nu_{i,j} \cdot k_j \cdot \frac{\beta_{p,j}}{C_p^\circ} \cdot \prod_{q=1}^{comp} \left(C_q^\circ \right)^{\beta_{q,j}} \cdot C_p \right\} \tag{23}$$

Details of this derivation are given in Appendix A. The discretizations of the differentials are identical to the schemes applied by Cornelisse et al. (1980). Leaving the subscripts i out of the following equations, the differentials in Eq. (10) are transformed to:

$$\frac{\partial C}{\partial t} \rightarrow \frac{1}{f'(s)} \cdot \frac{3 \cdot C_m^{n+1} - 4 \cdot C_m^n + C_m^{n-1}}{2 \cdot \Delta s} \tag{24}$$

$$\frac{\partial^2 C}{\partial x^2} \rightarrow \left\{ \frac{1}{g'(z)^2} \cdot \frac{1}{\Delta z^2} - \frac{3}{2} \cdot \frac{g''(z)}{g'(z)^3} \cdot \frac{1}{\Delta z} \right\} \cdot C_{m-1}^{n+1} - 2 \cdot \left\{ \frac{1}{g'(z)^2} \cdot \frac{1}{\Delta z^2} - \frac{g''(z)}{g'(z)^3} \cdot \frac{1}{\Delta z} \right\} \cdot C_m^{n+1}$$
$$+ \left\{ \frac{1}{g'(z)^2} \cdot \frac{1}{\Delta z^2} - \frac{1}{2} \cdot \frac{g''(z)}{g'(z)^3} \cdot \frac{1}{\Delta z} \right\} \cdot C_{m-1}^{n+1} \tag{25}$$

The derivatives of the transformation functions are given by:

$$f'(s) = 4 \cdot \tau_p \cdot s^3 \tag{26}$$

$$g'(z) = p + 4 \cdot (1-p) \cdot z^3 \tag{27}$$

$$g''(z) = 12 \cdot (1-p) \cdot z^2 \tag{28}$$

The boundary condition at the gas/liquid interface, Eq. (13), is included as the flux condition in the transformed and discretized equation (Cornelisse et al., 1980).

$$-D_i \cdot \left. \frac{\partial C_i}{\partial x} \right|_{x=0} = k_g \cdot \left(C_{i,gas} - \frac{C_{i,x=0}}{mgl_i} \right) \tag{29}$$

Application of the transformation for x and a number of straightforward rearrangements leads to

$$\left. \frac{\partial^2 C}{\partial x^2} \right|_{x=0} \rightarrow \frac{1}{g'(z)^2} \cdot \frac{2}{\Delta z^2} \cdot \left(C_1^{n+1} - C_0^{n+1} \right) + \left(\frac{1}{g'(z)} \cdot \frac{2}{\Delta z} + \frac{g''(z)}{g'(z)^2} \right) \cdot \frac{k_g}{D} \cdot \left(C_{gas} - \frac{C_{g(z)=0}}{mgl} \right) \tag{30}$$

The boundary conditions at $x=\infty$ are approximated by extending the grid to a depth in the liquid sufficiently larger than the penetration depth as defined by Eq. (18). Taking the range of the depth in the liquid as 5 times the penetration depth is assumed to be sufficient. This assumption has been checked on a number model calculations by inspection of the gradients. All checks revealed that the gradients were sufficiently close to zero at $x=5\cdot\delta_p$.

In the first time step the three-point backward discretization is replaced by a two-point Euler discretization because before t=0 no time step exists. Since the first time step is very small (due to the transformation of t), the larger truncation error of the Euler step is considered to be acceptable. While the gas phase concentration is kept constant for a contact period τ_P the enhancement factor is calculated according to:

$$E = \frac{\int_0^{\tau_P} -D \cdot \left.\frac{dC}{dx}\right|_{x=0} dt}{k_L \cdot \tau_P \cdot \left(C|_{x=0} - C_{bulk}\right)} \tag{31}$$

The gradient at x=0 is calculated by means of Eq. (29). The integral from 0 to τ_P is approximated by the summation of the gradients over all time steps (integration by trapezium rule).

4. Model simulations

The number of parameters that can be varied in the models is too large to treat all in detail, therefore only the most interesting parameters have been selected. The emphasis has been set on reaction rate constants and diffusion coefficients in order to examine the influence of the reactive intermediates. Therefore, the gas phase concentrations and gas-liquid partition coefficients are kept constant as well as the liquid phase concentrations at t=0 and in the liquid bulk. In addition, k_g and k_l were kept constant. For k_g the value was chosen sufficiently high to eliminate gas film resistances (e.g. 100 m/s). The liquid side mass transfer coefficient k_l has been fixed at $5\cdot10^{-5}$ m/s, a typical value for gas-liquid reactors. All constant input parameters are listed in Table 2 and Table 3. The number of spatial grid points has been set to 800 for all simulations. The number of grid points for the time coordinates was standard set to 60. In cases where a higher precision in the calculated enhancement factors was desired, the number of grid points was increased to 600.

Table 2. Default parameter values for model simulations.

Model	Component	Gas phase concentration C_g (kmol/m^3)	Liquid phase concentration C (kmol/m^3)	Diffusion coefficient D (m^2/s)	Solubility coefficient mgl (-)
ABP	A	1	10^{-40}	$1{\cdot}10^{-9}$	3
	B	10^{-40}	2	$1{\cdot}10^{-9}$	10^{40}
	P	10^{-40}	10^{-40}	$1{\cdot}10^{-9}$	10^{40}
BPdot	A	1	10^{-40}	$1{\cdot}10^{-9}$	3
	B	10^{-40}	2	$1{\cdot}10^{-9}$	10^{40}
	P	10^{-40}	10^{-40}	$1{\cdot}10^{-9}$	10^{40}
	B•	10^{-40}	$1{\cdot}10^{-5}$	$1{\cdot}10^{-9}$	10^{40}
	P•	10^{-40}	10^{-40}	$1{\cdot}10^{-9}$	10^{40}
3T	A	1	10^{-40}	$1{\cdot}10^{-9}$	3
	B	10^{-40}	2	$1{\cdot}10^{-9}$	10^{40}
	P	10^{-40}	10^{-40}	$1{\cdot}10^{-9}$	10^{40}
	B•	10^{-40}	$1{\cdot}10^{-5}$	$1{\cdot}10^{-9}$	10^{40}
	P•	10^{-40}	10^{-40}	$1{\cdot}10^{-9}$	10^{40}
	In•	10^{-40}	10^{-40}	$1{\cdot}10^{-9}$	10^{40}
	In	10^{-40}	10^{-40}	$1{\cdot}10^{-9}$	10^{40}
	T1	10^{-40}	10^{-40}	$1{\cdot}10^{-9}$	10^{40}
	T2	10^{-40}	10^{-40}	$1{\cdot}10^{-9}$	10^{40}
	T3	10^{-40}	10^{-40}	$1{\cdot}10^{-9}$	10^{40}

Table 3. Default second order reaction rate constants (in kmol/m^3/s) for model simulations.

Reaction	Model		
	ABP	BPdot	3T
A + B → P	$1{\cdot}10^{6}$		
A + B• → P•		$1{\cdot}10^{8}$	$1{\cdot}10^{8}$
P• + B → P + B•		$1{\cdot}10^{9}$	$1{\cdot}10^{9}$
2 B• → T_1			$1{\cdot}10^{5}$
B• + P• → T_2			$1{\cdot}10^{5}$
2 P• → T_3			$1{\cdot}10^{5}$
B + In• → B• + In			$1{\cdot}10^{9}$

4.1. Position and shape of the reaction front

For fast reactions between A and B the region in the liquid where both A and B exist in significant concentrations is very small. For infinitely fast reactions this region coincides with a single point. This is the point (or region) where the reaction rate between A and B is maximum and is called reaction front. The diffusion coefficients of reactant B and intermediate B• influence the position and shape of the reaction front. For comparison the results of the reaction A + B $\rightarrow$ P are included. The analytical solutions have been calculated with Eqs. (3) and (4). The positions of the reaction fronts are given in Table 4. The positions are scaled with the penetration depth as defined by Eq. (18).

Table 4. Reaction front positions.

Model	$D_c(B)$	$D_c(B\bullet)$	δ_r/δ_p	
	m^2/s	m^2/s	analytical	numerical
ABP	$1\cdot10^{-9}$	-	0.336	0.335
BPdot	$1\cdot10^{-9}$	$1\cdot10^{-9}$		0.335
	$1\cdot10^{-9}$	$1\cdot10^{-8}$		0.333
3T	$1\cdot10^{-9}$	$1\cdot10^{-9}$		0.335
	$1\cdot10^{-9}$	$1\cdot10^{-8}$		0.331
ABP	$1\cdot10^{-8}$	-	0.194	0.196
BPdot	$1\cdot10^{-8}$	$1\cdot10^{-9}$		0.202
	$1\cdot10^{-8}$	$1\cdot10^{-8}$		0.196
3T	$1\cdot10^{-8}$	$1\cdot10^{-9}$		0.205
	$1\cdot10^{-8}$	$1\cdot10^{-8}$		0.196

For model ABP the differences between the analytical and numerical solutions are small (less than 0.5% for the cases studied). Both the analytical solution and the numerical results agree on the large shift in position of the reaction front by changing the diffusion coefficient of B. The shift of the position of the reaction front is illustrated in Figure 2. In this figure the local reaction rates of the overall reaction A + B $\rightarrow$ P, based on the actual concentrations of the various species, are calculated from the concentration profiles emerging at the end the contact time. For the analytical solution this results in a front that is a sharp single line, indicated by the dotted lines in Figure 2.

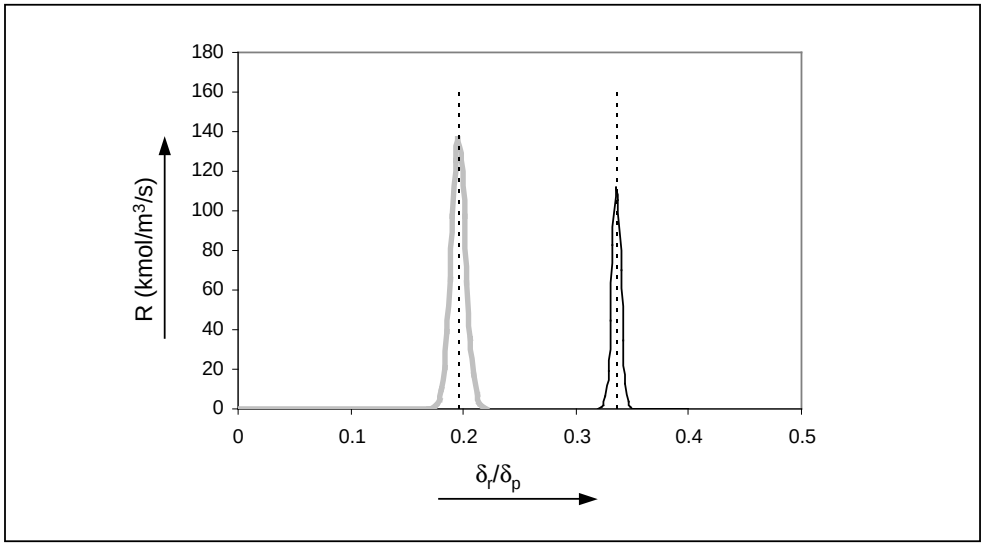

Figure 2. Reaction rate as function of penetration depth for model ABP. Solid lines are numerical calculated results, dotted vertical lines are reaction front positions according to Eq. (1) and (2). $D_c(B) = 1 \cdot 10^{-8}$ m²/s (left peak) and $D_c(B) = 1 \cdot 10^{-9}$ m²/s (right peak).

With a diffusion coefficient of B of $1 \cdot 10^{-9}$ m²/s all models predict the position of the reaction front within close distance from each other. However, on a smaller scale of the penetration depth the profiles of the overall reaction rates of model BPdot and model 3T deviate as shown in Figure 3. This behaviour is also observed with $D_c(B) = 1 \cdot 10^{-8}$ m²/s (Figure 4).

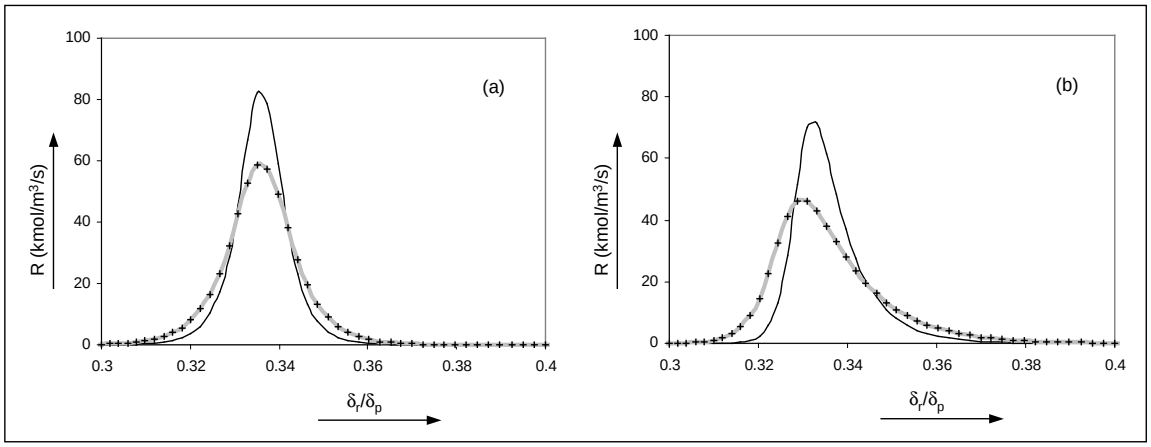

Figure 3. Reaction rates in the liquid for $D_c(B) = 1 \cdot 10^{-9}$ m²/s at time τ_p for model BPdot (thin lines) and model 3T (grey lines and symbols), (a) $D_c(B\bullet) = 1 \cdot 10^{-9}$ m²/s, (b) $D_c(B\bullet) = 1 \cdot 10^{-8}$ m²/s.

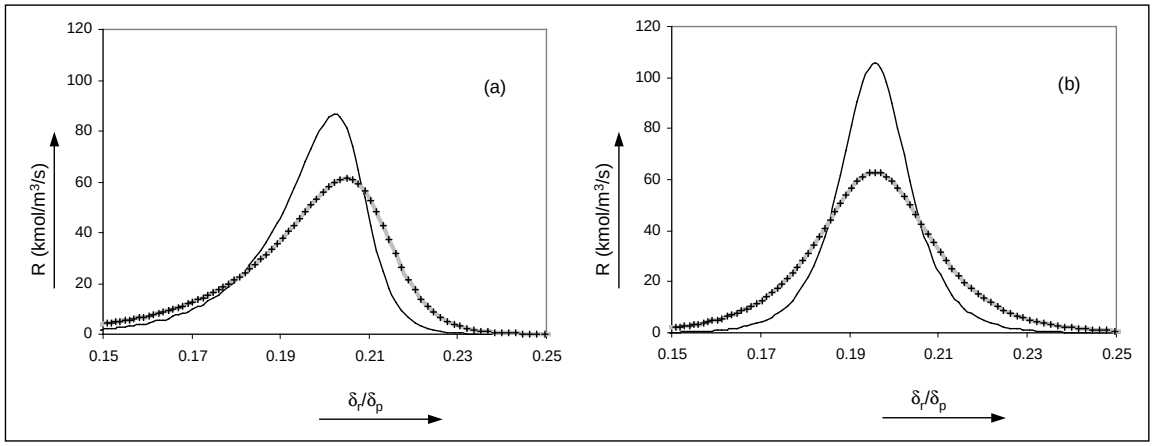

Figure 4. Reaction rates in the liquid for $D_c(B) = 1 \cdot 10^{-8}$ m²/s at time τ_p for model BPdot (thin lines) and model 3T (grey lines and symbols), (a) $D_c(B\bullet) = 1 \cdot 10^{-9}$ m²/s, (b) $D_c(B\bullet) = 1 \cdot 10^{-8}$ m²/s.

Comparing Figs. 3 and 4, it is observed that the reaction rate profiles are more symmetrical when the diffusion coefficients of B and B• are equal. From Table 4 it appears that in all models for equal diffusion coefficients the calculated location of the reaction rate maximum is exactly equal to the analytical solution of the ABP-model. The numerical value for the diffusion coefficients appears to have no influence on this observation as long as $D_c(B\bullet) = D_c(B)$. If the diffusion coefficient of B differs from that of B• the shape of the reaction rate profile is non-symmetrical. For $D_c(B\bullet) > D_c(B)$ the reaction profile is stretched in the direction of the bulk of the liquid because the higher diffusion rate of B• results in lower concentration of B• in the vicinity of the reaction front. This in turn causes a (small) increase in the concentration of A in the bulk direction (see also Figure 5).

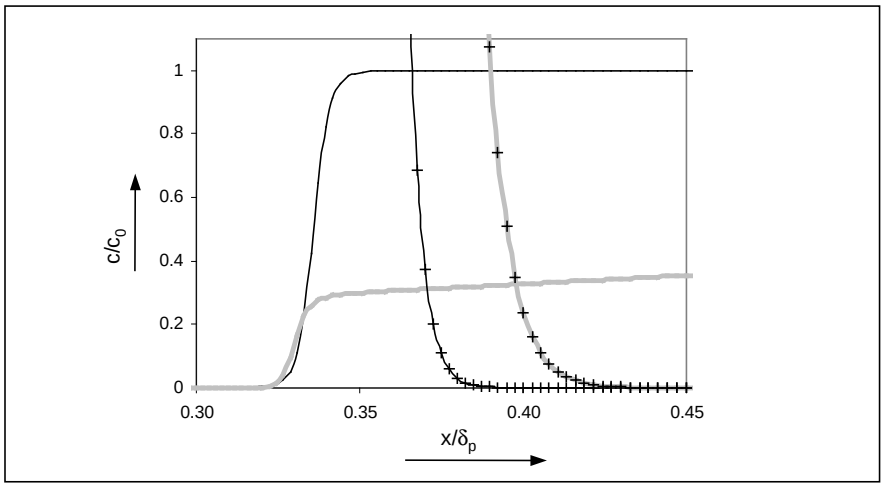

Figure 5. Model BPdot: concentrations of B• (lines) and A (lines and symbols) for $D_c(B\bullet) = 1 \cdot 10^{-9}$ m²/s (thin black lines), $D_c(B\bullet) = 1 \cdot 10^{-8}$ m²/s (wide grey lines). Scale factor c_0 is the total concentration of radicals at t=0.

The differences in concentrations of A in Figure 5 are only visible on the scale of the concentrations of the radicals, i.e. 10^{-5} kmol/m^3. To demonstrate the difference in concentrations of A the scale factor applied for the radical concentrations as also used for A. When the interface concentration would be applied to scale A, the differences shown in Figure 5 would be too small to notice.

4.2. Influence of radical intermediates on the concentration profiles

The influence of the diffusion coefficient of B• on the concentration profiles near the gas-liquid interface has been examined for the BPdot- and the 3T- model. All the results for these simulations are presented in the form of concentration profiles at the end of the contact time. A comparison of the effects of termination reactions is made. All model calculations have been performed with the basic parameter setting shown in Tables 2 and 3 unless indicated otherwise. For the model BPdot the B• and P• concentration profiles for varying D_c(B•) are shown in Figs. 6 and 7 respectively.

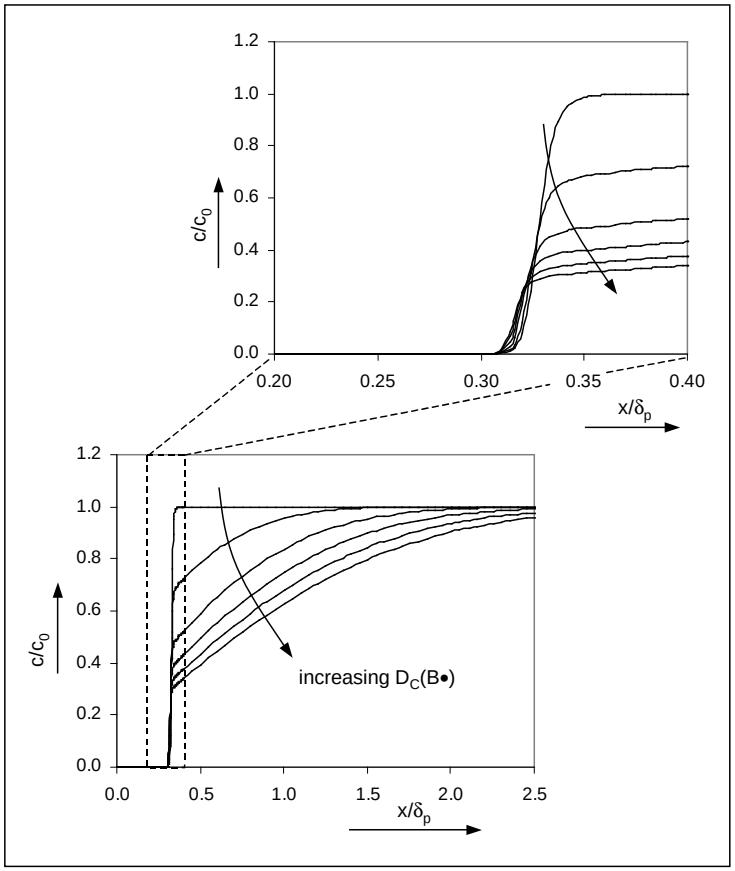

Figure 6. Concentration profiles of B• in model BPdot with varying D_c(B•) between $1\cdot10^{-9}$ and $1\cdot10^{-8}$ m^2/s.

The left and right frames are identical profiles; the scale of the graph is adapted to show the details. The concentrations for the radical intermediates are scaled to the total concentration of radicals at t=0.

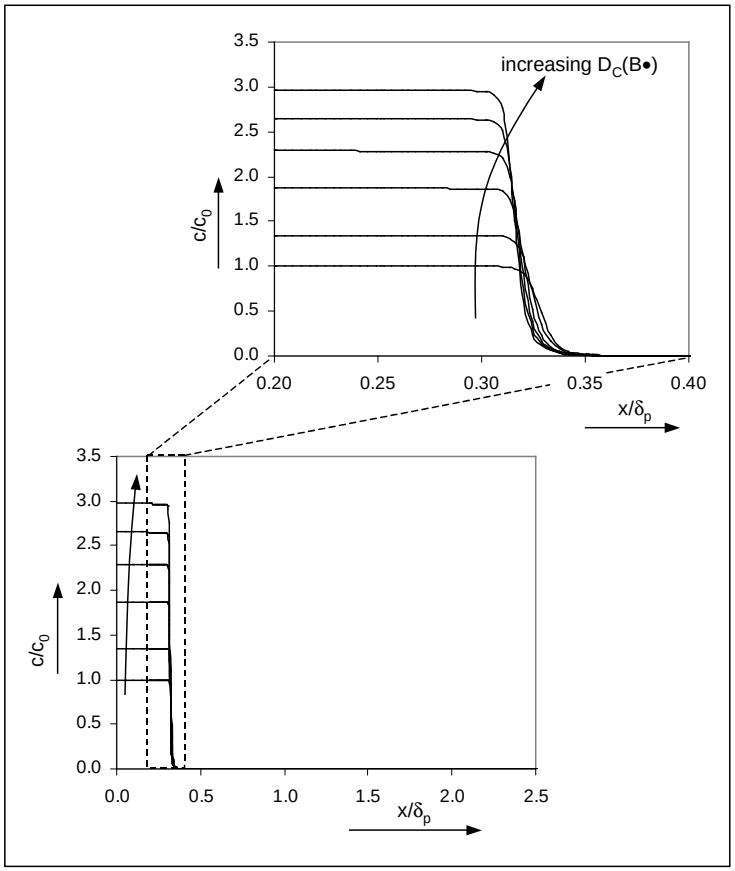

Figure 7. Concentration profiles of P• in model BPdot with varying D_c(B•) between $1 \cdot 10^{-9}$ and $1 \cdot 10^{-8}$ m^2/s.

From Figure 6 the concentration profiles for B• appear to have two distinct regions: one where the concentration has been lowered by pure diffusion of B• to the reaction zone ($x/\delta_{film} > 0.4$). Secondly, a region near the reaction zone where the concentration of B• rapidly has been decreased much more rapidly as a result of reaction (x/δ_{film} between 0.3 and 0.35). The reversal of the order of concentration profiles as function of D_c(B•) in this region as compared to $x/\delta_{film} > 0.4$ is caused by a small shift in the reaction front. For high values of the diffusion coefficient of B• the position of the maximum reaction rate between A and B• is shifted towards the G/L interface, see Figure 8.

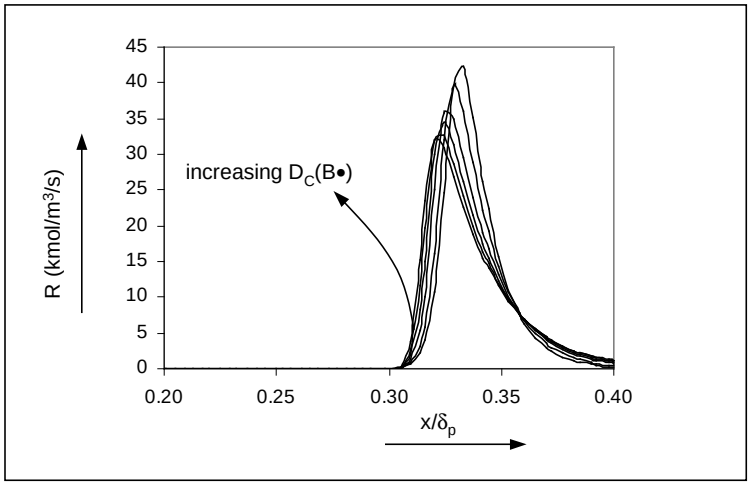

Figure 8. Reaction rate profile for A + B• → P• in model BPdot. Values for D_c(B•) vary between $1 \cdot 10^{-9}$ and $1 \cdot 10^{-8}$ m^2/s.

The reaction rate profile of the reaction between P• and B is nearly identical to the profile of the reaction rate for A and B• shown in Figure 8. Also with P• a high value for D_c(B•) shifts the reaction zone towards the interface hence the concentration of P• is lowered in comparison to the situation with a lower diffusivity of B•.

The concentration of P• builds up in the direction of the interface as D_c(B•) is increased. Starting at t=0 the reaction front is formed at the interface and moves deeper into the liquid as time progresses. Between the G/L interface and the reaction front the concentration of B is zero, any P• formed cannot react hence all radicals are present as P•. As soon as D_c(B•) is higher than D_c(P•) the concentration of P• is higher than the initial concentration of B• in the liquid because radicals from the liquid bulk are transported in the direction of the G/L interface due to the higher diffusivity of B• relative to P•.

Figures 9 and 10 give the results of the parallel calculations with model 3T. In Figure 9 it is clear that the concentration of B• is lowered with respect to the values obtained with model BPdot (Figure 6) but for the rest there is not much difference. The picture of the P• profile is somewhat different however: with the 3T-model the increase in the concentration of P• near the interface is much more suppressed as compared to the BPdot-model where no termination products are formed.

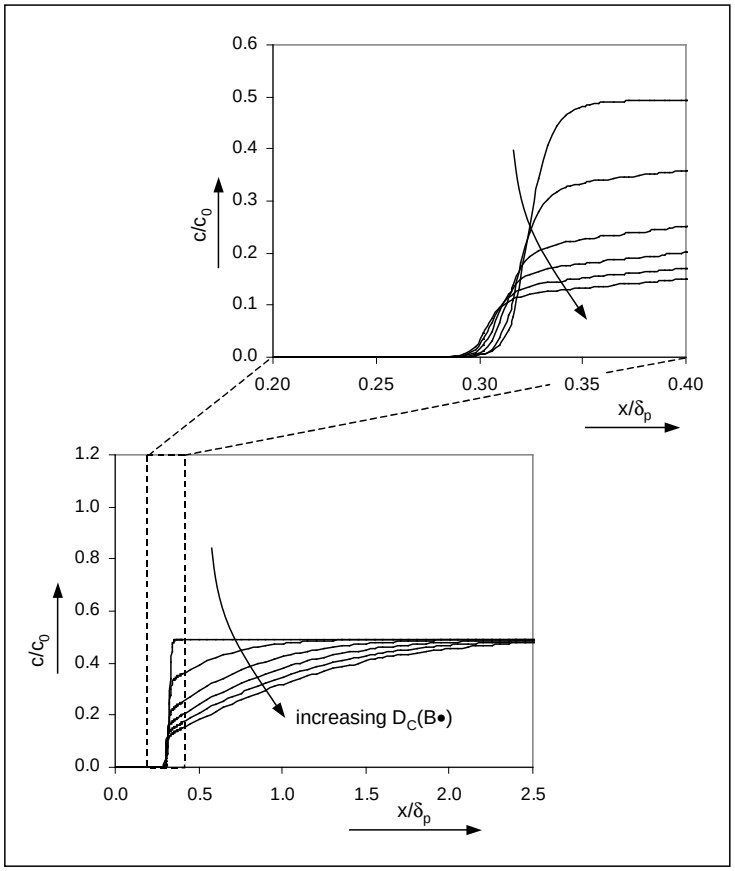

Figure 9. Concentration profiles of B• for model 3T. D_c(B•) is varied between $1 \cdot 10^{-9}$ m^2/s to $1 \cdot 10^{-8}$ m^2/s.

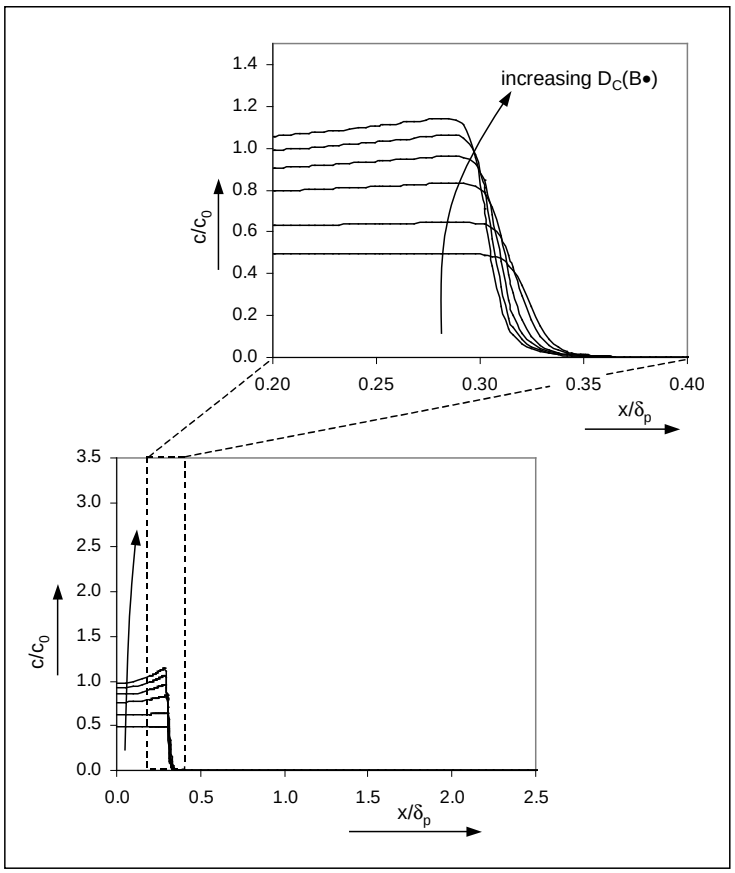

Figure 10. Concentration profiles of P• for model 3T. D_c(B•) is varied between $1 \cdot 10^{-9}$ m^2/s to $1 \cdot 10^{-8}$ m^2/s.

In model 3T the formation of termination products lowers the concentrations of both B• and P• in comparison to model BPdot. For diffusion coefficients of B• higher than those of P• the concentration of P• has a maximum located quite close to the reaction zone. Near the G/L interface there is no formation of P• because B• is zero. The termination reaction between P• radicals reduces the concentration near the interface. The consumption of P• is compensated via diffusion from the reaction zone where P• is product. For higher values of D_c(B•) the production of P• is increased (comparable to model BPdot, see Figure 8) leading to higher concentrations of P• near the reaction zone. Comparing Figs. 9 and 10 it appears that B• does not build up concentrations in the same way as P•. Any concentration gradient of B• building up as a result of reaction is reduced by the large diffusion coefficient of B•.

The profiles of B• and P• are reflected in the termination products. For equal reaction rate constants the ratio between the symmetrical termination products (T_1 and T_3) varies depending on the relative diffusion coefficients of the radical intermediates, see Figure 11.

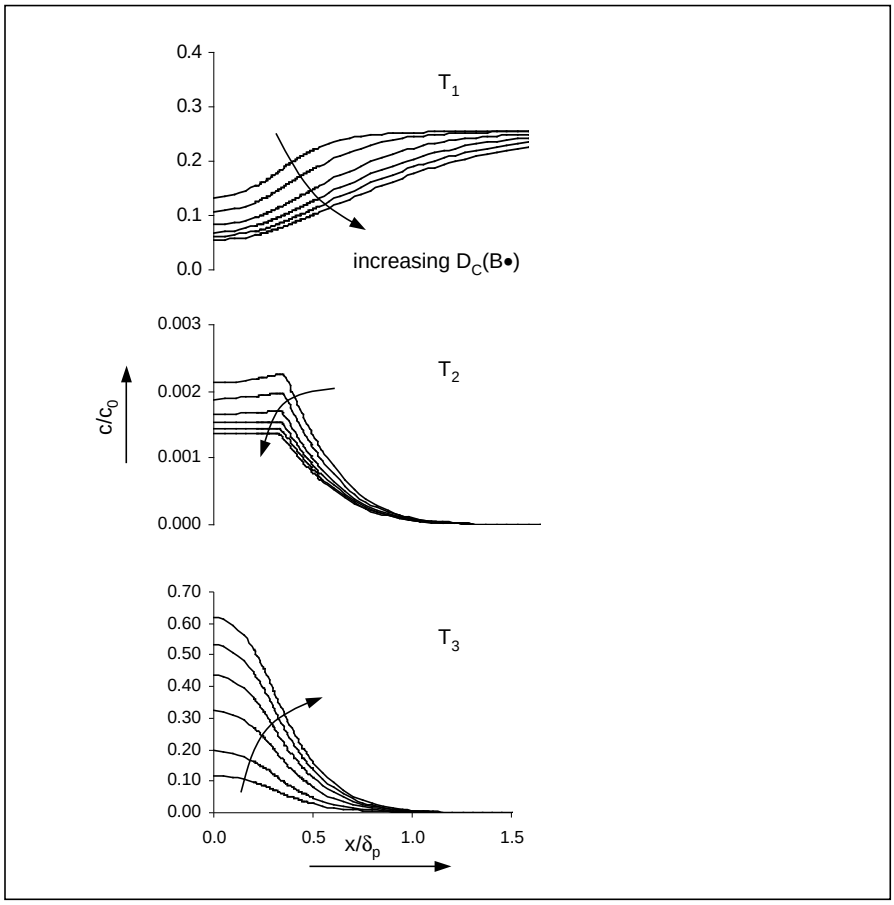

Figure 11. Concentration profiles of termination products T_1, T_2 and T_3 for model 3T. $D_c(B\bullet)$ is varied between $1 \cdot 10^{-9}$ m^2/s and $1 \cdot 10^{-8}$ m^2/s.

The mixed termination product T_2 has in all cases the lowest concentrations because the regions where both B• and P• are present in non-zero quantities are very limited. A maximum in the concentration profile of T_2 is observed in the vicinity of the reaction zone (see Figure 8 for model BPdot) where B• and P• are both present. From this position T_2 diffuses in both directions. For high values of $D_c(B\bullet)$ no gradient in the direction of the G/L interface exists because a high value of $D_c(B\bullet)$ lowers the concentrations in the reaction zone for P• (see Figure 10) which in turn lowers the reaction rate for the formation of T_2.

The reaction rate constants of the radicals are so high that at locations with A or B present, all radical intermediates are present in one type. The radical P• only exists in the part of the liquid where A exists, which is from the G/L interface to the reaction zone. The occurrence of unequal diffusion coefficients for radicals with similar molecular weights is not unlikely. For example, where B• has the option of an exchange reaction with B, the radical product P• has not:

$$B + B\bullet \rightleftharpoons B + B\bullet \qquad (32)$$

The effective diffusion coefficient for B• can be higher by the exchange reaction (Ruff and Friedrich, 1971). In autoxidation reactions radical types corresponding to the solvent are well known, i.e. the benzyl radical in oxidation of toluene and the cyclohexyl radical in the oxidation of cyclohexane.

5. Design aspects

One of the key parameters for the design of a gas-liquid reaction system is the absorption rate of the gaseous component. Estimation of this rate from other (known) parameters is often very much desired. To quantify the absorption rates, the effect of a number of variables on calculated enhancement factors is demonstrated for the models described in this paper. The different number of parameters applied in each model require additional consideration, however. One example is the dependency of E on reaction rate constants in the models BPdot and 3T respectively versus model ABP; whereas model ABP only has a single rate constant, the model BPdot has two reactions and model 3T has six reactions. The next section is focussed on model BPdot to demonstrate some basic features without the complications involved with handling the multiple reactions of model 3T. The enhancement factor as function of the Hatta number (φ) is a simple plot for model ABP as shown in Figure 12. The definition for Hatta for this type of reaction is:

$$\varphi = \frac{\sqrt{k_1 \cdot c_B \cdot D_A}}{k_L} \qquad (33)$$

The kinetic rate constant k_1 is related to model ABP (not to be confused with the k_1 from model 3T, Eq. (7)).

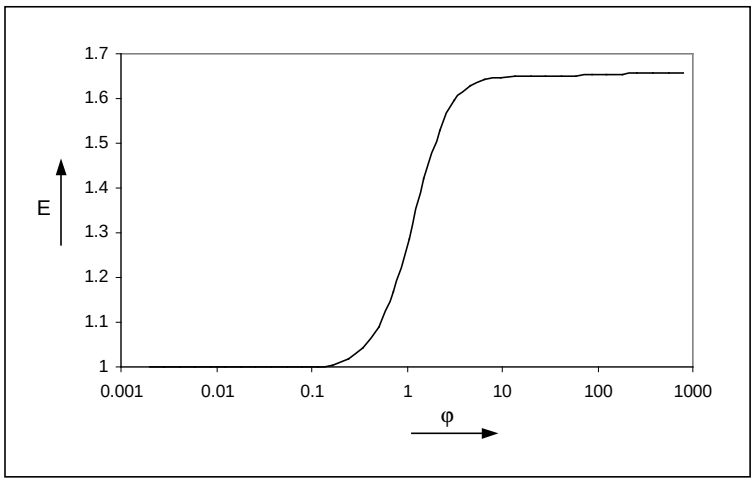

Figure 12. Enhancement factor as function of the Hatta number for model ABP, E=1.657 for high values of Hatta.

For models comprising more than one reaction of the gaseous reactant, the definition of the Hatta number is not straightforward because in more complex reaction schemes reactant A can be consumed in various ways, e.g. parallel, consecutive and combinations of these paths. For the case of the BPdot-model, two parameters are proposed based on the Hatta number of a single reaction:

$$\varphi_2 = \frac{\sqrt{k_2 \cdot c_{dot} \cdot c_B \cdot D_A}}{k_L} \tag{34}$$

$$\varphi_3 = \frac{\sqrt{k_3 \cdot c_{dot} \cdot c_B \cdot D_A}}{k_L} \tag{35}$$

The concentration c_{dot} is the concentration of initiator (In•) at t=0. It is easily verified that:

$$\varphi = \sqrt{\varphi_2^2 + \varphi_3^2} \qquad \text{or} \qquad k_1 = (k_2 + k_3) \cdot c_{dot} \tag{36}$$

The 3D-representation of the enhancement factor calculated with model BPdot is shown in Figure 13.

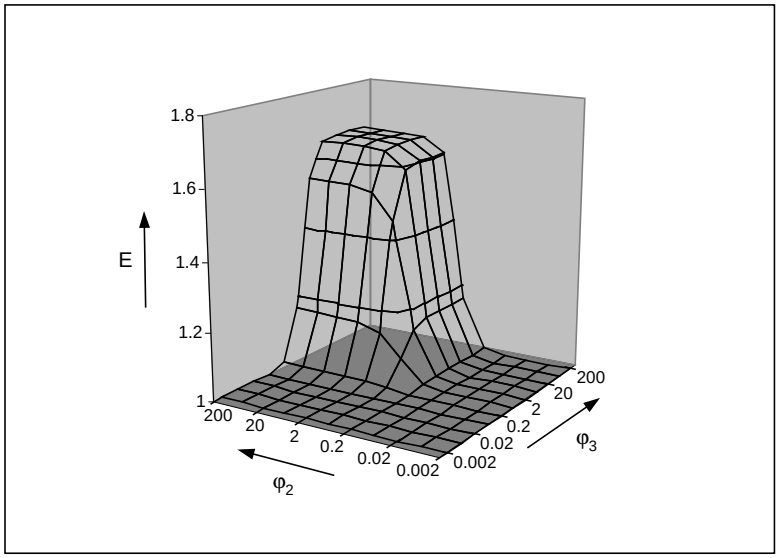

Figure 13. Enhancement factor as function of the parameters φ_2 and φ_3 of model BPdot, E=1.656 for high values of φ_2 and φ_3.

The representation of the one-dimensional curve of the enhancement factor for model ABP can also be transformed to a 3-D view by application of Eq. (36). For any combination of φ_2 and φ_3 the Hatta number according to the ABP-model can be calculated with Eq. (36) and subsequently the enhancement factor for the ABP-model can be determined (Figure 14).

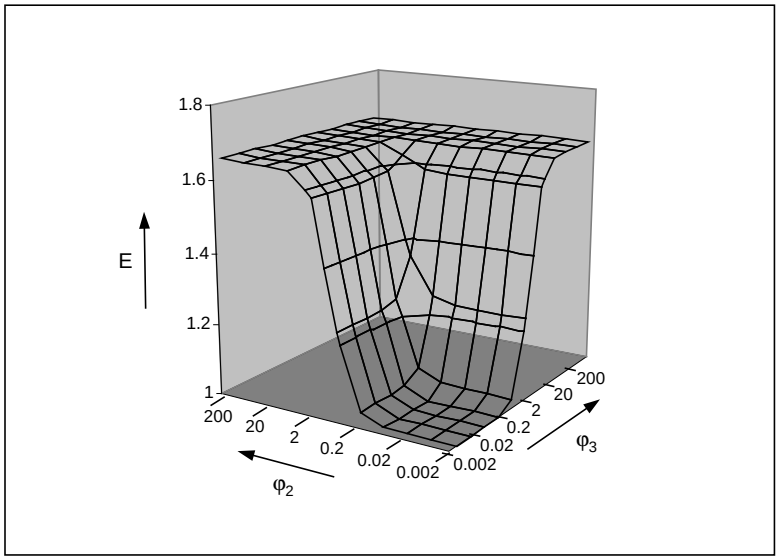

Figure 14. Enhancement factor for model ABP as function of the parameters φ_2 and φ_3.

From the comparison of Figure 13 and 14 it is directly clear that only for a limited number of combinations of φ_2 and φ_3 the enhancement factor of the BPdot-model coincides with the factor calculated for the ABP-model. The relative differences between model ABP and BPdot are shown in Figure 15. The deviation of model ABP compared to model BPdot is scaled by the enhancement factor at infinitely high reaction ($E_{A,\infty}$) according to:

$$\Delta(E) = \frac{E_{(ABP)} - E_{(BPdot)}}{E_{A,\infty} - 1} \tag{37}$$

The graph in Figure 15 is slightly rotated compared to the previous two figures to show the area for high φ_2 and φ_3 values more clearly.

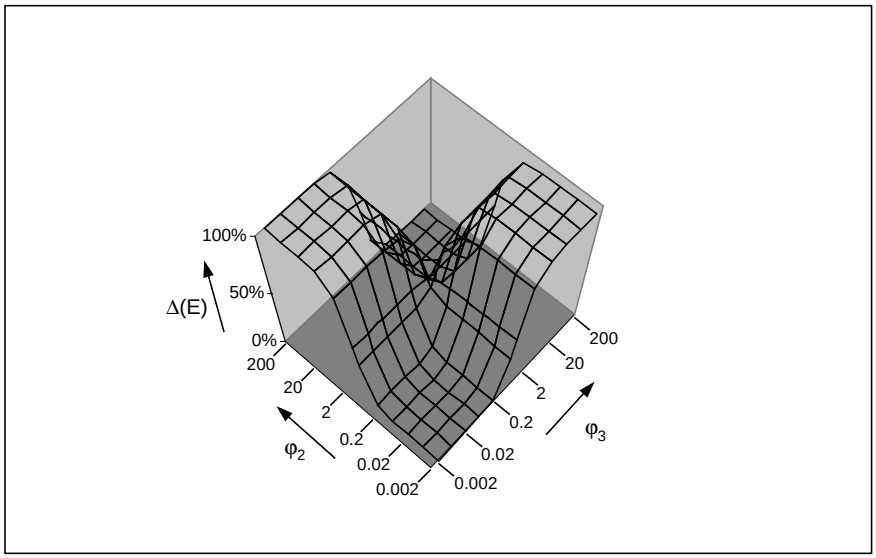

Figure 15. Deviation of enhancement factors as calculated by model ABP compared to model BPdot as function of the parameters φ_2 and φ_3.

For the design of a reactor system the areas where the use of the simplified model leads to good approximations can be easily identified from Figure 15. The symmetry in Figure 15 suggests that as long as the reaction rates of the radical intermediates are more or less balanced the approximation of a reaction without intermediates is valid regardless of the value of the enhancement factor. In the areas where the values of φ_2 and φ_3 differ significantly the radicals in model BPdot exist effectively only in one kind, B• or P• depending on which of the two parameters is larger. In this way the reaction path is blocked and no enhancement of mass transfer occurs, e.g. E = 1. The mathematical correlation for the translation to the ABP-model, Eq. (36), assigns a value for k_1 that is still quite large and therefore an enhancement factor bigger than 1 is derived.

Although Eq. (36) has been proposed on basis of the definition for the Hatta number of a second order reaction, there is no mathematical reason to reject other functions that calculate k_1 from k_2 and k_3. One example is the function shown in Eq. (38):

$$k_1 = \frac{k_2 \cdot k_3}{k_2 + k_3} \cdot c_{dot} \tag{38}$$

This correlation does not introduce additional parameters but for unequal values of k_2 and k_3 (or φ_2 and φ_3) the value of k_1 is determined by the smallest value of k_2 or k_3. The result for this transformation resembles the enhancement factors of model BPdot (Figure 13) much closer than in case of the application of Eq. (36). The differences between the model ABP with the transformation according to Eq. (38) and model BPdot is shown in Figure 16.

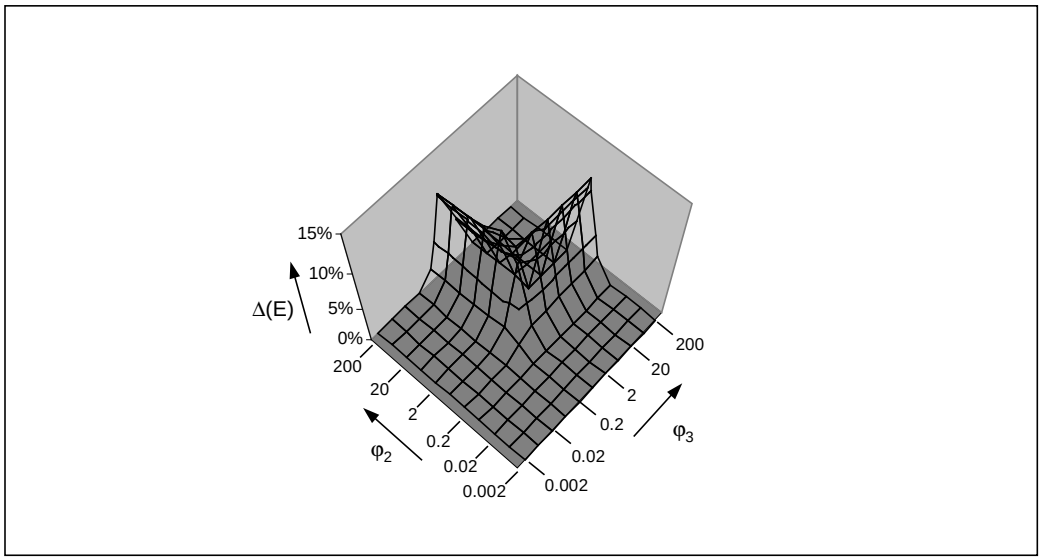

Figure 16. Deviation of enhancement factors as calculated by model ABP with transfer by Eq. (38) compared to model BPdot as function of the parameters φ_2 and φ_3.

Comparing Figs. 15 and 16 it is clear that by the translation through Eq. (38) a better match between model ABP and model BPdot is obtained. In addition, the software code for model ABP does not have to be changed upon application of Eq. (38).

In principle other functions than Eqs. (36) or (38) could be evaluated and selected on basis of some user-defined criterion by a trial-and-error procedure or a systematic approach. Although the use of mathematical functions like Eqs. (36) and (38) demonstrates that two variables can be reduced to a single parameter in various ways, the connection with a physical background or explanation is still lacking.

However, when the BPdot-model is simplified through a Bodenstein approximation (Helfferich, 2001a) and the resulting expressions are evaluated as part of the ABP-model a combination of mathematics and physical representation is obtained. The derivation of the equation is given in Appendix B, the resulting transfer equation is:

$$k_1 = \frac{k_2 \cdot k_3 \cdot c_{dot}}{k_2 \cdot c_A + k_3 \cdot c_B} \tag{39}$$

In contrast to Eqs. (36) and (38) this function contains the concentrations for A and B meaning that these concentrations need to be included in the calculations. An adaptation in the model ABP is required as the linearization of the reaction term, Eq. (23), is not valid for fractional reaction rate expressions as in Eq. (39). Instead of the generic expression for power laws presented in Appendix A, the analytical derivatives of Eq. (39) can easily be applied. These derivatives are also included in Appendix B. The results for model ABP transformed by application of Eq. (39) are nearly identical to the exact solution (calculated with model BPdot), see Figure 17. The small scatter in the graph is mainly caused by the numerical precision because by reducing the precision this scatter is significantly increased.

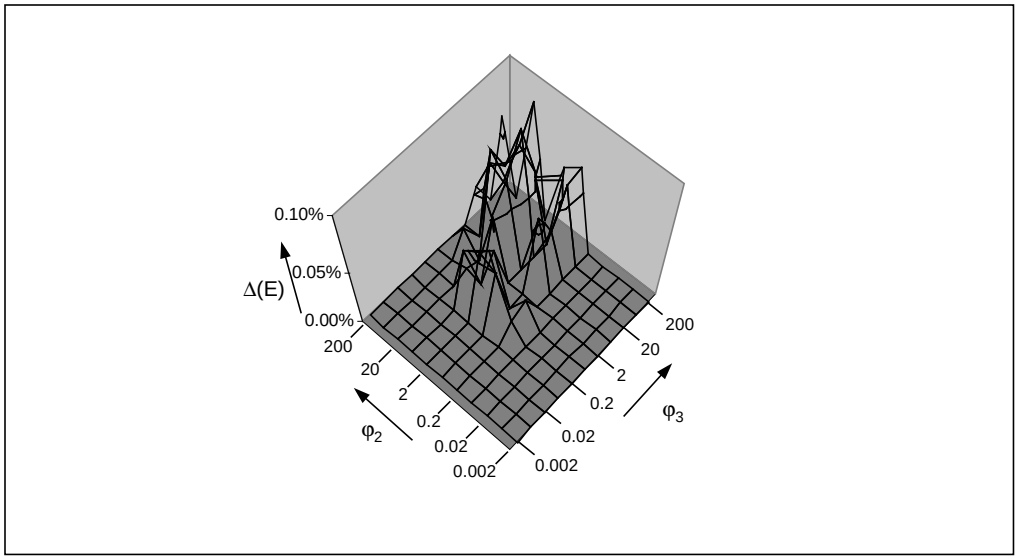

Figure 17. Deviation of enhancement factors as calculated by model ABP with transfer by Eq. (39) compared to model BPdot as function of the parameters φ_2 and φ_3.

Previous examples have demonstrated that complex models can be translated to more simple model versions by application of functions that correlate the parameters of the different model versions. The number of functions is in principle unlimited.

The form of the function and the inclusion of additional parameters determine the quality of the results of the simplified model in comparison to the complex model as well as the effort that has to be delivered to obtain the simplified model results.

A simplified model should meet the requirements for a specific job like for example incorporation in a CFD application or for the purpose of a process control study. Assuming that a complex model (derived from fundamental principles) is available and the requirements for the simplified model are known, it is possible to assign a very simple model as basic version. Then, by application of a number of transfer functions alternatives of the basic version can be evaluated very easily.

Whether the availability of a complex model is essential for the proposed procedure is not clear yet. When the complex model can be replaced by for example discrete observations from experiments, this procedure can also be a recipe to determine a suitable simple model directly from experimental observations.

The study of the models ABP and BPdot is of course a very simplified exercise compared to most of the radical reaction networks known from literature. The complexity of the analysis rapidly increases with the number of components, but as long as the translation of process parameters in the complex reaction system towards simplified models can be performed by means of comparing observable responses, such as for example enhancement factors, is it possible to obtain a validated, fit-for-purpose simplified model.

Model 3T has been left out of the analysis of this section because the complexity of this model is not increased in terms of the intermediates or reaction pathways. Instead, the number of non-radical by-products is increased which requires the ABP-model to be extended with reactions leading to those by-products. This would give an example where both the complex and simple model contain more variables, increased number of parameters and possible combinations, but the principles of the transfer functions are quite similar to the exercise with the BPdot and ABP-models.

6. Conclusions

The calculation of enhancement factors applied in the design of a G/L reaction system can be performed with simplified models where the reactive intermediates do not occur in the expressions for the reaction rates. The optimum model for a specific design purpose can be found by tuning the function that correlates the parameters of the complex model to the reduced number of parameters of the simplified model.

Depending on the choice of the form of the transfer function a large number of alternatives can be evaluated very easily. With transfer functions involving not only parameters but also process variables more effort in adaptations of the software routines in the model is required, but the agreement with the exact solution can be significantly improved.

The diffusion coefficients of radical intermediates have significant influence on the profiles of concentrations and reaction rates near the G/L interface. For fast reactions, all reactions take place in a small region that shifts away from the G/L interface as the time of the contact increases. In the snapshots of the results obtained at the end of the specific contact times shifts in position and value occur, the directions depend on the ratios of the diffusion coefficients of the radicals. With the model BPdot, increasing the diffusion coefficient of solvent radical (B•) reduces the concentration of B• near the reaction front while at the same time shifting the B• profile in the direction of the G/L interface. In the region between the G/L interface and the reaction front the concentration of the product radical (P•) builds up to higher values than the initial radical concentration at the start. These effects also occur when the formation of termination products is also included, but the extend is reduced.

It is shown that for very fast reactions differences in diffusion coefficients of the intermediates can cause shifts in the by-product formation in other ways than often assumed (Helfferich, 2001b). The example for model 3T shows that the mixed termination product (T_2) from two radical intermediates B• and P• is only formed in low quantities because the two radicals do not occur in high concentrations simultaneously. In case the concentration of the gaseous reactant is gradually reduced, there will be no gradual shift in observed termination product from T_1 (coupling of 2 B•) via T_2 to T_3 (formed out of 2 P•). Instead, by lowering the interfacial concentration of the gaseous reactant the reaction front will move in the direction of the G/L interface and therefore more T_1 will be formed at the cost of T_3. The concentration of T_2 will remain at lower levels than the other two termination products all the time.

The numerical study of reaction mechanisms comprising reactive intermediates and fast reactions is very helpful in gaining insight in effects that are difficult to study experimentally. This study has shown that systems with radical intermediates can be simplified to models where the intermediates are omitted. There is no reason that this methodology should be restricted to radical reactions. The extension to other systems as well the application on more complex systems than presented in this study is subject for future evaluations.

Nomenclature

Notation

a,b	stoichiometric coefficients	-
C,c	concentration	$kmol/m^3$
c_{dot}, c_0	concentration radical species at t=0	$kmol/m^3$
D, D_c	diffusion coefficient	m^2/s
E	enhancement factor	-
E_∞	enhancement factor at infinitely fast reaction	-
f, g	transformation functions	-
J	flow across gas-liquid interface	$kmol/m^2/s$
k	reaction rate constant	s^{-1} or $m^3/kmol/s$
k_g	gas side mass tranfer coefficient	m/s
k_L	liquid side mass transfer coefficient	m/s
mgl	solubility coefficient defined as c_{liquid}/c_{gas}	-
p	constant for curvature in x-variable transform function	-
R	reaction rate	$kmol/m^3/s$
s	transformed time variable	-
t	time variable	s
x	distance variable	m
z	transformed distance variable	-

Greek

β	constant defined in Eq (1)	-
$\beta_{i,j}$	exponent: component i in reaction j	-
δ_p	penetration depth	m
δ_r	location of maximum reaction rate	m
φ	Hatta number	-
φ_2, φ_3	constants derived from φ	-
$\nu_{i,j}$	stoichiometric constant: component i in reaction j	-
τ_p	contact time	s

Sub- and superscripts

$^\circ$	reference
bulk	liquid bulk
gas, liquid	phase
i	any component
j	any reaction
n	time count finite difference equations
m	distance count finite difference equations
p,q	any component or reaction

Abbreviations

A	gas phase reactant
B	liquid phase reactant
B•	radical derived from B
In	deactivated radical initiator
In•	radical initiator
P	liquid phase product
P•	radical derived from P
T_1	termination product formed out of reaction between 2 B•
T_2	termination product formed out of reaction between B• and P•
T_3	termination product formed out of reaction between 2 P•

References

Baker, G.A., Oliphant, T.A., (1960), An implicit, numerical method for solving the two-dimensional heat equation, *Quart. Appl. Math.* **17**, 361-373.

Burns, W.G., Hopper, M.J., Reed, C.R.V., (1970), Effects of L.E.T. and temperature in the radiolysis of cyclohexane. Part 2. Diffusion kinetic models, *Trans. Faraday Soc.* **66**, 2182-2191.

Carey, F.A., Sundberg, R.J., (1990), Advanced Organic Chemistry, Part A: Structure and Mechanisms, Plenum, NewYork, pp. 676-677.

Cornelisse, R., Beenackers, A.A.C.M., Van Beckum, F.P.H., Van Swaaij, W.P.M., (1980), Numerical calculation of simultaneous mass transfer of two gases accompanied by complex reversible reactions, *Chem. Eng. Sci.* **35**, 1245-1260.

Flores-Fernandez, G., Mann, R., (1978), Gas absorption with radical multiplying chain-type reactions, *Chem. Eng. Sci.* **33**, 1545-1549.

Froment, G.F., Bischoff, K.B., (1990), Chemical Reactor Analysis and Design, John Wiley & Sons, New York, pp. 275-282.

Helfferich, F.G., (2001a), Kinetics of homogeneous multistep reactions, in: Compton, R.G., Hancock, G., (Eds.), *Comprehensive Chemical Kinetics, vol. 38*, Elsevier, Amsterdam, pp. 72-77.

Helfferich, F.G., (2001b), Kinetics of homogeneous multistep reactions, in: Compton, R.G., Hancock, G., (Eds.), *Comprehensive Chemical Kinetics, vol. 38*, Elsevier, Amsterdam, pp. 283-286.

Juvekar, V.A., (1978), Gas absorption with autocatalytic reaction, *Chem. Eng. Sci.* **31**, 91-92.

Ruff, I., Friedrich, V.J., (1971), Transfer diffusion. IV. A numerical test of the correlation between prototrope mobility and proton exchange rate of H3O+ and OH- ions with water, *J. Phys. Chem.* **75**, 3297-3302.

Sim, M.-T., Mann, R., (1975), Gas absorption with autocatalytic reaction, *Chem. Eng. Sci.* **30**, 1215-1218.

Sitarski, M., (1981), Effect of Brownian diffusion on chemical kinetics, *Int. J. Chem. Kin.* **13**, 125-133.

Van Swaaij, W.P.M., Versteeg, G.F., (1992), Mass transfer accompanied with complex reversible chemical reactions in gas-liquid systems: an overview, *Chem. Eng. Sci.* **47**, 3181-3195.

Versteeg, G.F., Blauwhoff, P.M.M., Van Swaaij, W.P.M., (1987), The effect of diffusivity on gas-liquid mass transfer in stirred vessels. Experiments at atmospheric and elevated pressures, *Chem. Eng. Sci.* **42**, 1103-1119.

Versteeg, G.F., Kuipers, J.A.M., Van Beckum, F.P.H., Van Swaaij, W.P.M., (1989), Mass transfer with complex reversible chemical reactions - I. Single reversible chemical reaction, *Chem. Eng. Sci.* **44**, 2295-2310.

Westerterp, K.R., Van Swaaij, W.P.M., Beenackers, A.A.C.M., (1990), Chemical Reactor Design and Operation, John Wiley & Sons, New York, pp. 357-494.

Appendix A. Linearization of the reaction term by a Taylor series expansion around $C^{\bullet}_i$

In these equations the subscript j is for the reaction indices and subscript i is for components, they are replaced by p and q where appropriate.

Linearization of Eq. (21)

$$R_j \rightarrow k_j \cdot \prod_{p=1}^{comp} \left(C_p^{\bullet}\right)^{\beta_{p,j}} + \sum_{p=1}^{comp} \left.\frac{\partial R_j}{\partial C_p}\right|_{\bullet} \cdot \left(C_p - C_p^{\bullet}\right)$$

$$\left.\frac{\partial R_j}{\partial C_p}\right|_{\bullet} = k_j \cdot \prod_{q=1, q\neq p}^{comp} \left(C_q^{\bullet}\right)^{\beta_{q,j}} \cdot \beta_{p,j} \cdot \frac{\left(C_p^{\bullet}\right)^{\beta_{p,j}}}{C_p^{\bullet}} \qquad \text{(A1)}$$

Subsituted in Eq. (22)

$$R_i = \sum_{j=1}^{reac} \nu_{i,j} \cdot k_j \cdot \left[\prod_{p=1}^{comp} \left(C_p^{\bullet}\right)^{\beta_{p,j}} + \sum_{p=1}^{comp} \left\{ \prod_{q=1, q\neq p}^{comp} \left(C_q^{\bullet}\right)^{\beta_{q,j}} \cdot \beta_{p,j} \cdot \frac{\left(C_p^{\bullet}\right)^{\beta_{p,j}}}{C_p^{\bullet}} \cdot \left(C_p - C_p^{\bullet}\right) \right\} \right] \qquad \text{(A2)}$$

Defining and simplification of the constant R-terms:

$$R_i^{const} = \sum_{j=1}^{reac} \nu_{i,j} \cdot k_j \cdot \left[\prod_{p=1}^{comp} \left(C_p^{\bullet}\right)^{\beta_{p,j}} - \sum_{p=1}^{comp} \left\{ \beta_{p,j} \cdot \prod_{q=1}^{comp} \left(C_q^{\bullet}\right)^{\beta_{q,j}} \right\} \right] \qquad \text{(A3)}$$

$$R_i^{const} = \sum_{j=1}^{reac} \nu_{i,j} \cdot k_j \cdot \left[1 - \sum_{p=1}^{comp} \beta_{p,j} \right] \cdot \prod_{p=1}^{comp} \left(C_p^{\bullet}\right)^{\beta_{p,j}} \qquad \text{(A4)}$$

Terms of R dependent on concentrations:

$$R_i^{Cp} = \sum_{j=1}^{reac} \nu_{i,j} \cdot k_j \cdot \sum_{p=1}^{comp} \left\{ \prod_{q=1, q\neq p}^{comp} \left(C_q^{\bullet}\right)^{\beta_{q,j}} \cdot \beta_{p,j} \cdot \frac{\left(C_p^{\bullet}\right)^{\beta_{p,j}}}{C_p^{\bullet}} \cdot C_p \right\} \qquad \text{(A5)}$$

$$R_i^{Cp} = \sum_{p=1}^{comp} R_i(p) \qquad \text{(A6)}$$

$$R_i(p) = \sum_{j=1}^{reac} \nu_{i,j} \cdot k_j \cdot \beta_{p,j} \cdot \left(C_p^{\bullet}\right)^{\beta_{p,j}-1} \cdot \prod_{q=1, q\neq p}^{comp} \left(C_q^{\bullet}\right)^{\beta_{q,j}} \cdot C_p \qquad \text{(A7)}$$

Eqs. (A4) and (A5) subsituted in Eq. (A2)

$$R_i = \sum_{j=1}^{reac} \nu_{i,j} \cdot k_j \cdot \left[1 - \sum_{p=1}^{comp} \beta_{p,j} \right] \cdot \prod_{p=1}^{comp} \left(C_p^{\bullet}\right)^{\beta_{p,j}} + \sum_{p=1}^{comp} \left\{ \sum_{j=1}^{reac} \nu_{i,j} \cdot k_j \cdot \frac{\beta_{p,j}}{C_p^{\bullet}} \cdot \prod_{q=1}^{comp} \left(C_q^{\bullet}\right)^{\beta_{q,j}} \cdot C_p \right\} \qquad \text{(A8)}$$

Appendix B. Bodenstein approximation for model BPdot

Assumption 1: the rate of formation and disappearance of B• are approximately equal:

$$R_1 = R_2$$

$$k_2 \cdot c_A \cdot c_{B\bullet} = k_3 \cdot c_B \cdot c_{P\bullet} \tag{B1}$$

Assumption 2: the total radical concentration is constant and equal to the initial initiator concentration:

$$c_{B\bullet} + c_{P\bullet} = c_{dot} \tag{B2}$$

Rearrangement of Eq. (B1) and substitute in Eq. (B2)

$$c_{B\bullet} = \frac{c_{\bullet tot}}{1 + \frac{k_2 \cdot c_A}{k_3 \cdot c_B}} \tag{B3}$$

Eq. (B3) is substituted in the expression for R_1:

$$R_1 = \frac{k_2 \cdot k_3 \cdot c_{dot}}{k_2 \cdot c_A + k_3 \cdot c_B} \cdot c_A \cdot c_B \tag{B4}$$

The corresponding expression for model ABP is:

$$R_1 = k_1 \cdot c_A \cdot c_B \tag{B5}$$

Reaction rates for the components are

$$R_i = \nu_i \cdot R_1$$

$$\nu_i = -1 \quad \text{for i = A or B}$$

$$\nu_i = 1 \quad \text{for i = P} \tag{B6}$$

The partial derivatives are defined by:

$$\frac{\partial R_i}{\partial c_A} = \nu_i \cdot \frac{k_2 \cdot k_3 \cdot c_{dot} \cdot c_B \cdot (k_2 \cdot c_A + k_3 \cdot c_B) - k_2^2 \cdot k_3 \cdot c_{dot} \cdot c_A \cdot c_B}{(k_2 \cdot c_A + k_3 \cdot c_B)^2} \tag{B7}$$

$$\frac{\partial R_i}{\partial c_B} = \nu_i \cdot \frac{k_2 \cdot k_3 \cdot c_{dot} \cdot c_A \cdot (k_2 \cdot c_A + k_3 \cdot c_B) - k_2 \cdot k_3^2 \cdot c_{dot} \cdot c_A \cdot c_B}{(k_2 \cdot c_A + k_3 \cdot c_B)^2} \tag{B8}$$

$$\frac{\partial R_i}{\partial c_P} = 0 \tag{B9}$$

5

Modelling of mass transfer in combination with a homogeneous catalysed reaction

Abstract

The mass transfer rates of a gaseous reactant into a liquid where the reactions are catalysed by homogeneous catalysts have been evaluated by the numerical solution of the diffusion-reaction equations according to Higbie's penetration theory. The concentration profiles as well as enhancement factors are discussed as function of the kinetic rate constants and the diffusion coefficients of the catalytic intermediates. In addition to the complex catalytic model two simplified models were applied in order to facilitate design calculations. One version was obtained by application of the Bodenstein approximation, the simplest version comprised only the stoichiometric reaction. The Bodenstein model provides a very good approximation except for deviating diffusion coefficients of the catalytic intermediates. The applicability of the stoichiometric model is not as wide as with the Bodenstein model but for some conditions acceptable approximations are achieved.

1. Introduction

Homogeneous catalysis is broadly applied in process industry and extensively studied in academia. Although the mechanisms of a very large number of homogeneously catalysed systems are quite thoroughly known, for only a limited number of systems exact kinetic expressions and well validated kinetic parameters are determined. The reason is not a lack of industrial relevance but the exact quantification of a single reaction in an extensive network is extremely difficult. A complete description of a catalytic network requires the precise determination of all concerned reactions.

The work of Halpern et al. (1973; 1976; 1981) contains one of the few examples where the detailed kinetics of a homogeneously catalysed system has been elucidated. A series of papers describing the rhodium catalysed hydrogenation by means of combination of analytical techniques and kinetic experiments is very often cited in textbooks. The scheme presented in Figure 1 has been adapted from Halpern (1981). In this publication a summary is given of two earlier papers where kinetic data were presented (Halpern and Wong, 1973; Halpern et al., 1976).

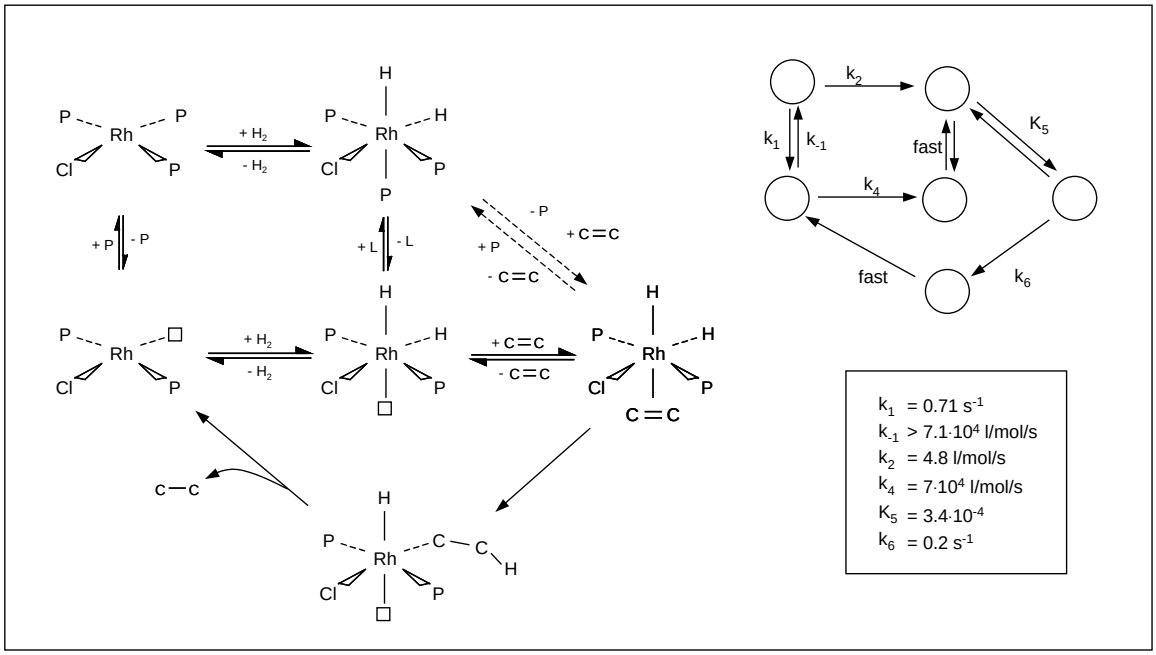

Figure 1. Part of the catalytic cycle of a rhodium catalysed hydrogenation. The upper right part indicates the reaction rate constants that have been quantitatively identified. P indicates PPh_3.

The reaction rates in Figure 1 are expressed as first order in the specific catalyst intermediate and first order in reactant where appropriate respectively. The kinetic constants in the rate expressions have been determined from measurements. The rate constants in Figure 1 are partly derived from spectrally determined equilibrium constants, therefore in case of k_{-1} a minimum is given rather than an exactly measured value. An overview of kinetics and mechanisms in other hydrogenation systems is given by Sanchez-Delgado and Rosales (2000). Most often, however, the kinetic rate expressions are determined for the overall reactions.

Outside the field of homogeneous catalysis with precious metals other examples are available where the kinetics of the individual reaction steps have been studied in detail. In the catalytic cycle of iron chelate complexes nitrous and sulphur oxides are absorbed in water, NO is reduced and the produced sulphite is oxidized (Zang and van Eldik, 1989). Main products are a series of nitrogen and sulphur containing components (Figure 2).

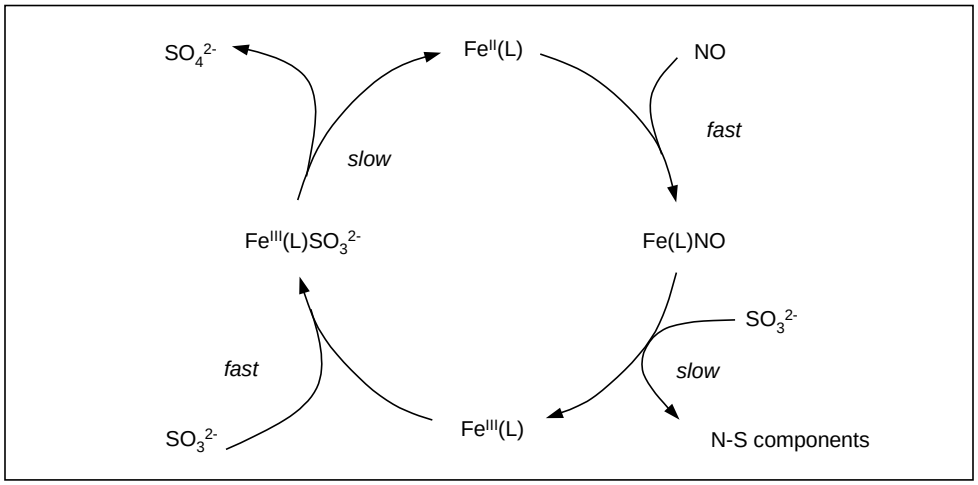

Figure 2. Main catalytic cycle of simultaneous absorption and reaction of nitrous and sulphur oxides. The ligand L is a chelating component like EDTA.

The differences in reaction rates indicated with slow or fast in Figure 2 are orders of magnitude. The second order rate constant of the reaction of NO with Fe^{II}(EDTA) is higher than $6 \cdot 10^7$ l/mol/s whereas the reduction of Fe^{III}(EDTA) by sulphite proceeds much slower. Given a first order reaction rate constant of $4 \cdot 10^{-5}$ s^{-1} as observed for 0.05 mol/l sulphite solution the derived (pseudo) second order rate constant is equivalent to $8 \cdot 10^{-4}$ l/mol/s, indicating a difference of 10^{11} with the former reaction.

Despite the occurrence of very fast reactions in solution for the majority of homogeneously catalysed reactions described in literature the aspects of mass transfer and mass transfer limitations are only briefly addressed.

Very frequently reaction conditions are chosen in such a way that limitations are avoided (Cavalieri dÓro et al., 1980). In some occasions, the mass transfer rates of the gaseous components are taken into account by application of mass transfer coefficients (Kelkar et al., 2001). The influence of mass transfer on the stability of a hydroformylation reactor has been investigated by van Elk et al. (2001). The kinetic model applied in this study was an overall empirical rate expression. The calculation of the rate of mass transfer in the absorption of gases followed by (complex) chemical reactions is one of the key issues in the design and scale-up of gas-liquid reactors. In textbooks as well as in practice the simplification of a reaction network to a single first-order irreversible reaction is often applied giving the advantage of simple concepts of Hatta number and enhancement factor. A great number of researchers have extended the analytical solutions for other than first order irreversible reactions. The spectrum of reactive systems includes single and multiple reactions (parallel and in-series), irreversible as well as reversible reactions, auto catalytic reactions. A comprehensive overview on the literature on mass transfer accompanied by complex chemical reactions can be found in a paper by van Swaaij and Versteeg (1992). An early numerical study on homogeneously catalysed gas-liquid reactions in combination with mass transfer effects is presented by Ponzi and Lemcoff (1981). They studied a reaction system comprising absorption of two gases; one gaseous reactant and one component for the regeneration of the catalyst as is applied in for example the production of acetaldehyde from ethene (Wacker process).

There are a number of reasons to study the combination of homogeneously catalysed reactions in the mass transfer limited regime. As industrial conditions in reactors often deviate from laboratory experimental set-ups it is likely that in plant reactors conditions occur where mass transfer limitations or enhancement of mass transfer through reaction influence the performance of the reactor. In addition mass transfer limitations are often difficult to separate from "ordinary" kinetic observations. It is therefore very well possible that in a number of laboratory scale reactors mass transfer limitations have been left out of consideration. Starting with the assumption that the reactions concerning the gaseous reactant can be in principle very fast, a general method to incorporate the transport equations with the elementary reactions would be very helpful. Once a fundamental model has been established, it is interesting to determine the conditions for which a simplified model gives results very close to the fundamental model. The simplified model is useful in for example design studies, plant simulations and for control purposes. This approach has been recently exercised in a diffusion-reaction system involving radical intermediates (Hoorn and Versteeg, 2005).

2. Mass transfer and reaction model

Three models are considered in this paper. All models comprise A as a gaseous component from the gas phase transferring to the liquid and reacting with B to form product P. The models differ in the reaction pathways and their association with a reaction rate expression.

2.1. Model ABP

This is the stoichiometric model for the reaction A + B → P. The Hatta number for this type of reaction is defined by:

$$\varphi = \frac{\sqrt{k_1 \cdot c_B \cdot D_A}}{k_L} \tag{1}$$

2.2. Model HC

This model is a representation of the reaction proceeding through homogeneous catalysis in which a minimum of catalyst intermediates is involved. The reactions and notation are indicated in Figure 3 along with the expressions for the reaction rates.

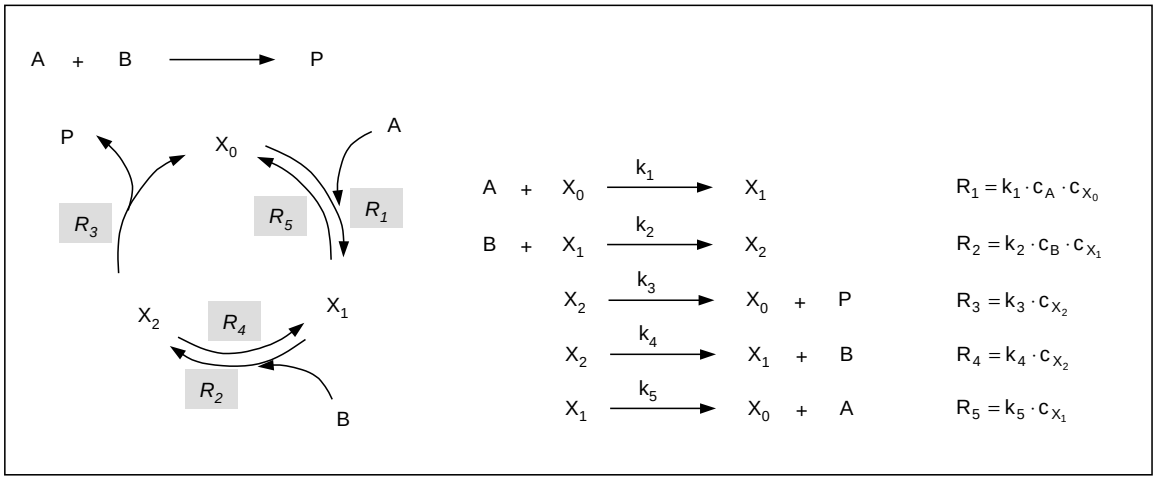

Figure 3. Components and reactions in the model HC.

The catalyst complexes in the reactions are noted by X_i where i=0 to 2. The index zero is to identify the stable catalyst configuration being the dominant species in the bulk of the liquid.

Although the reaction cycle shown in Figure 3 comprises several equilibria the overall sequence reflects essentially an irreversible reaction. For the reversible reactions between X_0 and X_1 and between X_1 and X_2 the following equilibrium constants are defined:

$$K_{15} = \frac{k_1}{k_5} = \frac{c_{X_1}}{c_{x_0} \cdot c_A}$$

$$K_{24} = \frac{k_2}{k_4} = \frac{c_{X_2}}{c_{x_1} \cdot c_B} \qquad (2)$$

2.3. Model Bo

Assuming a single reaction as in model ABP the reaction rate expression is derived from the HC-model by a Bodenstein approximation in order to eliminate the concentrations of the catalytic intermediates. There are many options and assumptions to arrive at simplified expressions (Helfferich, 2001), here the choice has been made to assume quasi-stationary behaviour of the catalytic intermediates. Reduction of the network in Figure 3 to the single reaction A + B $\rightarrow$ P gives the reaction rate expression:

$$R = \frac{\frac{k_1 \cdot k_2 \cdot k_3}{k_5 \cdot (k_3 + k_4)} \cdot c_{cat} \cdot c_A \cdot c_B}{1 + \frac{k_1}{k_5} \cdot c_A + \frac{k_2 \cdot k_3}{k_5 \cdot (k_3 + k_4)} \cdot c_B + \frac{k_1 \cdot k_2}{k_5 \cdot (k_3 + k_4)} \cdot c_A \cdot c_B} \qquad (3)$$

The total catalyst concentration c_{cat} is assumed to be constant, the naming of the constants in this equation is identical to the constants in Figure 3.

2.4. Absorption model

To reduce the number of variables studied in the previously defined models a number of assumptions have been made:

- diffusion is described by Fick's laws; there are no convective contributions in the liquid phase to mass transport,
- the solvent is inert,
- the temperature is constant; heat effects of reactions and absorption are not included,
- the density of the liquid is constant,
- mass transfer resistance in the gas phase is negligible.

For the description of mass transfer the penetration theory according to Higbie is applied. The disadvantage of more complicated numerical calculations in the penetration theory in comparison to the film theory is compensated by more physically realistic descriptions (Versteeg et al., 1987). In the penetration theory the equation for a single diffusing and reacting component (i) is given by:

$$\frac{\partial c_i}{\partial t} = D_i \cdot \frac{\partial^2 c_i}{\partial x^2} + R_i \tag{4}$$

Initial condition: $t = 0$ and $x \geq 0$ $\quad c_i = c_{i,bulk}$ (5)

Boundary conditions: $t > 0$ and $x = \infty$ $\quad c_i = c_{i,bulk}$ (6)

$t > 0$ and $x = 0$ $\quad J_{i,gas} = J_{i,liquid}$ (7)

The second boundary condition states that the flux of component i in the gas phase is equal to the flux in the liquid phase. All concentration profiles and derived properties are evaluated at the end of the contact time, τ_p. The contact time for absorption according to the penetration model is related to the liquid mass transfer coefficient and the diffusion coefficient of component A:

$$\tau_p = 4 \cdot \frac{D_A}{\pi \cdot k_L^2} \tag{8}$$

For displaying concentration profiles in a more convenient way a scaling factor is applied. According to the penetration model of Higbie, the solution for a non-reacting diffusion system is given by Westerterp et al. (1990):

$$c_A(x,t) = c_{A,i} \cdot \left[1 - \mathrm{erf}\left(\frac{x}{2\sqrt{D_A \cdot t}} \right) \right] \tag{9}$$

Given some time t, the value of x for which the error function is close enough to unity to reduce the concentration of A to zero is not precisely determined. The value for which the error function is close to 0.99 is the square root of π and (by taking τ_p for t) a very simple expression is obtained for the scaling factor or penetration depth, δ_p:

$$\frac{\delta_p}{2\sqrt{D_A \cdot \tau_p}} = \sqrt{\pi} \tag{10}$$

Substitution of Eq. (8) for τ_p gives:

$$\delta_p = 4 \cdot \frac{D_A}{k_L} \tag{11}$$

A method presented by Cornelisse et al. (1980) is applied to solve the system of coupled non-linear parabolic partial differential equations. This approach is based on a three-point backward scheme for finite-differencing originally proposed by Baker and Oliphant (1960). For an efficient use of grid point allocation, transformation of both the time and spatial variables has been applied (Versteeg et al.,1989). Further details on the implementation of the numerical methods can be found in Hoorn and Versteeg (2005).

The boundary conditions at $x=\infty$ are approximated by extending the grid to a depth in the liquid sufficiently larger than the penetration depth as defined by Eq. (11). Taking the range of the depth in the liquid as 5 times the penetration depth is assumed to be sufficient. This assumption is checked for each model calculation by inspection of the gradients near $x=5\cdot\delta_p$. The gas phase concentration is constant for a contact period τ_P therefore the enhancement factor is calculated according to:

$$E = \frac{\int_0^{\tau_p} -D \cdot \left.\frac{dc}{dx}\right|_{x=0} dt}{k_L \cdot \tau_P \cdot \left(c\big|_{x=0} - c_{bulk}\right)} \tag{12}$$

The gradient at x=0 is calculated from the numerical results for the concentrations at different grid points. The integral from 0 to τ_P is approximated by the summation of the gradients over all time steps (trapezium rule).

The reaction rate constants and diffusion coefficients have been varied. Where not indicated otherwise, a default value for reaction rate constants has been applied at $k_i = 10^5$ m^3/kmol/s (i=1,2) or $k_i = 10^6$ s^{-1} (i=3,4 or 5). All diffusion coefficients have been given values of $1 \cdot 10^{-9}$ m^2/s. Other parameter values have been kept constant to keep the number of variations within reasonable proportions. The gas phase concentrations and gas-liquid partition coefficients were kept constant as well as the liquid phase concentrations at t=0 and in the liquid bulk. All mass transfer coefficients were kept constant as well. For k_g the value was chosen sufficiently high to eliminate gas film resistances (e.g. 100 m/s). The liquid side mass transfer coefficient k_l has been fixed at $5 \cdot 10^{-5}$ m/s as a typical value for gas-liquid reactors. All default input parameters are listed in Table 1. The number of spatial grid points has been set to 800 for all simulations. The number of grid points for the time coordinates was set to 600.

Table 1. Default parameter values for model simulations.

Model	Component	Gas phase concentration C_g (kmol/m^3)	Liquid phase concentration C (kmol/m^3)	Solubility coefficient mgl (-)
ABP, Bo	A	1	10^{-40}	3
	B	10^{-40}	2	10^{40}
	P	10^{-40}	10^{-40}	10^{40}
HC	A	1	10^{-40}	3
	B	10^{-40}	2	10^{40}
	P	10^{-40}	10^{-40}	10^{40}
	X_0	10^{-40}	0.0001	10^{40}
	X_1	10^{-40}	10^{-40}	10^{40}
	X_2	10^{-40}	10^{-40}	10^{40}

For displaying convenient values in graphs the concentrations are scaled. Components B and P are scaled by the initial concentration of B, whereas A is scaled with equilibrium interface concentration of A (all indicated with c_0). The catalytic intermediates are scaled by the total catalyst concentration (c_0 or $c_{x,0}$).

3. Results simulations

3.1. Irreversible reaction system

3.1.1. Influences of rate constants

When the reaction rate constants of reactions 4 and 5 in the HC-model are kept sufficiently small, i.e. $k_i = 10^{-2}$ s^{-1}, the reaction cycle shown in Figure 3 can be regarded as irreversible. The calculated enhancement factor as function of k_1 while k_2 and k_3 have been fixed to values of 10^{10} is shown in Figure 4. The results obtained by application of the ABP-model is also plotted in Figure 4. The enhancement factor at infinitely fast reaction is for both models equal to 40.8.

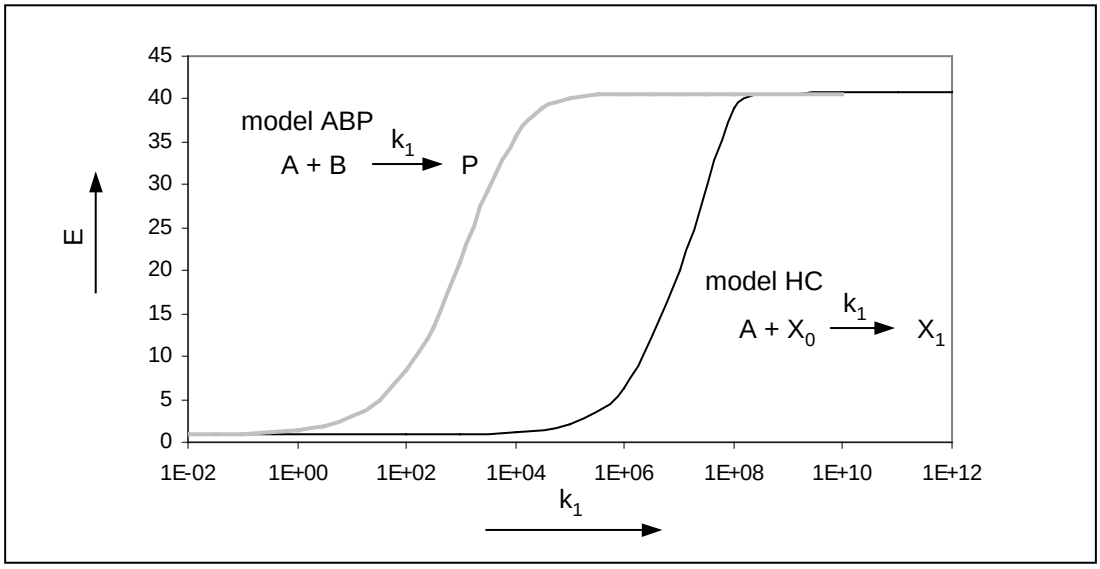

Figure 4. Enhancement factor as function of the rate constant for model HC and model ABP.

The shift in the curves in the direction of k_1 for model HC versus model ABP in Figure 4 corresponds to the concentration of the initial total catalytic intermediate concentration, e.g. $k_1(ABP) = c_{x,0} \cdot k_1(HC)$. A few number of concentration profiles corresponding to points in Figure 4 for the HC-model are given in Figure 5.

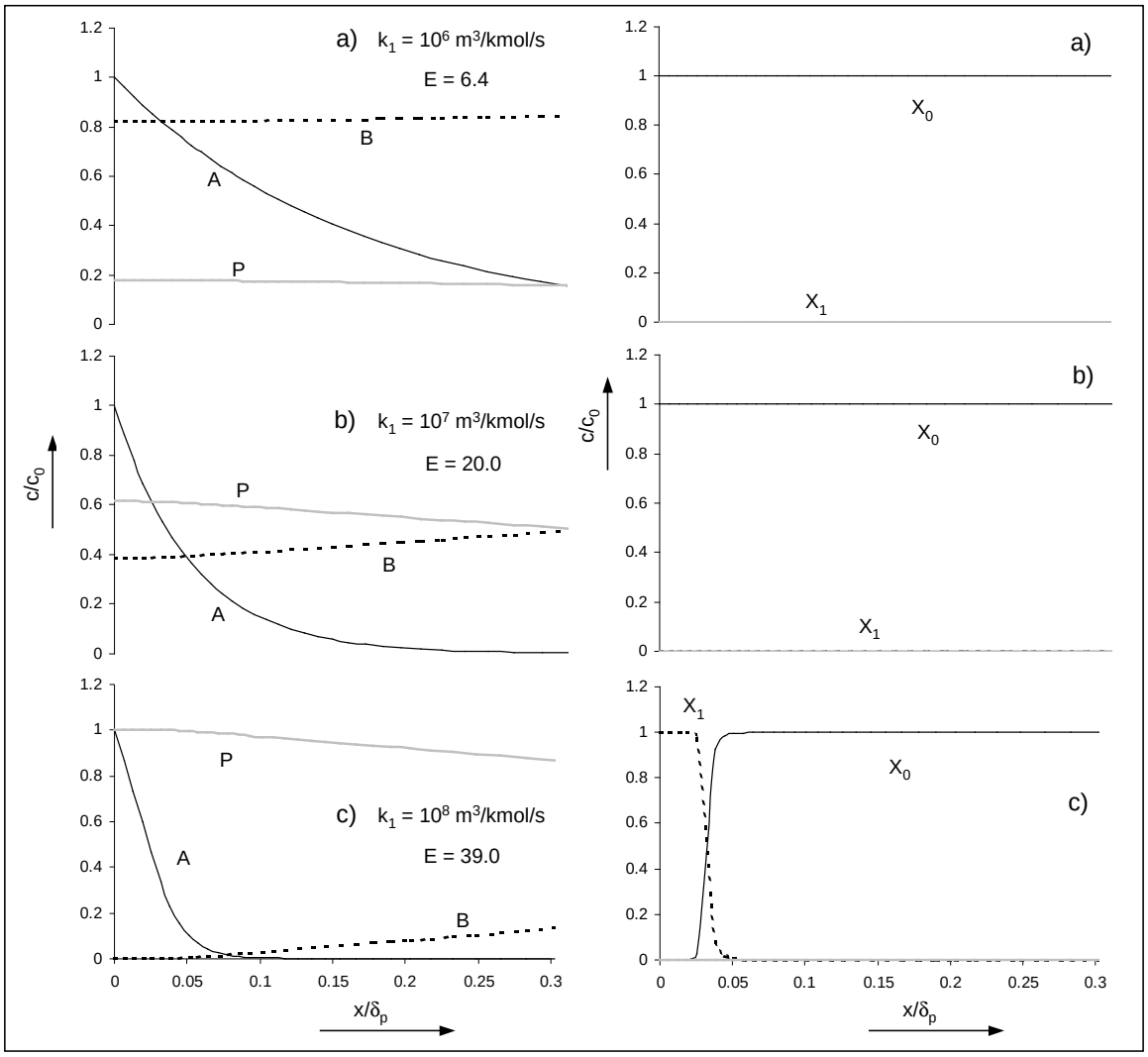

Figure 5. Concentration profiles at the end of the contact time τ_p for different values of k_1.

Already at low values for k_1 the absorption of A is enhanced but there is not much effect on the profiles of B and P (Figure 5a). Concentrations of B are non-zero throughout the penetration depth and the concentration gradients for P are quite small. All catalytic species are in the form of X_0. When A diffuses into the liquid it reacts with X_0 to form X_1, but as the succeeding reactions are (much) faster X_0 is formed very quickly again out of X_1 via X_2 (not present in significant amounts). Upon increasing the value to $k_1 = 10^7$ m^3/kmol/s the concentration of B near the interface is gradually reduced and the concentration of P increases (Figure 5b). The ratios between the catalytic intermediates remain unaffected. Increasing k_1 by another factor of 10 the enhancement factor for A approaches the value for infinitely fast reaction; 39.0 compared to 40.8. In this situation the concentration of B near the interface is practically zero and X_1 is the dominant catalytic intermediate in this region (Figure 5c).

The intermediate X_2 is still only present in very low concentrations all through the liquid because the reaction to X_0 remains very fast (high value for k_3). For values of k_1 higher than 10^8 m^3/kmol/s the profiles do not change a lot, the enhancement factor increases gradually with k_1 to the limit value of 40.8.

Given the values in Figure 5 and varying k_2 instead of k_1 (k_1 fixed at 10^{10} m^3/kmol/s) the results are comparable to those in Figure 5. The enhancement factor at high reaction rate is almost identical: 40.7. The profiles for A, B and P are similar and the concentrations of X_2 are also low. The ratio between X_0 and X_1 is different, however (Figure 6).

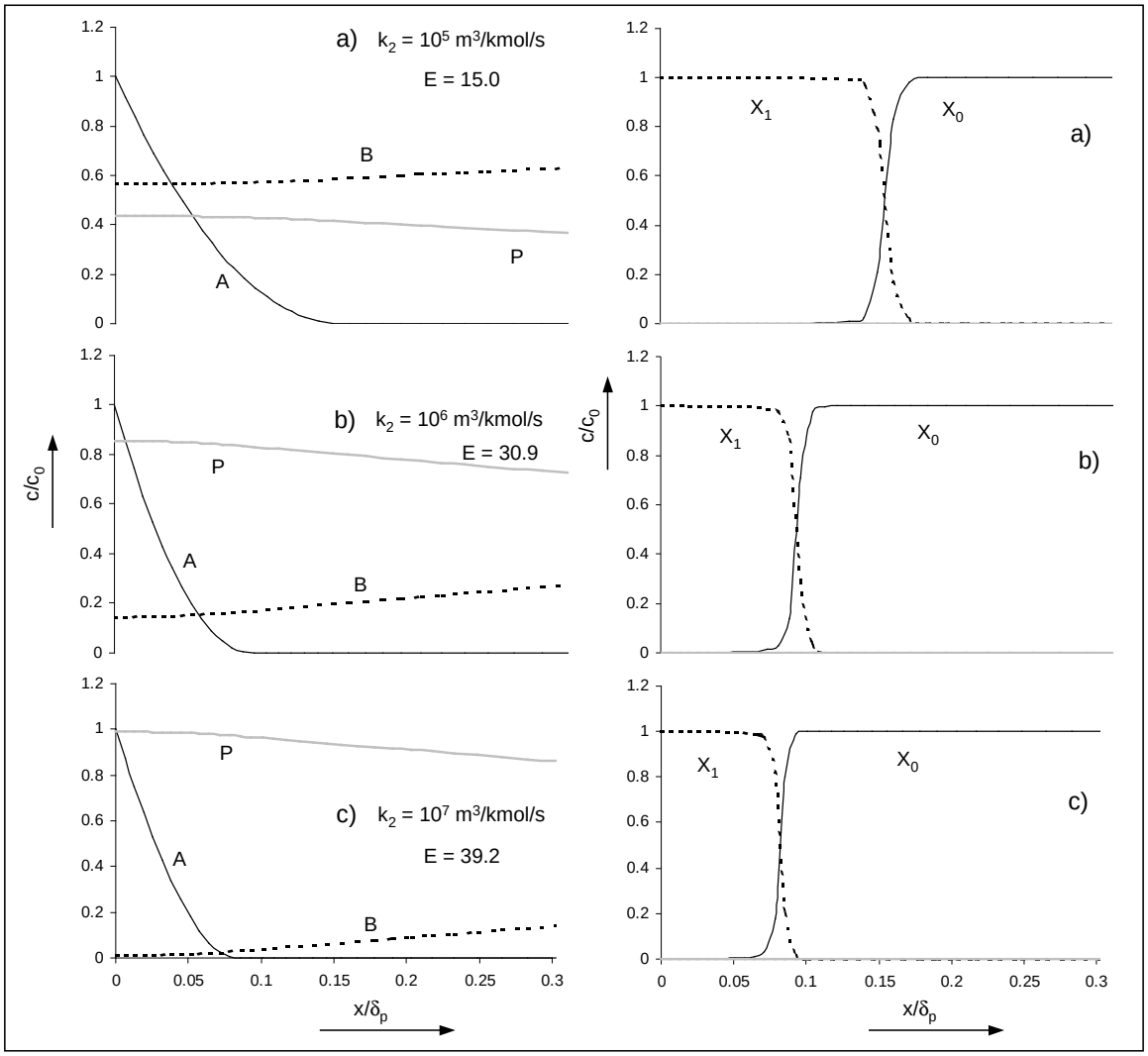

Figure 6. Concentration profiles at the end of the contact time τ_p for different values of k_2.

In Figure 6 it is clear that with all k_2 values two regions in the penetration area are present with different intermediates as the dominant species.

As k_2 increases the front between X_0 and X_1 does not change in shape but the position in the liquid is shifted towards the G/L interface (Figures 6a and 6b). Because of the high value for k_3, the intermediate X_2 is rapidly converted to X_0 and therefore concentrations of X_2 are low throughout the liquid. In the area where A diffuses into the liquid X_0 reacts with A to form X_1, hence X_1 is the dominant reactive intermediate near the interface. The bulk of the liquid contains only X_0 so there has to be a location where the ratio of the two intermediates is inverted. By increasing k_2 the reaction rate towards X_0 (via X_2) is increased thereby shifting the concentration profiles of A as well as X_0 towards the interface.

The concentration of X_2 can have noticeable values when k_3 is varied and k_1 and k_2 are kept constant at 10^{10} m^3/kmol/s, see Figure 7. The maximum attainable enhancement factor at high reaction rate is also 40.7.

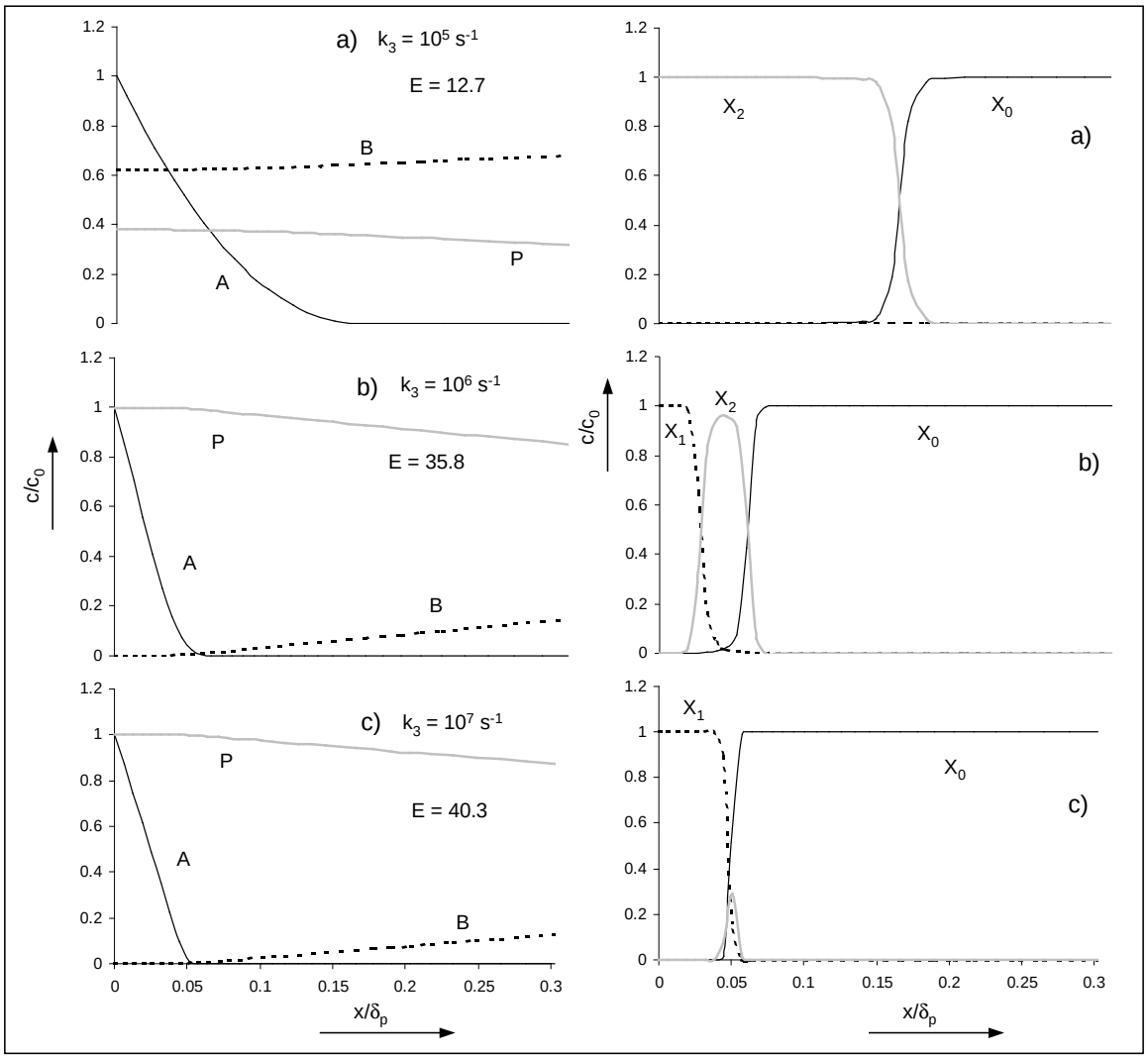

Figure 7. Concentration profiles at the end of the contact time τ_p for different values of k_3.

In Figure 7a (low values of k_3) the dominant intermediates are X_0 and X_2 since by the high value of k_2 X_1 reacts very fast to X_2 while the concentration of B is sufficiently high. For high values of k_3 the concentration of X_2 becomes low because the conversion of X_2 into X_0 is increased while the formation of X_2 is decreased because the concentration of B is reduced at the same time (Figure 7c). For intermediate values of k_3 the circle is more balanced leading to the occurrence of all the three intermediates (Figure 7b). The flux of A as function of k_3 as shown in Figure 8 is similar in shape to the enhancement factor (Figure 4). This is expected from Eq. (12) since k_L and Δc have equal values in calculating the enhancement factor and the flux.

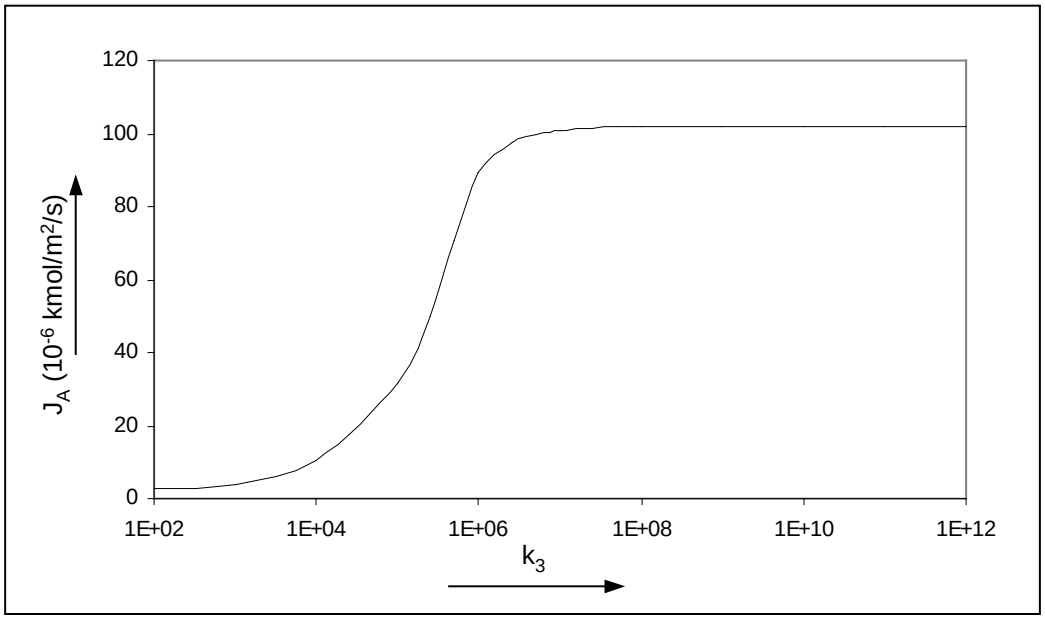

Figure 8. Flux of A across the G/L interface as function of k_3.

3.1.2. Influence of diffusion

The shape of the catalytic intermediate profiles is affected by differences in diffusivity of the intermediates. A number of case studies with varying diffusion coefficients were evaluated on basis of a single set of kinetic parameters (k_1,k_2 = 10^{10} m^3/kmol/s, k_3 = 10^{10} s^{-1}, k_4,k_5 = 10^{-2} s^{-1}). In Figure 9 the concentration profiles for the intermediates are shown where the diffusion coefficients of three intermediates have been alternating set to a lower value while keeping the others at default.

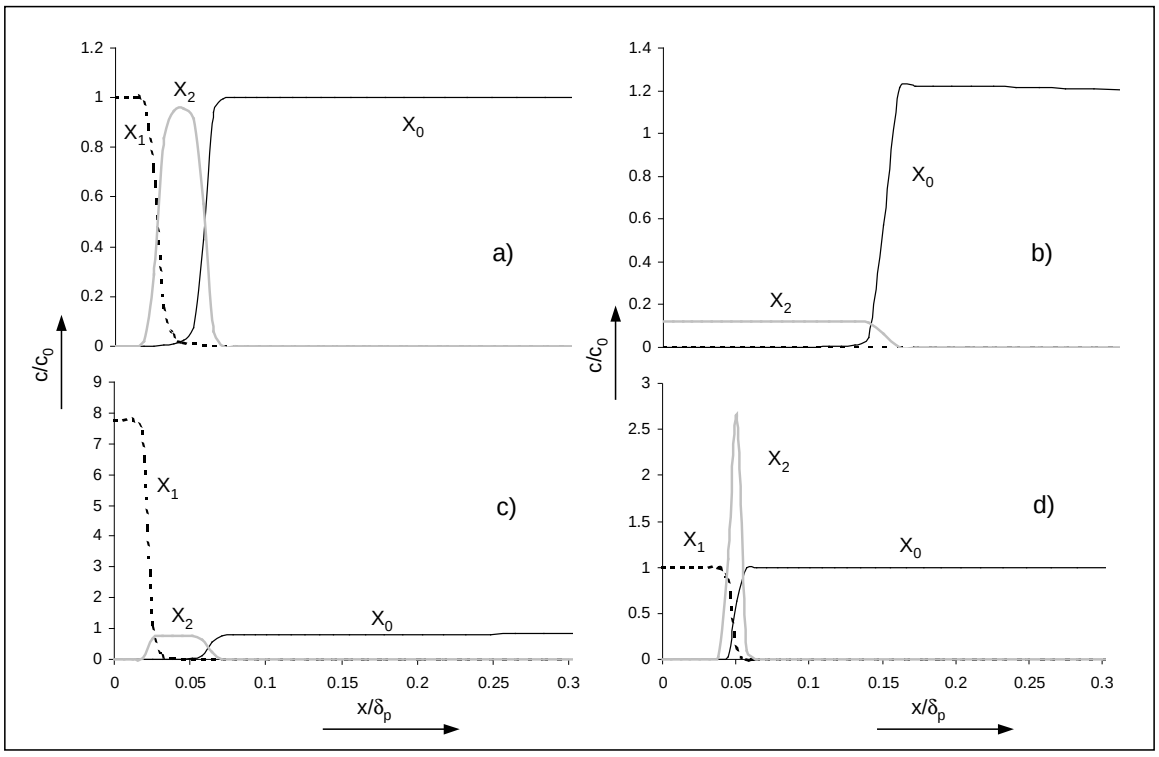

Figure 9. Concentration profiles at the end of the contact time τ_p with varying diffusion coefficients; a) default; b) $D_c(X_0) = 10^{-10}$ m²/s; c) $D_c(X_1) = 10^{-10}$ m²/s; d) $D_c(X_2) = 10^{-10}$ m²/s.

Note that the scaling of the c/c_0-axis in Figure 9 are not equal to the preceding Figures. The catalytic intermediate with the lowest diffusion coefficient locally builds up a concentration that is higher than the initial total concentration of catalyst. The shifts in the positions of the switches between the catalytic intermediates suggest that also in the enhancement factors differences might occur. For the default case as well as with $D_c(X_1) = 10^{-10}$ m²/s (Figures 9a and 9c) the enhancement factor is equal to 35.8. With $D_c(X_0) = 10^{-10}$ m²/s the enhancement factor is significantly lowered to E = 15.1. In contrast, the lowering of $D_c(X_2)$ to 10^{-10} m²/s results in an increase in the enhancement factor to E = 40.0. The observation that with $D_c(X_1) = 10^{-10}$ m²/s (Figure 9c) the enhancement factor is identical to the default case is not surprising since X_1 as dominant species near the G/L interface is not involved in the reaction with A. The decrease in E with $D_c(X_0) = 10^{-10}$ m²/s is caused by the reduction in concentration near the G/L interface (Figure 9b). The intermediates X_1 and X_2 diffuse in the direction of the bulk of the liquid, at the point where A diminishes to zero the reaction cycle stops at X_0 and since this intermediate has the lowest diffusion coefficient the diffusion rate of X_0 in the direction of the G/L interface is much smaller than the supply of X in the form of X_1 and X_2. The slight increase in the enhancement factor in case of $D_c(X_2)$ to 10^{-10} m²/s is more difficult to address (Figure 9d).

Probably the increase in concentration in X_2 is suitably located between X_1 at the G/L interface and X_0 in the liquid bulk thereby increasing the overall concentration of catalyst in the region where A penetrates into the liquid. In the alternate situation where the values for diffusion coefficients are chosen higher instead of lower the effects appear to be quite similar to those shown in Figure 9 but in the details differences exist, see Figure 10.

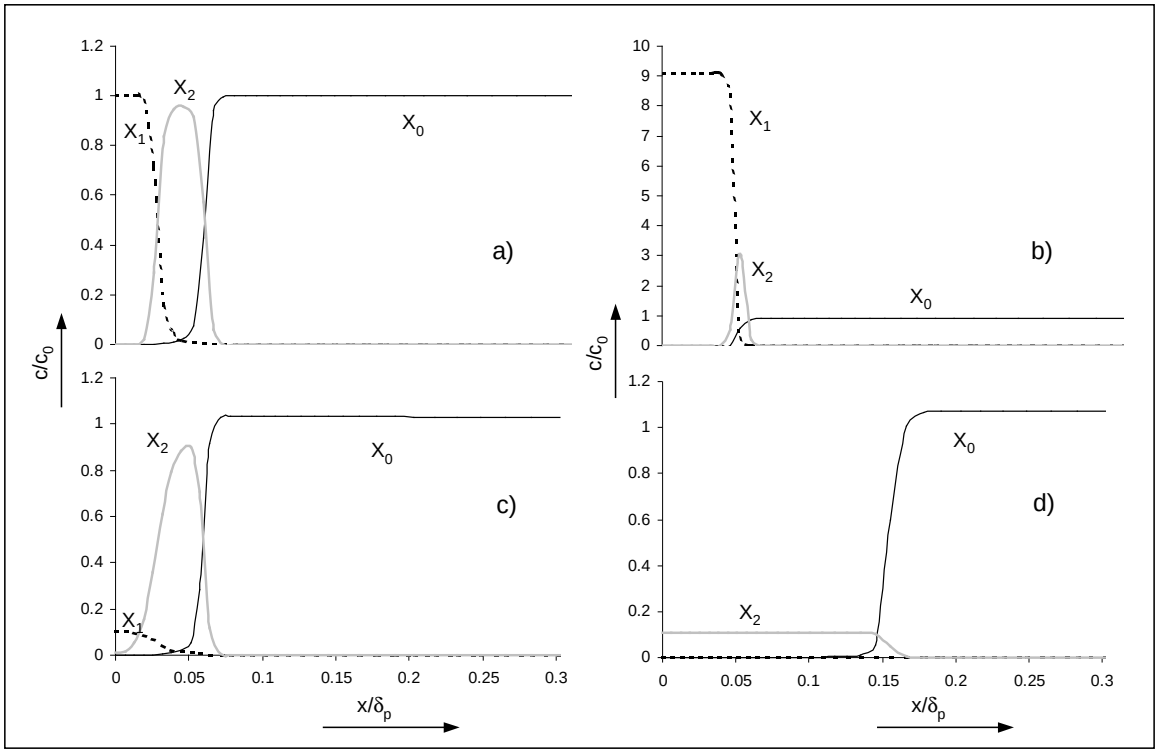

Figure 10. Concentration profiles at the end of the contact time τ_p with varying diffusion coefficients; a) default; b) $D_c(X_0) = 10^{-8}$ m^2/s; c) $D_c(X_1) = 10^{-8}$ m^2/s; d) $D_c(X_2) = 10^{-8}$ m^2/s.

In case $D_c(X_0) = 10^{-8}$ m^2/s (Figure 10b) the diffusion of X_0 in the direction of the G/L interface is larger than the diffusion of X_1 and X_2 in the opposite direction, therefore the concentrations of the latter two intermediates are increased. The enhancement factor is increased with respect to the default case (E = 40.2 versus 35.8). The profile in Figure 10c is a result of the high diffusivity of X_1: near the interface the concentration of X_1 is lowered by the diffusion in the direction of the liquid bulk. This diffusion is not balanced by X_0 and X_2. However, the enhancement factor is hardly effected by the changes in profile. The explanation is identical to the discussion with Figure 9c: since X_1 as dominant species near the G/L interface is not involved in the reaction, the enhancement of the absorption of A is not affected. The enhancement factor for the profiles in Figure 9d is significantly lower at E = 13.5.

Figure 10d ($D_c(X_2) = 10^{-8}$ m^2/s) is quite similar to Figure 9b ($D_c(X_0) = 10^{-10}$ m^2/s). While in both simulations the concentrations of X_1 in the liquid are close to zero, the rate of the catalytic cycle is determined only by X_0 and X_2 and apparently in this situation the ratio between the diffusion coefficients is more important than the absolute values.

3.1.3. Simplification

Frequently, reaction rate expressions for homogeneous catalysed systems are simplified by inclusion of the catalyst concentration in the rate constant. As illustration of this method Figure 11 shows the enhancement factors calculated by the HC-model in comparison to model ABP with application of the transformation $k_1(ABP) = c_{x,0} \cdot k_1(HC)$, as was already mentioned with Figure 4.

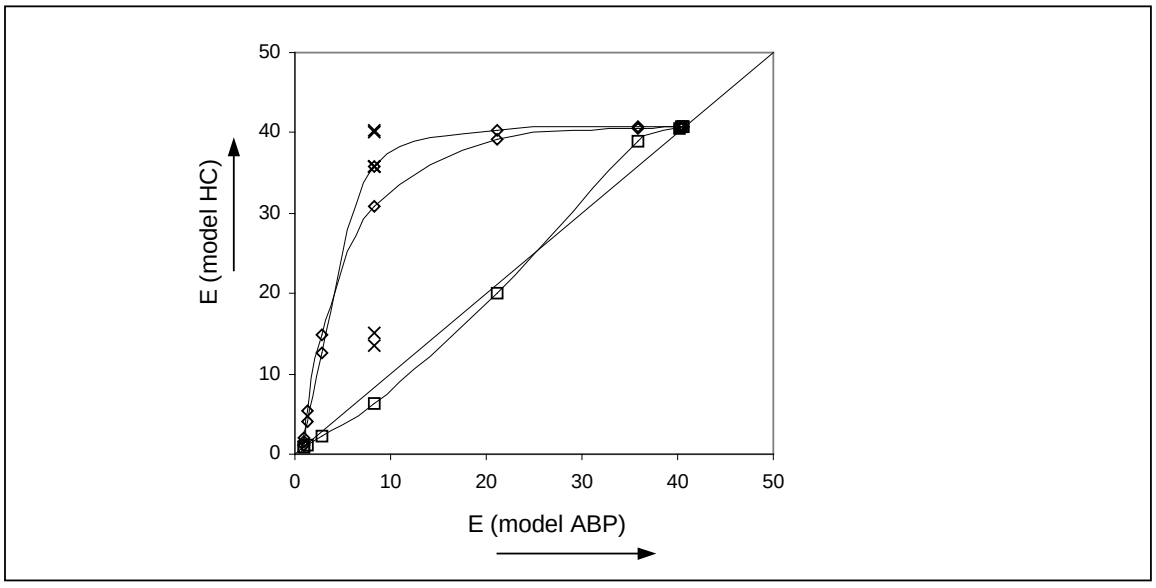

Figure 11. Enhancement factors for model HC compared to model ABP with correlation for k_1 by means of catalyst concentration. Symbols refer to simulations shown in: Figure 5 (□); Figure 6 (◊); Figure 7 (Δ); Figure 9 (×); Figure 10 (×).

Figure 11 clearly shows that only for a limited number of system parameters the simplification on the catalyst concentration leads to acceptable estimations of the absorption rate.

3.1.4. Conclusion concerning irreversible reactions

In a complete irreversible catalytic cycle the variation of reaction rate constants determines the concentrations of all components including the catalytic intermediates. With the concentration profiles the enhancement of the absorption can be explained. In addition to the kinetics also differences in the diffusivity of the catalytic intermediates can be involved. Simplification of systems of homogeneously catalysed reactions with mass transfer by means of incorporation of the catalyst concentration into the reaction rate constant could easily result in the prediction of erroneous absorption rates.

3.2. Effect of reversibility

3.2.1. Influences of rate constants

It is well known from literature that reversibility of reactions has a significant effect on the mass transfer rate of an absorbing reactant (Versteeg et al., 1989). To study this effect quantitatively the simulations for the HC-model where k_3 was varied (results shown in Figure 7) were carried out with several values for k_4 and k_5, see Figure 12. The rate constants k_1 and k_2 were fixed at 10^{10} m^3/kmol/s and k_4 and k_5 were translated to the corresponding equilibrium constants. In addition, the profiles of the catalytic intermediates for a selected value of k_3 (where the differences in E are maximum) are shown in Figure 13.

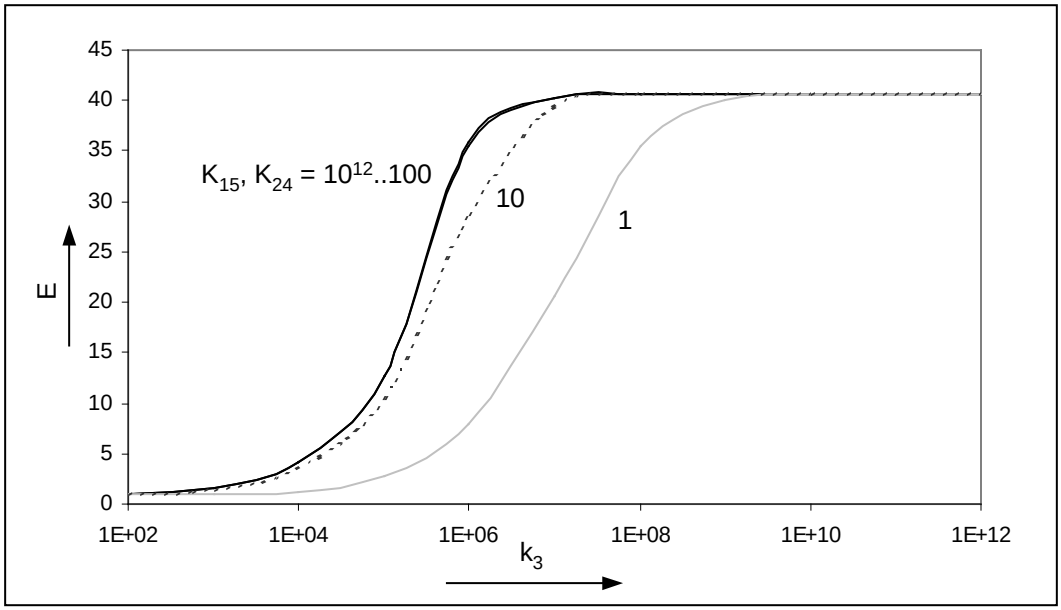

Figure 12. Enhancement factor as function of the rate constant for the reaction $X_2 \rightarrow X_0 + P$ for various equilibrium constants.

As is observed from Figure 12 for values of K_{15} and K_{24} between 100 and 10^{12} m^3/kmol, the calculated enhancement factor is not affected. However, decreasing the equilibrium values below 100 m^3/kmol significant changes in the simulated values of the enhancement factor occur. Therefore, in line with previous published results (Versteeg et al., 1989), it can be concluded that lower values of the equilibrium constant result in a reduction of the enhancement factor. In Figures 13a and 13d the concentration profiles of the intermediate components are given for the irreversible (13a) and the reversible case (13d) respectively.

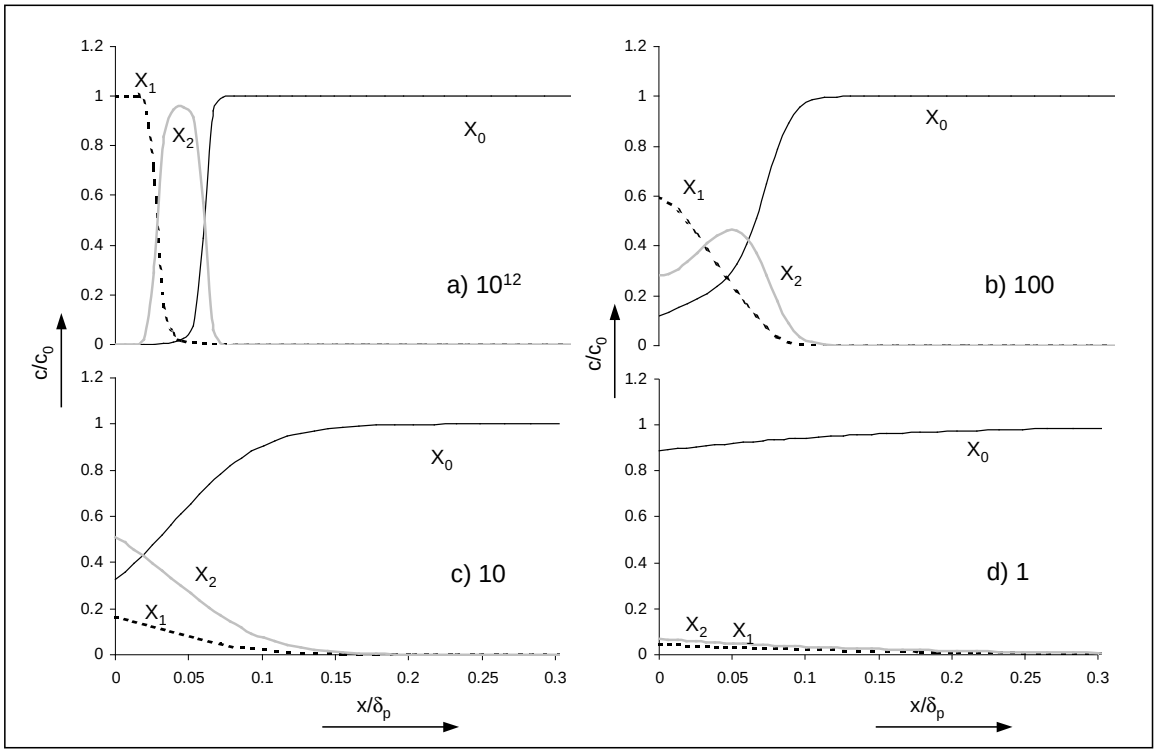

Figure 13. Concentration profiles for $k_3 = 10^6$ m^3/kmol/s with varying values of K_{15} and K_{24} as indicated.

Figure 13a is identical to Figure 7e and so the corresponding profiles for A, B and P could be found in Figure 7b. These profiles only change gradually when K_{15} and K_{24} are decreased from 10^{12} to 100. The position of the maximum in the concentration of X_2 does not vary either for these simulations. However, it can be seen in Figure 7b that the profiles are less steep and that the species X_0, X_1 and X_2 are occurring simultaneously over a wide range. Figure 13d is the representation of two fast reversible reaction sequences followed by R_3 as the rate-determining step.

The shifting of enhancement factors with k_3 as shown in Figure 12 also occurs with other reaction rate constants. In the following examples k_2, k_3 and k_4 have been fixed at various values as to keep the equilibrium between X_1 + B and X_2 constant. In Figure 14 k_2, k_3 and k_4 are set to 10^{10} creating a very fast equilibrium between X_1 + B and X_2 and a fast reaction from X_2 to X_1. The variation in k_5 ranges from 10^6 to 10^{11}. In Figure 14 the enhancement factor is shown as function of k_1.

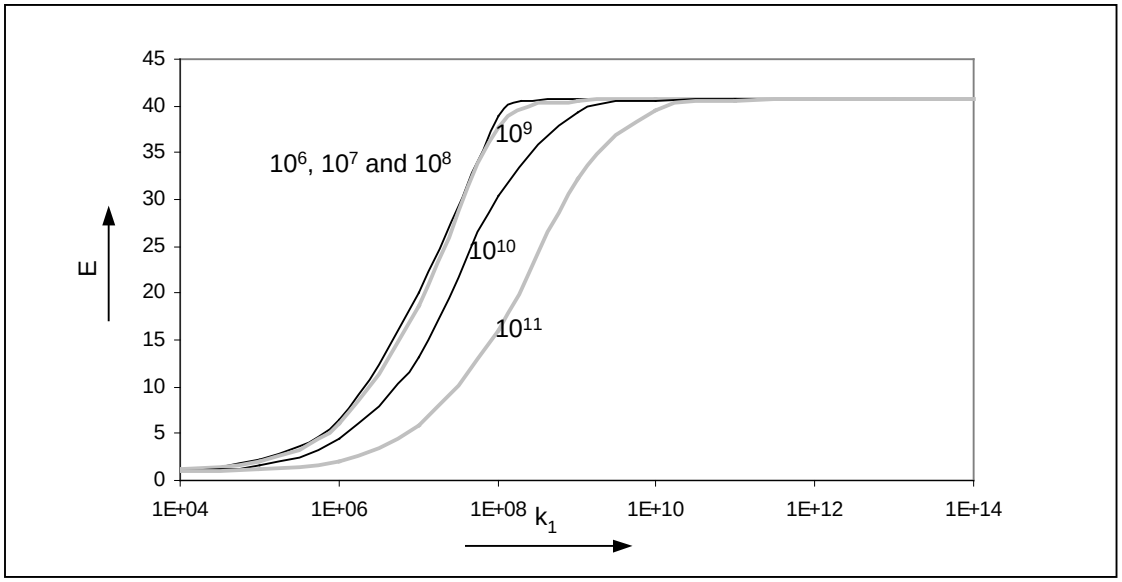

Figure 14. Enhancement factor as function of the rate constant for the reaction $X_0 + A \rightarrow X_1$ for various values of k_5 (indicated near the lines; k_2, k_3 and k_4 are equal to 10^{10}).

The shape of the enhancement curves is similar to earlier observations, i.e. Figures 4 and 12. Starting with $k_5 = 10^9$ s^{-1} and increasing it is observed that the value of the enhancement factor becomes smaller at identical values of k_1. This is no surprise as an increase in the rate of R_5 has to be compensated by a higher rate for R_1 to maintain the equilibrium. For values of k_5 lower than 10^8 s^{-1} there is no shift in the enhancement factors, in this regime the pathway towards X_0 is faster via X_2 (reaction R_2 and R_3) since the profiles for the concentration of B do not vary much as function of k_5. The equilibrium constant of the reaction between X_0 and X_1 can be expressed as the ratio of k_1 and k_5 and from Figure 14 it is concluded that E_∞ is independent of the value of the equilibrium constant. This is in contrast to the findings of the reversible system A + B $\leftrightarrow$ P where the E_∞ is a function of the equilibrium constant (Versteeg et al., 1989). The major difference between the straightforward reversible system and the reactions of model HC is that in the latter system one reaction is irreversible, therefore the catalytic cycle is not fully reversible and can not be represented by a single equilibrium from which the catalytic intermediates are eliminated.

Since Figure 14 suggests that the effect of the value of k_5 is also related to the size of the other rate constants, the simulation was repeated for k_2, k_3 and k_4 equal to 10^6. Results are shown in Figure 15.

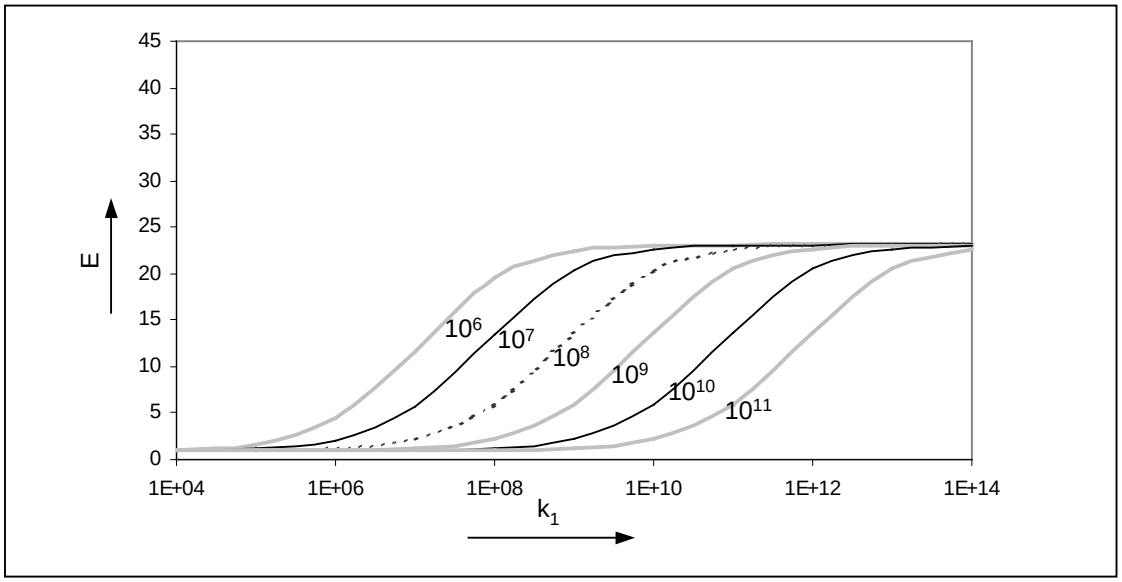

Figure 15. Enhancement factor as function of the rate constant for the reaction $X_0 + A \rightarrow X_1$ for various values of k_5 (k_2,k_3,k_4 = 10^6).

Comparing Figures 14 and 15, the reduction in E_∞ is immediately clear: the value is reduced from 40.8 to 23.1. Secondly, the distinction between low and high values for k_5 has disappeared from Figure 15 (it has been shifted to lower values than 10^6). When the pathway from X_1 to X_0 via X_2 is much slower than with Figure 14, the direct reaction by means of R_5 is the dominant pathway for the conversion of X_1 to X_0 hence any increase in k_5 can be compensated by a similar increase in k_1. The explanation for the reduction in E_∞ is less straightforward. Apart from the rate of the equilibrium between X_1 and X_2 (R_2 and R_4) the only difference between the simulations in Figures 14 and 15 is the constant k_3. To demonstrate the influence of k_3 more clearly, the results of a simulation with $k_3 = 10^{10}$ m^3/kmol/s are given in Figure 16. By increasing k_3 to 10^{10} the E_∞ is larger compared to Figure 15 (where $k_3 = 10^6$) but still not to the original level indicated by Figure 14.

The influence of the values of k_2 and k_4 is demonstrated by Figure 17 where calculated values for E_∞ as function of k_2,k_4 are given. The reaction rate constants k_1 and k_5 have been fixed at 10^{14} and 10^6 respectively to ensure that the asymptotic solution of E_∞ is reached (this has been verified by comparison of the result for $k_1 = 10^{12}$; in none of the parameter combinations the enhancement factor differed by more than 0.05%).

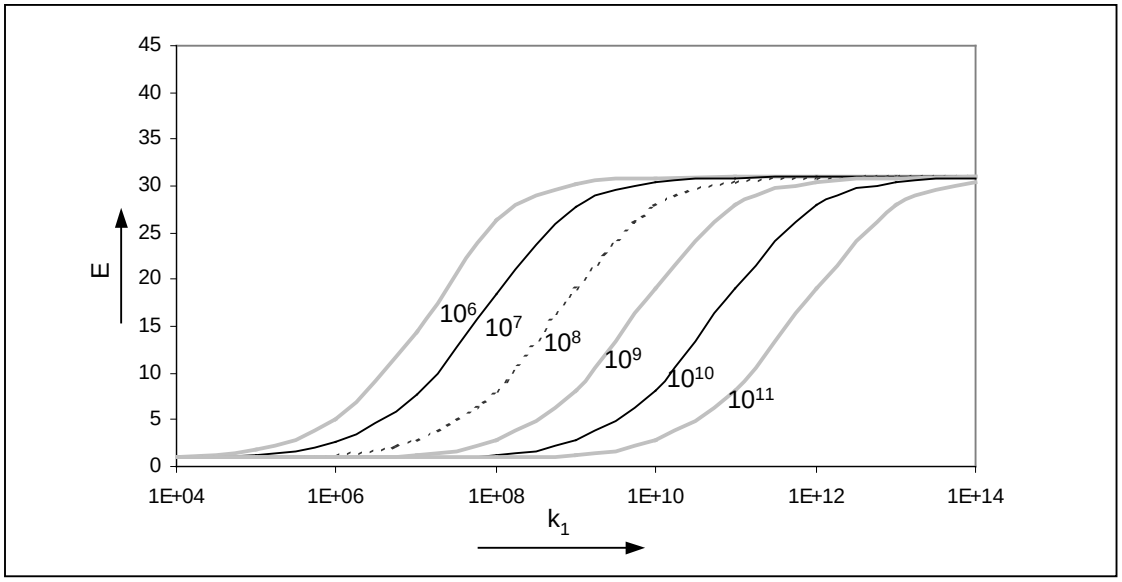

Figure 16. Enhancement factor as function of the rate constant for the reaction $X_0 + A \rightarrow X_1$ for various values of k_5 (k_2,k_4 = 10^6; k_3 = 10^{10}).

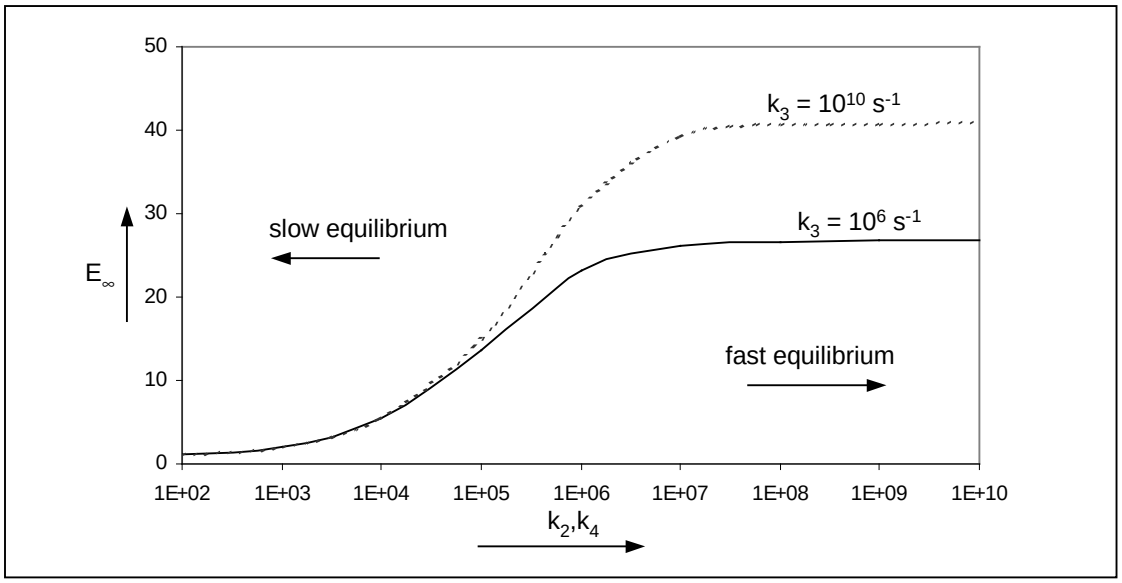

Figure 17. Enhancement factor at infinitely fast reaction for $X_0 + A \rightarrow X_1$ as a function the rate of the equilibrium of R_2 and R_4.

Figure 17 is presenting different information compared to the preceding Figures. In Figure 17 the influence of rate constants on E_∞ is elucidated. The values of k_2 and k_4 affect E_∞, for k_2 and k_4 lower than 10^5 s^{-1} variation of k_3 has no effect on the enhancement factor implicating that the enhancement of the absorption of A by the catalytic cycle is completely dominated by the rate of the equilibrium reactions R_2 and R_4. At values for k_2 and k_4 higher than 10^6 s^{-1} the maximum absorption rate of A is determined by the rate of reaction R_3.

3.2.2. Influence of diffusion

The diffusivity of the catalytic intermediates also influence the extend of the E_∞ as is shown in Figure 18. The two curves shown in Figure 17 have been included in Figure 18 as well as a reference (indicated by the symbols). In line with the simulations of Figure 10 the diffusion coefficients of the catalytic intermediates have been lowered in alternating fashion. The values for the rate constants other than given in Figure 18 were set at $k_1 = 10^{14}$ m^3/kmol/s and $k_5 = 10^6$ s^{-1} making the reaction between X_0 and A very fast en irreversible. The diffusion coefficients of the components and the other catalytic intermediates were kept constant at 10^{-9} m^2/s.

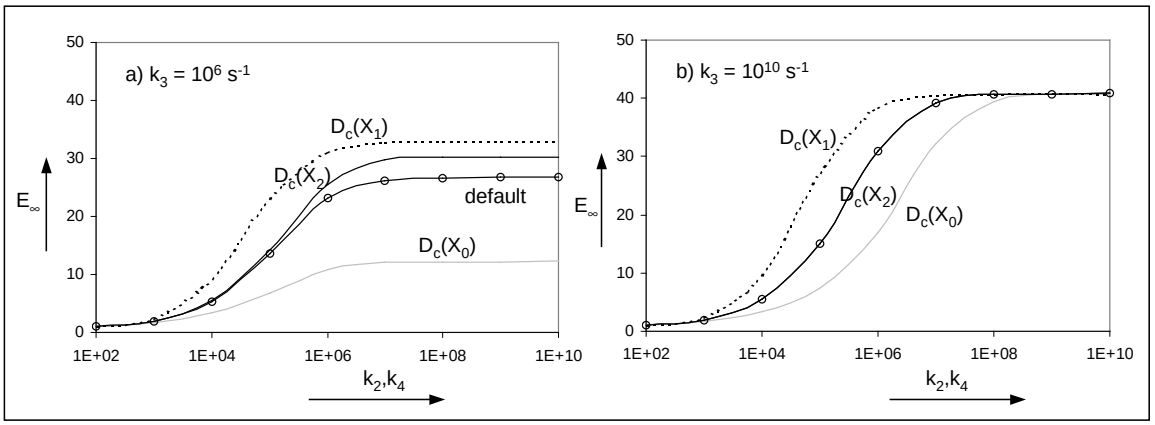

Figure 18. Enhancement factor at infinitely fast reaction for $X_0 + A \rightarrow X_1$ as a function the rate of the equilibrium of R_2 and R_4 evaluated for alternating lowered diffusion coefficients of catalytic intermediates compared to default (default is 10^{-9} m^2/s, the lower values of 10^{-10} m^2/s are valid for the intermediates as indicated).

As it is clear from Figure 18, E_∞ depends on the value of k_3. For the lower k_3 it is observed that the E_∞ for a lower $D_c(X_0)$ decreases and E_∞ increases with lower $D_c(X_1)$ and $D_c(X_2)$ while between the latter two also a small difference exists. This is in line with the findings in the irreversible system so it is likely that the mechanisms leading to these observations must be similar. Decreasing $D_c(X_0)$ has the effect that the concentrations X_1 and X_2 near the G/L interface decrease, on the other hand decreasing $D_c(X_1)$ or $D_c(X_2)$ leads to effectively higher concentrations of the corresponding intermediates in the absorption region for A. When the concentration of X_2 changes the reaction rate of R_3 changes and because the value of k_3 is small compared to the other kinetic constants R_3 is the rate-determining factor in the overall catalytic cycle.

With k_3 equal to 10^{10} the reaction R_3 is no longer the rate-determining step and E_∞ is only determined by the R_2/R_4 equilibrium. For high values of k_2 and k_4 there is no effect of the diffusivity of the catalytic intermediates because all the reaction steps in the cycle are very fast and a lower diffusivity of one of the intermediates is compensated by the others. For lower values of k_2 and k_4 the effects are identical to the observations with $k_3 = 10^6$ with the exception of the lower $D_c(X_2)$; the curve is exactly equal to the default case. While R_3 is very fast X_2 is almost instantaneously converted to X_0 and since this intermediate has a default diffusion coefficient there is no net effect.

For simulations with $D_c = 10^{-8}$ m^2/s, the results and effects are in line with those presented in Figure 18 and Figure 10 and therefore will not be discussed in detail.

3.2.3. Conclusion concerning reversibility

The occurrence of reversible reactions in the catalytic cycle has a profound effect on the absorption rate of the gaseous reactant. Not only the location of the equilibrium is important but also the rate of the equilibrium effects the absorption rate. The importance of the diffusion of the catalytic intermediates is comparable to the irreversible reaction system, however the explanation of the shifts in enhancement factors is more complicated.

4. Simplified models for design

In the following section, it is assumed that model HC represents the exact kinetic mechanism of a virtual process. The results from the simplified models ABP and Bo will be reflected on the predictions for the HC-model. It must be noted, however, that the scheme ABP is the exact representation of the irreversible molecular reaction scheme without homogeneous catalysis.

4.1. Model Bo

In the simulations with model HC leading to the results shown in Figures 14, 15 and 16 the effect of K_{15} on the absorption rate has been studied in relation to the other reaction rates. These simulations have been repeated with the Bo-model. Since the kinetic parameters between the models are equal, the calculated enhancements factors can be directly compared. The fit of the Bo-model in the range of applied parameters agrees very good to the results of the HC-model. The average deviation between the E-values is 0.16% while the maximum observed deviation is 0.30%.

As was noticed from the results shown in Figures 10 and 11 differences in diffusion coefficients can have significant influence on the total concentration distribution of the catalytic intermediates as well on the enhancement of the rate of absorption. As in the model Bo the intermediate species have been eliminated out of the kinetic rate expressions by application of the Bodenstein principle this model is a good test case to study the diffusion effects. For that, the results for the Bo-model are compared with the E_∞ values obtained with the HC-model in Figure 18. Because the results for the Bo-model match the default ($D_c = 10^{-9}$ m^2/s) case of the HC-model very well, Figure 18 is not only a graph for model HC with varying diffusion coefficients but represents the differences between model Bo and model HC as well. To express the differences in a more direct fashion, the equivalent parity plot is given in Figure 19.

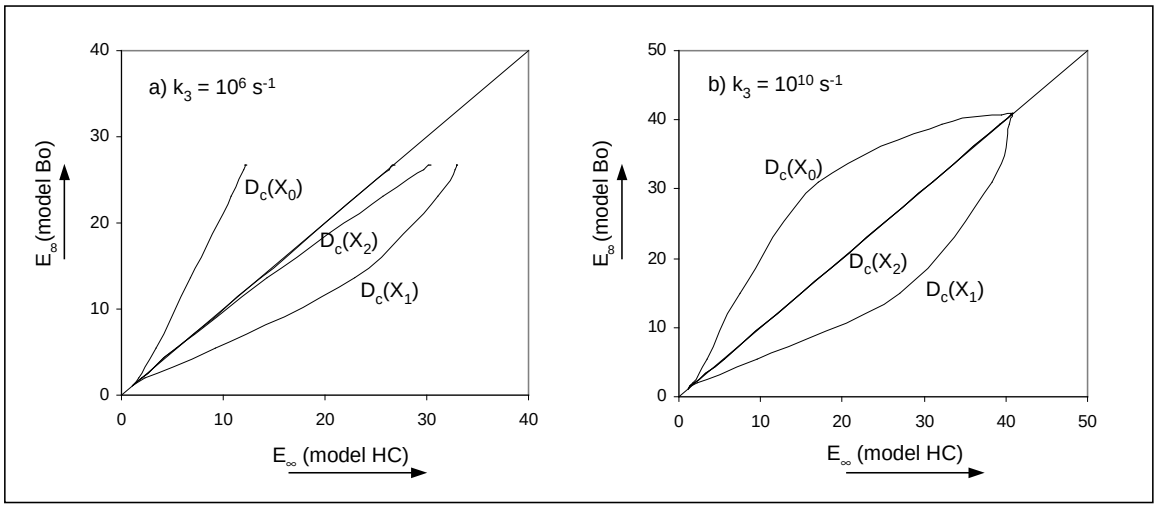

Figure 19. Parity plot of the enhancement factor at infinitely fast reaction for $X_0 + A \rightarrow X_1$ of model Bo as function of the values calculated by model HC. Evaluations for alternating lowered diffusion coefficients of catalytic intermediates compared to the default (default is 10^{-9} m^2/s, the lower value of 10^{-10} m^2/s indicated by the labels).

Figure 19 clearly indicates that for deviating diffusion coefficients the Bodenstein approximation leads to erroneous enhancement factors. Only when the diffusion of the catalytic intermediates is not important (see the discussion in 3.2.2), application of the Bodenstein approximation leads to accurate predictions.

4.2. Model ABP

Despite having the most simple expression for the reaction rate, the results for model ABP are more difficult to compare to the HC-model because the number of kinetic parameters does not match between the models. In a previous paper (Hoorn and Versteeg, 2005) it was shown that for some type of reaction networks the kinetic parameters of the reactions forming the principle pathway in the network of the detailed model can be compared with a simpler model by means of 3D-plots. This strategy is of limited use here because reversible reactions are involved in the HC-model. Except for the case of irreversible reactions where the catalytic cycle comprises in effect three reactions. Then, the enhancement factor as function of two of the three kinetic rate constants can be compared with the enhancement factor calculated by the ABP-model. An alternative approach to compare model ABP with model HC is derived from the realization that the characteristics of the Bo-model lie between those of the models ABP and HC. Because of the very good match between the Bo-model and the HC-model the results for model ABP can be compared to both models. Through the proper choice of k_1 in model ABP, the reaction rate calculated by the Bo-model (see Eq. (3)) matches the rate in the ABP-model quite closely. For simplification, Eq. (3) is put in the form of:

$$R = \frac{a_1 \cdot c_A \cdot c_B}{1 + a_2 \cdot c_A + a_3 \cdot c_B + a_4 \cdot c_A \cdot c_B} \qquad \text{with} \qquad a_1 = \frac{k_1 \cdot k_2 \cdot k_3}{k_5 \cdot (k_3 + k_4)} \cdot c_{cat}$$

$$a_2 = \frac{k_1}{k_5}$$

$$a_3 = \frac{k_2 \cdot k_3}{k_5 \cdot (k_3 + k_4)}$$

$$a_4 = \frac{k_1 \cdot k_2}{k_5 \cdot (k_3 + k_4)} \qquad (13)$$

Now, the k_1 in model ABP can be chosen as:

$$k_1 = \frac{a_1}{1 + a_2 \cdot c_A^* + a_3 \cdot c_B^* + a_4 \cdot c_A^* \cdot c_B^*} \qquad (14)$$

The principal method is to fix the concentrations c_A^* and c_B^* as reference concentrations. The choice for the reference concentrations determines the quality-of-fit between the reaction rate calculated by the Bo-model respectively the ABP-model, but the extend of this influence is variable because it depends on the value of the rate constants in the Bo-model (in the extreme when a_2 to a_4 are so small that all factors are much smaller than unity in the denominator of Eq. (14) the choice of c_A^* and c_B^* is arbitrary).

The enhancement factor as function of k_1 for model ABP is shown in Figure 4, so when k_1 has been calculated according to Eq. (14) the enhancement factor for the ABP-model is known and can directly be compared with E calculated for the Bo-model. The simulations with model HC leading to the results shown in Figures 14, 15 and 16 have been repeated with the ABP-model in addition to the already performed simulations with model Bo. After a few trails the reference concentrations were fixed at $c_A^* = 0.025$ kmol/m^3 and $c_B^* = 1.0$ kmol/m^3 (half the values for the interfacial respectively the bulk liquid concentration). The results for enhancement factors with model ABP compared to model Bo are shown in Figure 20.

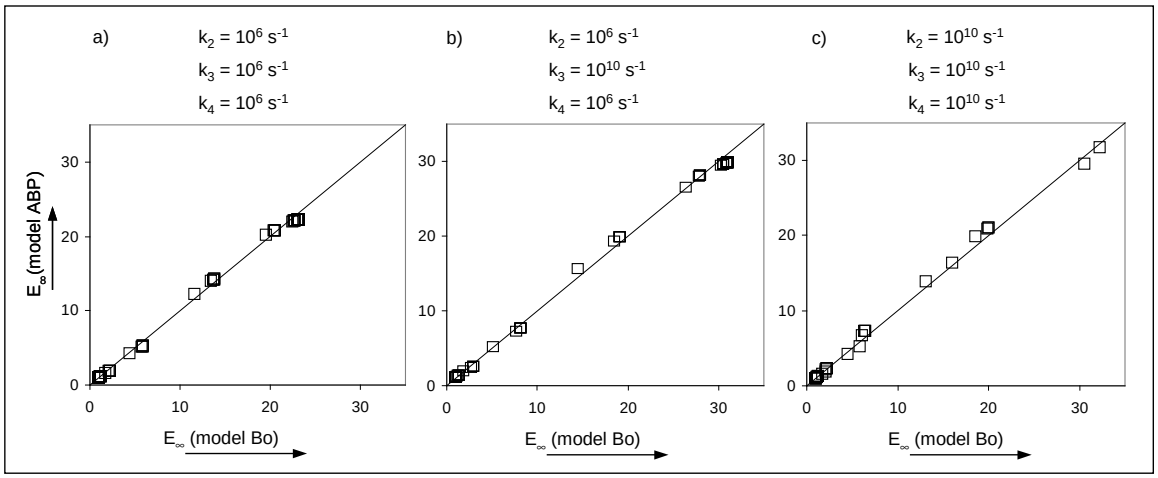

Figure 20. Parity plots of the enhancement factor for the reaction A + B → P of model ABP versus model Bo. Evaluations for varying values of k_1 ($10^2..10^{14}$ m^3/kmol/s) and k_5 ($10^6..10^{11}$ s^{-1}), $c_A^* = 0.025$ kmol/m^3 and $c_B^* = 1.0$ kmol/m^3.

The curve for E_∞ with all the diffusion coefficients equal to the default values of 10^{-9} m^2/s as performed with model HC (shown in Figure 18) repeated with model ABP with unaltered references gives also a reasonable agreement; the average difference in E-values is 7% with a maximum deviation of 20%.

4.3. Conclusion concerning model simplification

The Bodenstein approximation simplifies model HC to a large extend while the quality of the predictions remains very good. Only in case of changes in physical parameters that are not intrinsically present within the Bo-model, the fit of the Bo-model decreases. With the even more simple ABP-model the range in which accurate simulations for model HC are provided is limited, but the flexibility is good.

5. Conclusions

The mass transfer of a gaseous reactant into a liquid where the reactions are catalysed by homogeneous catalysts still offers challenges for chemists and chemical engineers. In this paper the diffusion-reaction equations according to Higbie's penetration theory have been numerically solved. The catalytic cycle of the reaction network comprised two equilibria and one irreversible reaction.

The least complicated case to study is when the equilibria are replaced with irreversible reactions. By varying a limited number of reaction rate constants several effects on the absorption rate of A have been observed. The variation of reaction rate constants determines the concentrations of all components including the catalytic intermediates and with the concentrations the enhancement of the absorption can be explained. In addition to the kinetics also diffusion can be involved, for example in case of differences in the diffusivity of the catalytic intermediates.

The occurrence of reversible reactions in the catalytic cycle has a profound effect on the absorption rate of the gaseous reactant. Not only the location of the equilibrium is important but also the rate of the equilibrium effects the absorption rate. The importance of the diffusion of the catalytic intermediates is comparable to the irreversible reaction system, however the explanation of the shifts in enhancement factors is more complicated.

Once a rigorous model for absorption with homogeneously catalysed reactions has been obtained the verification of simplified model versions is not difficult. It has been shown that with the Bodenstein approximation very good predictions for the absorption rates are obtained for a wide range of kinetic parameters. When the rigorous model contains physical parameters not included in the Bodenstein model the predictions are less reliable as for example in the case of deviating diffusivity's of the catalytic intermediates. The simple model $A + B \rightarrow P$ can be tuned to match the absorption rates as well as the Bodenstein model but the range of application for the parameters is limited. Simplification of systems of homogeneously catalysed reactions with mass transfer by means of incorporation of the catalyst concentration into the reaction rate constant could easily result in the prediction of erroneous absorption rates.

The catalytic system applied in this study is quite simple and extension of the reaction networks is one of the points of interest for further research. Also more complicated interactions of the catalytic intermediates such as ligand exchanges and deactivation are interesting from an industrial point of view. Finally, the study of the behaviour of a fully reversible catalytic cycle is the next step to be performed.

Nomenclature

Notation

c	concentration
D, D_c	diffusion coefficient
E	enhancement factor
E_∞	enhancement factor at infinitely fast reaction
J	flow across gas-liquid interface
k	reaction rate constant
k_g	gas side mass tranfer coefficient
k_L	liquid side mass transfer coefficient
mgl	solubility coefficient defined as c_{liquid}/c_{gas}
R	reaction rate
t	time variable
x	spatial variable

Greek

δ_p	penetration depth
φ	Hatta number
τ_p	contact time

Sub- and superscripts

bulk	liquid bulk
gas, liquid	phase
cat	catalyst
i	any component
j	any reaction

Abbreviations

A	gas phase reactant
B	liquid phase reactant
P	liquid phase product
X_0	catalytic complex
X_1	catalytic complex
X_2	catalytic complex

References

Baker, G.A., Oliphant, T.A., (1960), An implicit, numerical method for solving the two-dimensional heat equation, *Quart. Appl. Math.* **17**, 361-373.

Cavalieri d'Oro, P., Raimondi, L., Pagani, G., Montrasi, G., Gregorio, G., Adreetta, A., (1980), Propene hydroformylation with rhodium carbonyls and triphenylphosphine. II - Kinetics of butyraldehydes formation, *La chimica e l'industria* **62**, 572-579.

Cornelisse, R., Beenackers, A.A.C.M., van Beckum, F.P.H., van Swaaij, W.P.M., (1980), Numerical calculation of simultaneous mass transfer of two gases accompanied by complex reversible reactions, *Chem. Eng. Sci.* **35**, 1245-1260.

Halpern, J., Wong, C.S., (1973), Hydrogenation of tris(triphenylphosphine)chlororhodium(I), *J. Chem. Soc. Chem. Comm.*, 629-630.

Halpern, J., Okamoto, T., Zakhariev, A., (1976), Mechanism of the chlorotris(triphenylphosphine) rhodium(I) catalyzed hydrogenation of alkenes. The reaction with of chlorodihydridotris(triphenylphosphine)rhodium(III) with cyclohexene, *J. Mol. Cat.* **2**, 65-68.

Halpern, J., (1981), Mechanistic aspects of homogeneous catalytic hydrogenation and related processes, *Inorg. Chim. Acta* **50**, 11-19.

Helfferich, F.G., (2001), Kinetics of homogeneous multistep reactions, in: Compton, R.G., Hancock, G., (Eds.), *Comprehensive Chemical Kinetics, vol. 38*, Elsevier, Amsterdam, pp. 283-286.

Hoorn, J.A.A., Versteeg, G.F., (2005), Modelling of mass transfer and reaction: diffusion effects of radical intermediates, *submitted for publication*.

Kelkar, A.A., Jaganathan, R., Chaudhari, R.V., (2001), Hydrocarbonylation of methyl acetate using a homogeneous Rh(CO)Cl(PPh3)2 complex as a catalyst precursor: kinetic modeling, *Ind. Eng. Chem. Res.* **40**, 1608-1614.

Ponzi, E.N., Lemcoff, N.O., (1981), Influence of mass transfer on homogeneous catalytic gas-liquid reactions, *Rev. Latinoam. Ing. Quim. Quim. Apl.* **11**, 1-12.

Sanchez-Delgado, R.A., Rosales, M., (2000), Kinetic studies as a tool for the elucidation of the mechanisms of metal complex-catalyzed homogeneous hydrogenation reactions, *Coor. Chem. Rev.* **196**, 249-280.

van Elk, E.P., Borman, P.C., Kuipers, J.A.M., Versteeg, G.F., (2001), Modelling of gas-liquid reactors - Stability and dynamical behaviour of a hydroformylation reactor, *Chem. Eng. Sci.* **56**, 1491-1500.

van Swaaij, W.P.M., Versteeg, G.F., (1992), Mass transfer accompanied with complex reversible chemical reactions in gas-liquid systems: an overview, *Chem. Eng. Sci.* **47**, 3181-3195.

Versteeg, G.F., Blauwhoff, P.M.M., van Swaaij, W.P.M., (1987), The effect of diffusivity on gas-liquid mass transfer in stirred vessels. Experiments at atmospheric and elevated pressures, *Chem. Eng. Sci.* **42**, 1103-1119.

Versteeg, G.F., Kuipers, J.A.M., van Beckum, F.P.H., van Swaaij, W.P.M., (1989), Mass transfer with complex reversible chemical reactions - I. Single reversible chemical reaction, *Chem. Eng. Sci.* **44**, 2295-2310.

Westerterp, K.R., van Swaaij, W.P.M., Beenackers, A.A.C.M., (1990), Chemical Reactor Design and Operation, John Wiley & Sons, New York.

Zang, V., van Eldik, R., (1989), Reaction kinetics of iron chelates with sulfur oxides and nitrogen oxides in aqueous solution: waste gas purification by homogeneous catalysis?, *DECHEMA Monographien* **118**, 143-156.

Summary

Chemical reactors in which reactants are present in both gas and liquid occur frequently in industry. The study of these type of reactors is quite a challenge in many aspects. Clever design and optimisation increase the profit of the chemical plant, improve safety and reduce the impact on the environment. In design and optimisation activities models are indispensible since large scale experiments are often not feasible and scale-up from lab experiments is required. The majority of models for gas-liquid reactors are based on the two-film theory, Higbie's penetration theory or by Danckwerts modification. All theory's give relations for combined mass transfer between gas and liquid and reaction in the liquid. The quantification of these processes is a key factor in the construction of a model. This subject is studied from two angles; characterisation of mass transfer and reaction in an industrial application and by means of investigation of the behaviour of hypothetical reaction systems.

As industrial application the kinetics of the oxidation of toluene have been studied in close interaction with the gas-liquid mass transfer occurring in the reactor. Kinetic parameters for a simple model have been estimated on basis of experimental observations performed under industrial conditions. The conclusions for the mass transfer and reaction regime on basis of experimental observations and model calculations are in good agreement: toluene oxidation under industrial conditions can be characterized as a slow reaction with respect to mass transfer.

During the oxidation of toluene under semibatch conditions, the formation of benzyl alcohol is initially equal to the rate of formation of benzaldehyde. As the overall conversion increases the benzyl alcohol concentration at first decreases much faster than benzaldehyde, but this decrease slows down causing the benzyl alcohol concentration to reduce to zero only very slowly. To account for this phenomenon a new reaction pathway has been proposed where the formation of benzaldehyde out of benzylhydroperoxide is catalysed by benzoic acid. Incorporation of this new reaction in a model improves the description of benzyl alcohol concentration prophiles while maintaining good predictions for benzaldehyde and benzoic acid.

For the study of a hypothetical reaction system comprising radical reactions the diffusion-reaction equations for different model versions have been solved using a finite-differencing technique. In all models a reactant A is transferred from the gas to the liquid phase and reacts in the liquid with B to form P. The calculations comprised a simple stoichiometric model, a system with radical intermediates involved in the propagation steps and a version where also the termination reactions were included.

The results show that the diffusion coefficients of radical intermediates can have significant influence on the profiles of concentrations and reaction rates near the G/L interface. Furthermore, it is shown that for very fast reactions differences in diffusion coefficients of the intermediates influence the by-product formation. For systems of two radical intermediates, the so-called mixed termination product is only formed in low quantities whereas the other two termination products dominate. The calculation of enhancement factors required in the design of a G/L reaction system can be performed with simplified models where the reactive intermediates do not occur in the expressions for the reaction rates. The optimum model for a specific design purpose can be found by tuning the functions that correlate the parameters of the complex model to the parameters of the simplified model. In principle it is possible to very easily evaluate a large number of alternatives.

The second type of a theoretical system deals with homogeneous catalysis. Several models on the mass transfer of a gaseous reactant into a liquid where the reactions are catalysed by homogeneous catalysts have been evaluated by the numerical solution of the diffusion-reaction equations according to Higbie's penetration theory. The concentration profiles as well as enhancement factors are discussed as function of the kinetic rate constants and the diffusion coefficients of the catalytic intermediates. In addition to the complex catalytic model two simplified models were applied in order to facilitate design calculations. One version was obtained by application of the Bodenstein approximation, the simplest version comprised only the stoichiometric reaction. The Bodenstein model provides a very good approximation except for those situations where (substantial) differences exist between the diffusivities of the various catalytic intermediates. The applicability of the stoichiometric model is not as wide as with the Bodenstein model but in case of varying diffusion coefficients with the higher flexibility the complete model can be approached more closely.

Samenvatting

Chemische reactoren met reactanten in zowel de gas- als de vloeistoffase worden in de industrie veel toegepast. Het onderzoek aan dit type reactoren is een grote uitdaging op meerdere gebieden. Zorgvuldig ontwerp en goede optimalisatie vergroten de winst van de fabriek, verhogen de veiligheid en verminderen de belasting op het milieu. Binnen ontwerp en optimalisatie zijn modellen onmisbaar omdat experimenten op grote schaal veelal niet mogelijk zijn en een opschaling vanuit laboratorium experimenten vereist is. De meeste modellen voor gas-vloeistof reactoren zijn gebaseerd op de film theorie, Higbie's penetratie theorie of op de modificatie hierop van Danckwerts. Alle theorieën geven relaties voor gecombineerde stofoverdracht tussen gas en vloeistof en de reacties in de vloeistof. Het kwantificeren van deze processen vervult een sleutelrol in de constructie van een model. Dit nu wordt in dit proefschrift bestudeerd vanuit twee invalspunten; de karakterisering van stofoverdracht en reactie in een industriële reactor, en door middel van onderzoek naar het gedrag van hypothetische reactieve systemen.

Als industrieel voorbeeld is van de tolueenoxidatie de kinetiek in nauwe samenhang met de optredende gas-vloeistof stofoverdracht bestudeerd. Voor een vereenvoudigd model zijn de kinetische parameters bepaald op basis van experimentele resultaten waarbij de condities zo goed mogelijk leken op de fabrieksituatie. De conclusies voor wat betreft de stofoverdracht en het regiem op basis van experimentele observaties en de conclusies van de modelberekeningen zijn in goede overeenkomst: tolueenoxidatie bij industriële omstandigheden kan worden beschouwd als een langzame reactie in vergelijking tot stofoverdracht.

Tijdens het semi-batch bedrijven van de tolueenoxidatie is de vorming van benzylalcohol in eerste instantie gelijk aan de vormingssnelheid van benzaldehyde. Als de conversie van tolueen toeneemt, neemt de concentratie van benzylalcohol veel sneller af dan die van benzaldehyde, maar de afname vlakt af waardoor de benzylalcohol concentratie maar heel langzaam afneemt naar nul. Om dit gedrag te beschrijven is een nieuwe route in het reactiemechanisme voorgesteld waarbij de vorming van benzaldehyde uit benzylhydroperoxide gekatalyseerd wordt door benzoëzuur. Het inbrengen van deze nieuwe reactie in het mechanisme verbetert de modelbeschrijving van het verloop van de benzylalcoholconcentratie terwijl de voorspellingen voor benzaldehyde en benzoëzuur even goed blijven.

Voor het bestuderen van een hypothetisch reactiesysteem met radicaal reacties zijn de diffusie-reactievergelijkingen voor verschillende modelversies opgelost met een eindige-elementen methode. In alle modellen is reactant A een gasvormige component die naar de vloeistoffase wordt overgedragen alwaar deze reageert met B om zo P te vormen. De berekeningen zijn uitgevoerd voor een eenvoudig stoichiometrisch model, een systeem met radicalen als intermediair betrokken bij propagatiereacties en een versie waarbij tevens terminatiereacties zijn meegenomen. De resultaten laten zien dat de diffusiecoëfficiënten van de radicalen duidelijke invloed kunnen hebben op de concentratieprofielen en reactiesnelheden in de buurt van het gas-vloeistof oppervlak. Ook is aangetoond dat, bij zeer snelle reacties, verschillen in diffusiecoëfficiënten van de radicalen de bijproductvorming verandert. Bij systemen met twee radicaalintermediairen wordt het zogenaamde gemengde terminatieproduct alleen in heel kleine hoeveelheden gevormd terwijl de beide andere terminatieproducten domineren. De berekening van versnellingsfactoren zoals benodigd bij het ontwerpen van een gas-vloeistof systeem kan worden uitgevoerd met vereenvoudigde modellen waarbij de reactieve intermediairen geëlimineerd zijn uit de uitdrukkingen voor de reactiesnelheden. Het optimale model voor een specifiek ontwerpdoel kan worden gevonden door het trimmen van de functies welke het verband geven tussen de parameters van het complexe en vereenvoudigde model respectievelijk. In principe is het mogelijk om heel eenvoudig een groot aantal alternatieven te evalueren.

Het tweede type van een theoretisch systeem gaat over homogene katalyse. Verschillende modellen voor stofoverdracht van een gasvormige reactant naar een vloeistof waarbij de reacties worden gekatalyseerde door homogene katalysatoren zijn berekend door numerieke oplossing van de diffusie-reactievergelijkingen afgeleid van Higbie's penetratietheorie. De concentratieprofielen en de versnellingsfactoren zijn gecorreleerd aan de kinetische reactieconstanten en de diffusiecoëfficiënten van de katalytische intermediairen. Naast het complexe katalytische model zijn twee vereenvoudigde modellen ontwikkelt om ontwerp berekeningen te ondersteunen. Eén versie is verkregen vanuit een Bodenstein benadering, de meest eenvoudige versie bestond uit de stoichiometrische reactie. Het Bodenstein model levert een zeer goede benadering behalve in de situatie waarbij (aanzienlijke) verschillen bestaan tussen de diffusiecoëfficiënten van de verschillende katalytische intermediairen. De toepasbaarheid van het stoichiometrisch model is niet zo breed als de Bodenstein variant maar in geval van variërende diffusiecoëfficiënten kan door de grotere flexibiliteit het complete model dichter worden benaderd.

Dankwoord

Met veel plezier heb ik dit promotieonderzoek uitgevoerd. Gedurende het hele traject is de hulp en assistentie van een groot aantal personen onontbeerlijk geweest. Deze wil ik daarvoor heel hartelijk bedanken.

Mijn werkgever DSM ben ik zeer erkentelijk dat ik tijd en ruimte heb gekregen om mijn wetenschappelijke ambitie invulling te kunnen geven.

Met mijn promotor Geert Versteeg heb ik in de afgelopen 5 jaar plezierig samengewerkt. We hebben veel vruchtbare gesprekken gevoerd over de inhoud van het vak, maar ook over diverse maatschappelijke zaken in het algemeen. Daarnaast heeft hij me laten ervaren op welke manieren je een idee tot een concreet resultaat kunt brengen. De kunst om kort en duidelijk de essentie van een boodschap weer te geven heb ik zeer gewaardeerd. Geert, bedankt!

Sietse van der Sluis was op moment dat ik deze promotie wilde gaan uitvoeren sectiechef van onze afdeling en heeft dit vanaf het eerste moment gesteund. Sietse, ik vind het geweldig dat je deel uitmaakt van de commissie en hoop binnen DSM nog vaker met je te maken mogen krijgen.

Heel veel collega's en oud-collega's binnen DSM worden hartelijk bedankt voor ondersteuning en bijdragen in velerlei gedaante en belangstelling.

- Op gebied van projectmatig werken en algemene organisatie: Veerle Cauwenberg, Gerard Kwant, Chris Stoelwinder, Remko Bakker, Frank van den Brink†, Henk Oevering en Bert Bosman.
- Alle medewerkers uit de Tolox groep, voor hun kennis en kunde welke terug te vinden is in Hoofdstuk 2 en 3: Martijn Westermann, Daniëlle Petra, Rinke Altink, Llewellyn Rijk, Alex Vrinzen, Theo Cuypers, Jaap van Soolingen en Sylvia Vanhommerig.
- De opeenvolgende technology managers van DSM Fine Chemicals voor toestemming voor de publicaties van Hoofdstuk 2 en 3: Otto Plantema en Ubald Kragten.
- Voor het toetsen van de concept-artikelen en het vrijgeven voor publicatie: Edith Hermans, Peter Breepoel en Ralph Thomas.
- Voor de adviezen over promoveren binnen DSM: Cor van de Moesdijk, Ton Simons, Ton Loontjens, Ludo Kleintjens en Bert Bosman.
- Aangaande het scherp houden op inhoudelijk gebied: Ruud Guit, Paul Alstars, Paul van Geem.

- Een select gezelschap (voormalig) kamergenoten bestaande uit Robert Jan de Korte, Peter Roos en Pieter Vonk voor het incidenteel aanhoren van wat gemopper maar zeer zeker ook voor hun ervaring op gebied van AIO/promotie-activiteiten en het aanleveren van bruikbare software.
- Gerard Krooshof voor het beantwoorden van veel kleine vraagjes op gebied van thermodynamica.
- Johan Tinge en Rinke Altink voor de dropjes samen met de altijd grote belangstelling voor de voortgang en de daaruit volgende discussies over zeer uiteenlopende onderwerpen.
- Collega's "reactorkunde" voor gezelligheid en vakmatige vragen: Ioana Urseanu, Peter Markusse, Lei Hahn, Joop Lommen, Rudy Tuik, Bernd Ohlmeier, Gerben van Kranenburg, Bob Hoomans en Andrzej Stankiewicz.
- Alle overige collega's voor het tonen van belangstelling (op een enkele na dan).

Marieke Hoorneman heeft in het kader van de Twaio opleiding een project voor DSP Rotterdam uitgevoerd, waarvan ik het geluk had begeleider te mogen zijn. Samenwerken met Marieke was effectief en gezellig en heeft goede resultaten gebracht. Deze hebben in belangrijke mate bijgedragen aan de basis voor Hoofdstuk 2.

Eimert Roeters wordt bedankt voor het korte maar zeer effectieve coachingsgesprek.

Op de TU Twente heb ik niet veel tijd doorgebracht, maar de keren dat ik daar aanzeilde was Irene Gootjes altijd op kantoor. Afspraken, koffiemuntjes of een praatje, altijd goed! Edwin van Elk wil ik hartelijk bedanken voor het overdragen van zijn rekenmodellen en software.

Dit proefschrift was niet geschreven zonder de steun en toeverlaat van mijn ouders.....Ook mijn broer Marc, schoonzuster Mechteld en mijn vriendin Ellen betekenen veel meer dan in deze regels is aan te geven.....We vieren een feestje!

About the author

Born 1 December 1968 in Zaandam, The Netherlands. Graduated in 1993 (cum laude) at the Vrije Universiteit Amsterdam, specialisation in organic chemistry with prof. dr. G.W. Klumpp. Also in 1993 a degree in chemical engineering was obtained at the Technische Universiteit Delft with prof. dr. ir. J.A. Moulijn. In 1991 his research poster presenting experimental work performed at the Vrije Universiteit Amsterdam was awarded at the 1st Symposium Undergraduate Research, as a result of which a 3-months scolarship was fullfilled at Trinity University (San Antonio, Texas USA) with the group of prof. dr. M.P. Doyle.

Johan Hoorn has been employed at DSM Research since 1994. He is currently involved with process technology as expert chemical reaction engineering.

Publications

This thesis

Hoorn, J.A.A., van Soolingen, J., Versteeg, G.F., (2005), Modelling toluene oxidation, incorporation of mass transfer phenomena, Chem. Eng. Res. Des. 83, 187-195.

Hoorn, J.A.A., Alsters, P.L., Versteeg, G.F., (2005), A kinetic model for toluene oxidation comprising benzylperoxy benzoate ester as reactive intermediate in the formation of benzaldehyde, Int. J. Chem. Reactor Eng. 3, Article 6.

Hoorn, J.A.A., Versteeg, G.F., Modelling of mass transfer in combination with radical reactions, submitted for publication in Chemical Engineering Science.

Hoorn, J.A.A., Versteeg, G.F., Modelling of mass transfer in combination with a homogeneous catalysed reaction, submitted for publication in AIChE Journal.

Previous work

Dekker, N.J.J., Hoorn, J.A.A., Stegenga, S., Kapteijn, F., Moulijn, J.A., (1992), Kinetics of the CO oxidation by O2 and N2O over Cu-Cr/Al2O3, AIChE J. 38, 385-396.

Doyle, M.P., Winchester, W.R., Hoorn, J.A.A., Lynch, V., Simonsen, S.H., Ghosh, R., (1993), Dirhodium(II) tetrakis(carboxamidates) with chirakl ligands. Structure and selectivity in catalytic metal-carbene transformations, J. Am. Chem. Soc. 115, 9968-9978.